Master's thesis

NTNU
Norwegian University of Science and Technology
Faculty of Engineering
Department of Marine Technology

Ida Oline Håberg

Foil Motion Control of High-Speed Catamarans

Master's thesis in Marine Technology
Supervisor: Marilena Greco
June 2019

NTNU
Norwegian University of
Science and Technology

Ida Oline Håberg

Foil Motion Control of High-Speed Catamarans

Master's thesis in Marine Technology
Supervisor: Marilena Greco
June 2019

Norwegian University of Science and Technology
Faculty of Engineering
Department of Marine Technology

NTNU
Norwegian University of
Science and Technology

NTNU Trondheim
Norwegian University of Science and Technology
Faculty of Engineering Science and Technology
Department of MarineTechnology

MASTER THESIS IN MARINE TECHNOLOGY

Spring 2019

FOR

Ida Oline Håberg

Foil Motion Control of High-speed Catamarans

(Foil Motion Control av høyhastighets katamaraner)

High-speed vessels can benefit from use of submerged foil systems. They can provide foil-lift damping for the vertical-plane motions and can increase the vessel thrust, so enhancing the vessel efficiency. Moreover, use of foils in the bow part of the vessel can help avoiding deck-diving in following seas. Incorporating a foil motion control could enhance the seakeeping of high-speed catamarans. It can help in limiting the motions of the overall platform, as well as in preventing occurrence of unwanted phenomena, like ventilation and cavitation of the foils, with deterioration of the foil performances.
A preliminary project work has been performed to document the state of the art. From this, a catamaran geometry and its properties have been selected. DNV-GL seakeeping package was selected as research tool and applied to investigate the seakeeping of the catamaran without foils. Response Amplitude Operators (RAOs) in regular waves with different headings were estimated and results for selected conditions were compared against available numerical reference solutions. The main features of the foil system, with four fully submerged foils, have been decided and some important hydrodynamic-load contributions were discussed. A PID controller of the flap angles was selected for the foil motion control.

Objective
This master thesis aims to investigate the foil motion control of the selected high-speed catamaran. The target will be to incorporate a model of foil hydrodynamic loads in an available seakeeping solver for the vessel with forward speed and to associate a control algorithm, verifying its suitability.

The work should be carried out in steps as follows:

1. Summarize major findings/outcomes from the project thesis and, if necessary, complement the literature survey in order to identify state-of-the-art of the problem.
2. Describe the numerical DNV-GL package selected as research tool and its basic assumptions. Outline the foil system and discuss the hydrodynamic-load modelling required for the examined concept, including flap-angle effects. Explain the controller chosen for the foil motion control.
3. Complete the assessment studies of the project thesis, by providing numerical-convergence studies of the catamaran without foil.
4. Implement the foil loads in the seakeeping solver. Assume zero flap angle and investigate the relevance on trim and sinkage in steady-forward speed, and therefore on the mean-catamaran configuration. Then, perform seakeeping analysis of the vessel with foil system and discuss influence of foils on the catamaran motions in waves, as well as on the ship resistance.
5. Implement the control strategy in the numerical solver and investigate the behaviour of the catamaran in relevant wave conditions and the influence of controller features.

Rigid body motions and global loads should be examined to detect occurrence of undesired phenomena (e.g. slamming, cavitation, ventilation) or possible structural issues.

6. Draw the conclusions from the studies and discuss possible further research steps.

The work may show to be more extensive than anticipated. Some topics may therefore be left out after discussion with the supervisor without any negative influence on the grading.

The candidate should in her report give a personal contribution to the solution of the problem formulated in this text. All assumptions and conclusions must be supported by mathematical models and/or references to physical effects in a logical manner.

The candidate should apply all available sources to find relevant literature and information on the actual problem.

The thesis should be organised in a rational manner to give a clear presentation of the work in terms of exposition of results, assessments, and conclusions. It is important that the text is well written and that tables and figures are used to support the verbal presentation. The thesis should be complete, but still as short as possible. In particular, the text should be brief and to the point, with a clear language. Telegraphic language should be avoided.

The thesis must contain the following elements: the text defining the scope (i.e. this text), preface (outlining project-work steps and acknowledgements), abstract (providing the summary), table of contents, main body of thesis, conclusions with recommendations for further work, list of symbols and acronyms, references and (optional) appendices. All figures, tables and equations shall be numerated.

The supervisor may require that the candidate, in an early stage of the work, present a written plan for the completion of the work. The plan should include budget for the use of computer and laboratory resources that will be charged to the department. Overruns shall be reported to the supervisor.

From the thesis it should be possible to identify the work carried out by the candidate and what has been found in the available literature. It is important to give references to the original source for theories and experimental results.

Supervisor : Marilena Greco
Co-supervisor : Jens Helmers

Submitted : January 15th 2019
Deadline : June 11th 2019

Marilena Greco
Supervisor

Preface

This work is a master thesis written as part of the degree M. Sc. in Marine Technology with a specialization in hydrodynamics at NTNU. The thesis is executed in cooperation with DNV GL. The work was carried out in spring 2019. Before finalizing the thesis, a presentation was held at DNV GL presenting the work executed and obtaining feedback.

The thesis investigates foil motion control of a high-speed catamaran and contains a comprehensive literature study where relevant theory regarding foil motion control and seakeeping is discussed. In addition, the description of the modeling of a numerical catamaran model and results obtained for various seakeeping analyses is included. All work has been executed by the author of the thesis, Ida Oline Håberg.

Trondheim, June 5^{th}, 2019

Ida Oline Håberg

Acknowledgement

First and foremost, I would like to thank Professor Marilena Greco for expert knowledge and guidance throughout the thesis. From defining the scope to discussing the mathematical assumptions, our weekly meetings have provided me with knowledge, inspiration, and invaluable insight.

I would also like to direct a special thanks to Olav Rognebakke at DNV GL for enabling the cooperation, and for always being positive towards the work. Receiving guidance and being able to utilize the software used and created by DNV GL has been widely interesting. A big thank you is also directed to Håvard N. Austefjord, who was fortunately back from parental leave just in time, for always answering all kinds of questions regarding both conceptual understanding and the software. Jens B. Helmers has also provided valuable help and advice in the creation of the model, and in the execution of the work, and I would like to thank him for crucial guidance. In addition, I would like to thank Eivind Ruth at DNV GL for help with, and understanding of, the software.

I would also like to thank Odd Magnus Faltinsen for taking the time to discuss the scope and work. I am very grateful to have received help and guidance from world-leading experts within the field.

Lastly, I would like to thank my fellow students at office C.1058 for always being there for support and discussions. I would like to emphasize that their help and spirit has been very motivating when completing the work.

Ida Oline Håberg,

June 5^{th}, 2019

Trondheim, Norway

Abstract

Due to large motions and accelerations, high-speed vessels regularly experience large wave impact loads and wave-induced vibrations. A submerged foil system together with a ride control algorithm is a measure to reduce the severity of motion and loads. Done correctly, this technology can provide damping of the motions in the vertical plane and increase the vessel thrust, thereby enhancing the efficiency of the vessel. In addition, the foil motion control system can contribute to limiting unwanted phenomena such as ventilation and cavitation. This thesis is a study of the foil motion control of a high-speed catamaran based on investigations of a submerged foil system with a ride-control algorithm.

A high-speed catamaran earlier used by the *Division of Marine Hydrodynamics, NTNU* was selected for the work. The study is executed in cooperation with the Hydrodynamics, Advisory Department at DNV GL, who have contributed both with software and computational tools and guidance. A model of the vessel was created in *HydroD*, and linear hydrodynamic analyses on the model were run in *Wasim*. The geometry was validated with results for a similar high-speed catamaran from *Hydrodynamics of High-Speed Marine Vehicles* by Faltinsen, and was concluded to be satisfactory. A submerged foil system consisting of four T-foils with flaps was selected and investigated, and a relevant control algorithm was selected. Focus was devoted to the theoretical investigation and understanding of the foil loads and the implementation of the foil loads in the selected software. As this thesis combines hydrodynamic theory with control theory, an additional study was executed comparing the computational methods traditionally used in the said disciplines.

The influence from the foils on the vessel was investigated both passively, with zero flap angles, and actively, with motion control of the flaps. Linear analyses in regular waves were executed in *Waqum*, and the motions in the vertical plane were examined. The passive foil system was found to produce significant damping for both the surge, heave and pitch motions and accelerations. The resulting heave force and pitch moment produced by the passive foils was seen to be 180° out of phase with the respective motion velocities, providing maximum damping. A pure D-controller was selected for the final foil motion control, with the main objective of reducing the pitch motion. The active foils provided a reduction efficiency ratio of the pitch motion of 96% at the most, and a corresponding reduction of the pitch acceleration. Heave motion and acceleration were also reduced. The foils were also found to produce a positive horizontal force, increasing the vessel efficiency. Overall, the foil motion control system was seen to be of great benefit for the selected catamaran.

Sammendrag

Skip som opererer ved høye hastigheter utsettes regelmessig for kraftige bølgeinduserte belastninger og vibrasjoner forårsaket av store bevegelser og akselerasjoner. Et neddykket foilsystem kombinert med en kontrollalgoritme for kontroll av skipsbevegelsene er en måte å redusere bevegelsesnivået og størrelsen på disse kreftene. En slik type teknologi kan gi dempning av bevegelsene i det vertikale planet og øke fremoverhastigheten til skipet. Dette fører til en økning av skipseffektiviteten. Reduksjon av uønskede fenomen som ventilasjon og kavitasjon er et annet mulig resultat av foilkontroll. Denne oppgaven undersøker foilkontroll av en valgt høyhastighetskatamaran der et neddykket foilsystem kombinert med en kontrollalgoritme for kontroll av skipsbevegelsene har blitt studert.

En høyhastighetskatamaran tidligere brukt av *Divisjonen for Marin Hydrodynamikk, NTNU* ble valgt for arbeidet. Studiet ble utført i samarbeid med Hydrodynamics, Advisory på DNV GL som har bidratt med prorgramvare og veiledning. En numerisk modell av katamaranen ble laget i *HydroD* og analysert gjennom lineære hydrodynamiske analyser i *Wasim*. Geometrien ble validert ved bruk av resultater for en lignenede katamaran funnet i *Hydrodynamics of High-Speed Marine Vehicles* by Faltinsen. Resultatene ble vurdert som tilfredstillende. Et neddykket foilsystem bestående av fire T-foiler med klaffer kombinert med en relevant kontrollalgoritme ble valgt som konsept. Kreftene forårsaket av foilene ble vurdert teoretisk i tillegg til å bli implementert i den valgte programvaren.

Påvirkningen fra foilene på katamaranen ble undersøkt både ved passive foiler med null klaffvinkel, og ved aktive foiler med kontrollerte klaffer. Lineære analyser ble utført i *Waqum*, og bevegelsene i det vertikale planet ble undersøkt. Det ble sett at det passive foilsystemet forårsaket en signifikant dempning i jag, hiv og stamp. De resulterende hivkreftene og stampmomentene var i 180° fase med de respektive hastighetene, noe som gir maksimal dempning. En D-kontroller ble implementert med hovedmål om å redusere stampbevegelsene. Det aktive foilsystemet bidro til en reduksjons-effiktivitets-grad på maksimalt 96%. Stampakselerasjonen ble redusert tilsvarende. I tillegg ble det sett at foilsystemet produserer en positiv horisontal kraft, som bidrar til økt skipseffektivitet. Totalt sett bidrar de kontrollerte foilene til stor nytte for den valgte katamaranen.

Contents

List of Figures

List of Tables

Nomenclature

Latin letters

A	Added mass coefficient, Area of foil
B	Linear damping coefficient
b	Two-dimensional damping coefficient
C	Restoring coefficient
C_D	Drag coefficient
$C_{D,v}$	Viscous drag coefficient
$C_{D,i}$	Induced drag coefficient
$C_{DW,\Gamma}$	Drag coefficient due to circulation
C_F	Friction coefficient
C_L	Lift coefficient
c	Foil chord
D_f	Drag force
d	Depth
e	Control error
Fn	Froude number
Fn_h	Submergence froude number
Fn_∇	Displacement froude number
f	Frequency, Control force
g	gravitational acceleration
H	Wave height
H_s	Significant wave height
h	Submergence, Retadartion function
I_q	Integrated value of given quantity
K	Diagonal force coefficient matrix
k	Reduced frequency, Wave number
k_p	Proportional gain
k_d	Derivative gain
k_i	Integral gain
L	Length
L_f	Lift force
L_{pp}	Length between the perpendiculars

M Moment
p Distance between foils
R_T Resistance coefficient
Rn Reynolds number
R_{WS} Resistance component
rc flap length to foil chord ratio
S Wave spectrum
s Translational movement, Foil span
T Wave period, Thrust allocation matrix
T_z Zero up-crossing period
t Foil thickness
U Vessel speed
u Control input
V Velocity
z Submergence

Acronyms

COG Center of Gravity
DOF Degree of Freedom
ER Reduction Efficiency Ratio
KG Center of gravity above keel
LCG Lengthwise center of gravity
NED North East Down (Frame)
OA Order of Accuracy
PID Proportional Integral Derivative (Controller)
RAO Response Amplitude Operator
RMS Root Mean Square
WDB Waqum Database
WIG Wing in ground

Greek letters

α_t Angle of attack
α_f Flap angle
α_i Ideal angle of attack
α_0 Angle of zero lift
β Wave propagation angle
Γ Circulation
γ Phase angle
Δ Vessel weight
ϵ *Resistanceparameter*
ζ_a Wave amplitude
η Body motion, Surface elevation
θ Wave direction
Λ Aspect ratio
λ Wavelength
ν Kinematic viscosity
ρ Density
σ Strength of source
τ Control force
ϕ Velocity potential
ω Circular frequency

Chapter 1

Introduction

The demand for seaborne transport is forecasted to increase with 60% by 2050, DNV GL (2018a). Meanwhile, the Paris agreement states that the earth's temperature should not rise with more than 2°C during this century. Meeting both the increased energy demand and the UN's climate goal sets requirements regarding developing and utilizing more sustainable technology. The goal is finding solutions contributing to low emissions without compromising the efficiency of the technology.

A submerged foil system, together with a ride control algorithm, is a technology that enhances the efficiency and therefore decreases the carbon footprint of high-speed catamarans. The technology can provide foil-lift damping of the motions in the vertical plane and increase the vessel thrust. As a result, the vessel efficiency increases. Another usage of a foil motion control system is reducing the severity of the wave loads experienced by the vessel, which results in a more comfortable ride. An additional effect of a submerged foil system is the limitation of unwanted phenomena such as ventilation and cavitation, as well as the possibility of limiting deck-diving in following seas.

This thesis aims to investigate the foil motion control system of a selected high-speed catamaran with the target of incorporating the foil hydrodynamic loads in a seakeeping solver used by DNV GL. The selected vessel is a high-speed catamaran used in earlier work by textitDivision of Marine Hydrodynamics, NTNU, Faltinsen (1992). The target is to study the high-speed catamaran with forward speed and to associate a control algorithm with the foil system.

1.1 Background

1.1.1 Project thesis

As a preliminary study, a project thesis was carried out during the autumn of 2018. A high-speed catamaran model earlier used by the *Division of Marine Hydrodynamics, NTNU*, Faltinsen (1992), was selected for the preliminary study of the effect of foil motion control. The study was executed in cooperation with the Hydrodynamics, Advisory Department at DNV GL. A numerical model of the vessel was created, and a stability analysis in addition to linear hydrodynamic analyses in the time domain was run obtaining RAOs used for verification of the vessel model. DNV GL's software package *SESAM* was utilized; *HydroD* for the modeling, and *Wasim* for the hydrodynamic analyses. Only the lower part of the geometry was included as *HydroD* only takes the geometry below the waterline into consideration for such cases. The meshed simulation domain and the meshed vessel model of the catamaran are presented in Figure 1.1 and 1.2.

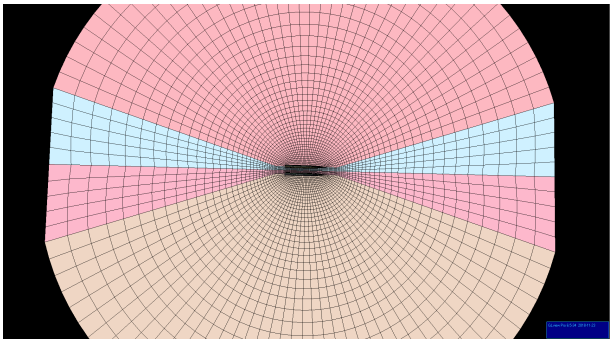

Figure 1.1: Simulation domain

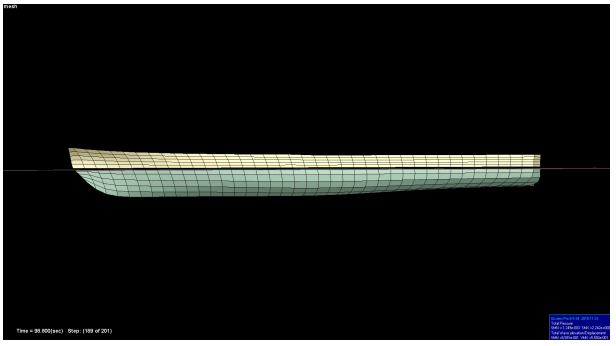

Figure 1.2: Catamaran from side

The analyses were run for three vessel speeds; 0kn, 19kn, and 35kn corresponding to the Froude numbers 0, 0.5 and 0.934, respectively. The obtained results were validated with data for a similar vessel from *Hydrodynamics of High-Speed Marine Vehicles* by Faltinsen (2006). Figure 1.3 to 1.4 show Response Amplitude Operators (RAOs) for heave and pitch for Froude number 0.5 in head seas. These degrees of freedom are especially considered as they can be decreased considerably by foil motion control. Figure 1.5 to 1.6 show RAOs for heave and pitch for Froude number 0.9 in head seas. Table 1.1 shows the main dimensions of the catamaran considered. The dimensions of the catamaran used for comparison are displayed in Appendix A.1.

Designation	Symbol	Unit	Value
Length between perpendiculars	L	$[m]$	37.78
Beam at waterline midship	B	$[m]$	9.18
Draft, even keel	d	$[m]$	2.35
Displacement	∇	$[m^3]$	257
Block coefficient	C_b	-	0.542
Breadth of one hull at waterline amidships	b	$[m]$	2.67
Distance between centre of hulls	$2p$	$[m]$	6.52
Transverse metacentric height	GM	$[m]$	5.56
Centre of gravity above keel	KG	$[m]$	3.32
Centre of gravity aft of amidships	LCG	$[m]$	2.96

Table 1.1: Dimensions of high-speed catamaran in the study

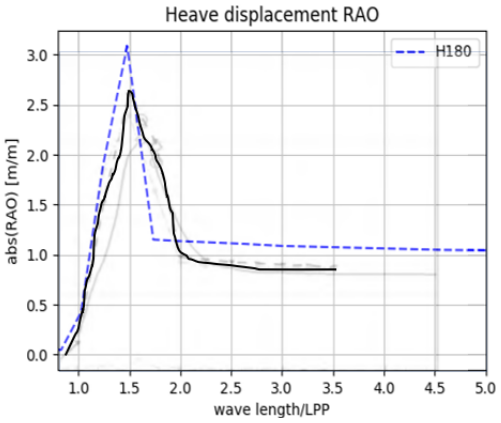

Figure 1.3: Heave RAO, Fn 0.5

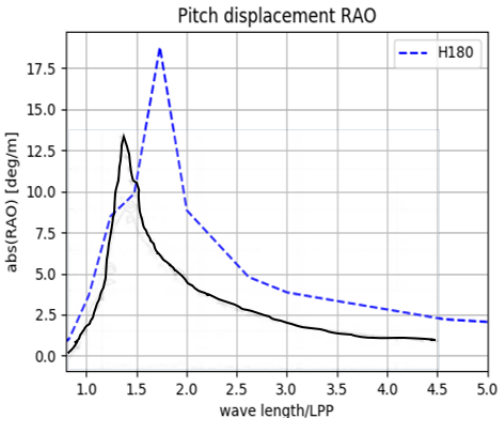

Figure 1.4: Pitch RAO, Fn 0.5

[- - - - -]= catamaran from project thesis, [———] = comparison catamaran

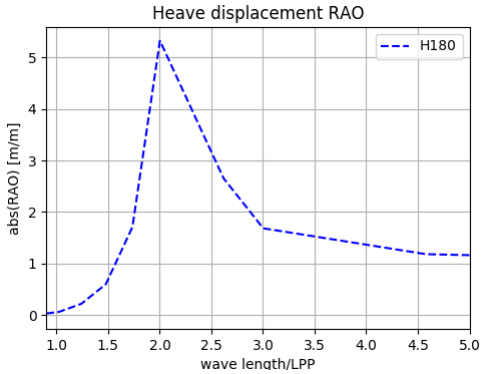

Figure 1.5: Heave RAO, Fn 0.9

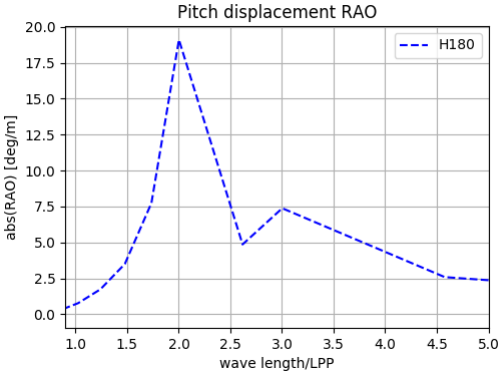

Figure 1.6: Pitch RAO, Fn 0.9

The RAOs in Figure 1.3 and 1.4 are seen to be quite similar to the RAOs from literature both regarding shape and value. The RAOs for Fn=0.9 have similar shapes, and higher maximum values than for the lower speeds, which is as expected. When viewing RAOs in all degrees of freedom for all headings, the largest responses were in general seen for head seas at 180°, while beam seas at 90° was found to give the smallest responses. Sea from 135° also resulted in a considerable response. As a result, head seas was selected as the heading of interest for further studies of motion reduction.

Only RAOs for Froude number 0.5 were used for validation of the results. Preferably, additional comparisons should have been done with RAOs for Froude number 0.9. However, no RAOs for fitting catamarans were found for Froude numbers close to this. RAOs for lower Froude numbers, as 0.3 and 0.4 were found, so an additional computation could have been included with one of these Froude numbers for further validation of the model. Only results for heave and pitch were found for comparison. Viewing results from the literature assessing additional degrees of freedom would have been useful to detect deviations and inconsistency.

Overall, the results indicate that the created model functions as desired concerning producing results that seem to be correct when undergoing hydrodynamic numerical analyses. This is considered a satisfying basis for moving forward with the same model in the master thesis. An underwater fore-aft foil system was selected and defined in terms of geometry and positioning. This geometry was assessed with respect to the forward speed, and simplifications and assumptions were discussed. This is described in further detail in Chapter 3. The influence of the foil system is to be investigated further in this thesis.

1.1.2 History

Humans have always been interested in finding solutions to utilize the surrounding environment as effectively as possible. In the marine environment, numerous vessel designs have been proposed and tested through the years to move across the ocean at high speeds, and at the same time minimize the power requirements. One problem addressed early was the issue of the large pitch and roll motions occurring in severe sea states which lessen both the safety and efficiency of the vessel, Huang et al. (2018). This history is relevant when viewing the foil motion control of high-speed catamarans as it sets the background of the development for a considerable part of the technology used for these aspects today.

Parametric roll is one issue that has resulted in comprehensive research being conducted on the reduction of pitch and roll movement throughout the years. Parametric roll can result in the loss of stability, and the large roll motions may cause damage of cargo and even capsizing. The parametric roll motions can be initiated through resonance when the pitch motion frequency coincides with the wave frequency. Therefore, a reduction of the

pitch motions can reduce the risk of parametric roll. Another relevant issue is seasickness, which can be caused by the vertical accelerations caused by the pitch and roll motions.

Various devices, both active and passive, have been designed to reduce the ship motions. Froude (1865) introduced bilge keels as a passive stability system as the first roll reducing mechanism in the 19th century. Another passive method studied is the use of antiroll tanks, for instance by Frahm (1911). Schlick (1904) made the first proposal for active gyrostabilizers where the effects of one or more spinning wheels are used to counteract the roll motion. The use of gyrostabilizers in the ride control of marine vessels was in newer time investigated by Townsend et al. (2007). Active and passive fins and rudders have been investigated in several studies, both for roll and pitch control. One example is the use of a fixed anti-pitch foil in the bow, which has been proved to reduce vertical motions, Avis (1989). Satisfactory performance in anti-rolling by using active fins has been demonstrated by Perez and Blanke (2012). The flapping foil developed by John Martin Kleven Godø and Sverre Steen at NTNU, Stensvold (2016), is a new and exciting idea that can revolutionize the high-speed vessel market by decreasing the energy needs by 30-50%.

1.1.3 Current state of high-speed vessels with foil motion control

High-speed vessels are expected to be of increasing importance in the future regarding marine applications, passenger- and cargo transportation, Fossen (1996). Through the last decades, there has been a focus on faster, more efficient high-speed multi-hulls. Modern, slender catamaran hull shapes and lightweight materials allow high speeds and low power usage at the same time. The major factors taken into consideration when designing high-speed vessels are cost, capacity, speed, range, sea keeping, environmental issues, safety, and reliability. As a solution, foil assisted catamarans have been developed, and multiple studies have been conducted throughout the years on various designs and concepts. The effect of using motion control systems such as T-foils, trim tabs, or interceptors with regards to damping, increases with increasing velocity. Therefore, the usage of these devices is generally more efficient for high-speed vessels, than for conventional vessels at moderate operating speeds, Faltinsen (2006).

Hydrofoil assistance has been found to benefit a number of the areas mentioned, especially in the increase of speed, reducing the cost and improving sea-keeping and range, Migoette and Hoppe (1999). Hydrofoil vessels where the hulls are completely lifted out of the water at operating speeds have for instance been built both in Norway and Japan, Faltinsen (2006). The *Foil Cat 2900* is a Norwegian example which has two fully submerged T-foils located at the bow, and one full-width at the stern. *Super Shuttle 400* is a Japanese foil catamaran with full-width fully submerged foils both at bow and stern. Until around the

year 2000, hydrofoil assistance was not considered efficient for semi-displacement catamarans with lower operational Froude numbers than for instance for hydrofoils with Froude numbers from around 3. Typical resistance tendencies are shown by Migoette and Hoppe (1999) in Figure 1.7. The graph is a function of the displacement Froude number Fn_∇, and the length-displacement ratio $\frac{L}{\nabla^{1/3}}$ as these are viewed as the dominating resistance parameters.

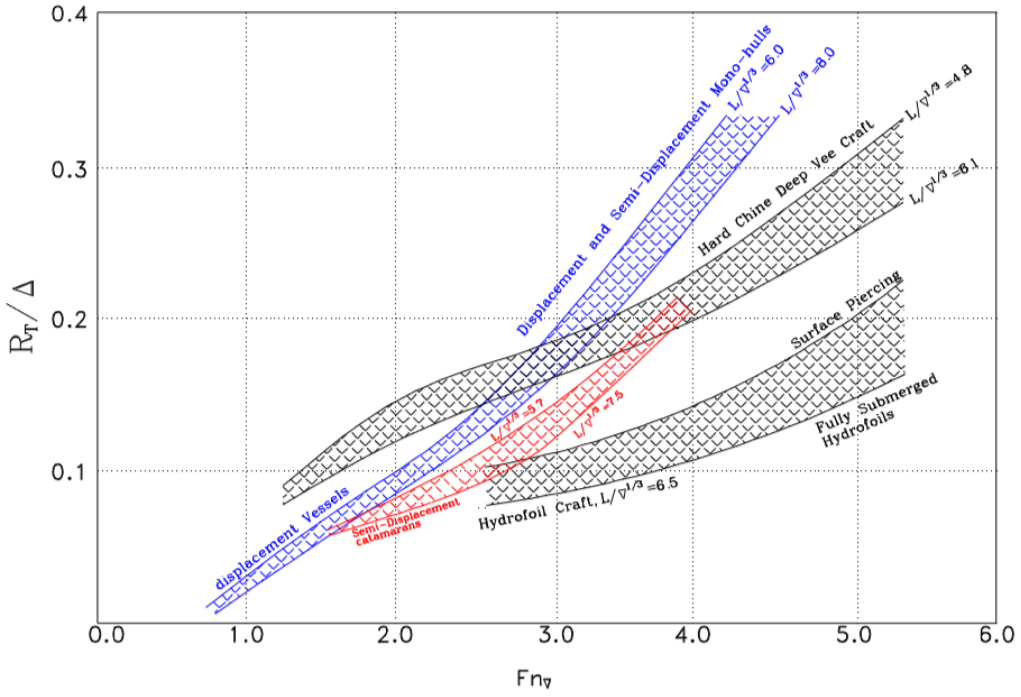

Figure 1.7: Typical resistance coefficients for sea craft, from Migoette and Hoppe (1999)

For the vessel studied, the displacement Froude number is 2.28. When the displacement Froude numbers are less than 2.25, the presence of foils is in general found to increase the resistance of a vessel opposed to reducing it. This can be seen from Figure 1.8 given by Migoette and Hoppe (1999), which shows the typical resistance for a semi-displacement catamaran with ϵ as a parameter describing the resistance. The dotted line shows the results with foils, while the solid line is without foils. It is important to note that this is the trend when neither foil control or retractability of the foil into the hull at low speeds is included. However, as a result, the design of foils for vessels operating at lower Froude numbers is crucial for optimal effect.

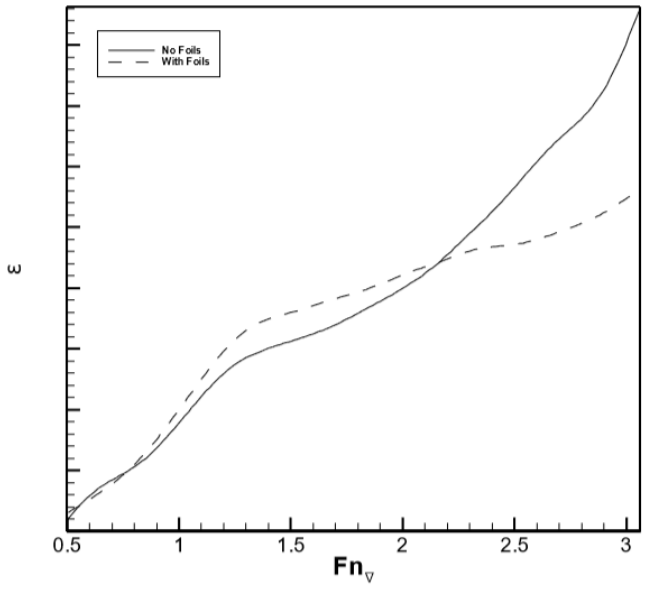

Figure 1.8: Foil influence on semi-submersible catamaran, from Migoette and Hoppe (1999)

It is hypothesized that a submerged foil system on the semi-submerged catamaran in the study together with a ride control algorithm can reduce the resistance of the vessel and therefore enhance the efficiency significantly. In addition, several studies have shown ride motion control of foils on vessels to contribute to reducing the wave-induced motions successfully. One example is the study done by Zhang et al. (2014) on a wave-piercing catamaran with a centered T-foil at the bow. In Figure 1.9 and 1.10, the pitch angles and heave displacements with and without control foils for numerical simulations are shown. For additional emphasis, the Motion Sickness Index is presented in Figure 1.11.

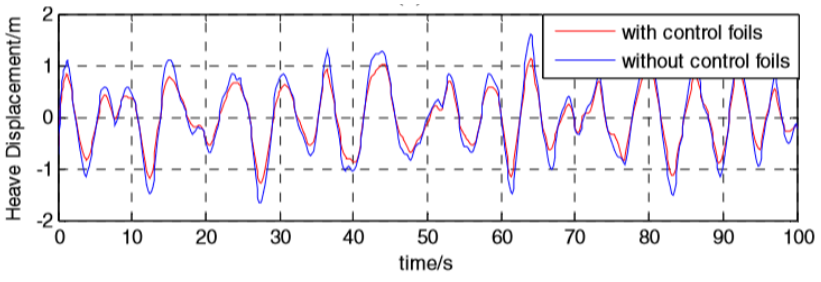

Figure 1.9: Heave reduction by control foils, from Zhang et al. (2014)

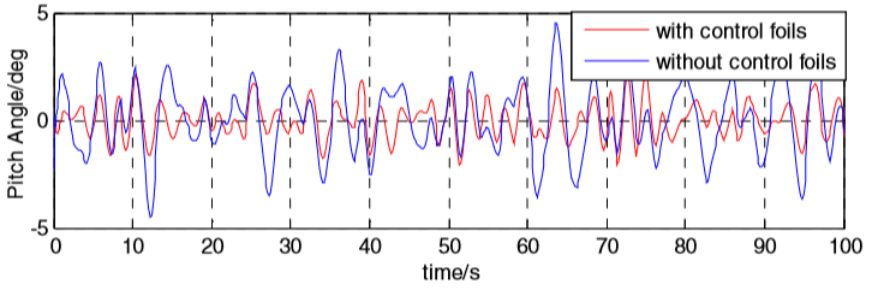

Figure 1.10: Pitch reduction by control foils, from Zhang et al. (2014)

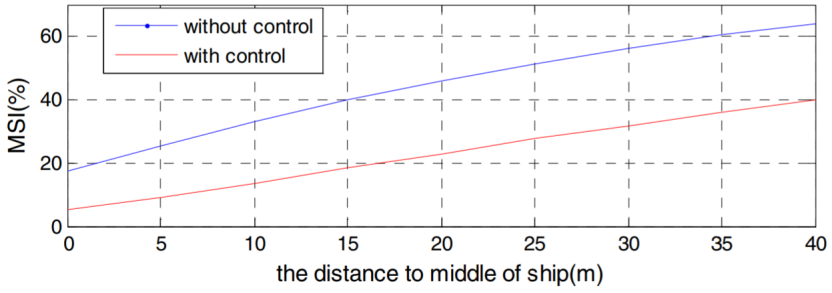

Figure 1.11: Motion sickness index, from Zhang et al. (2014)

1.2 Objective

Motivated by the recent research on foil motion control of high-speed catamarans together with the increasing demand for sustainable technologies, this master thesis aims to investigate the foil motion control of the selected high-speed catamaran. Reduction of the pitch motion was chosen as the main control objective, as limiting the pitch motion contributes to limiting the coupled vessel motions, parametric roll, and seasickness. The goal is to implement a model of the hydrodynamic loads caused by the foil system together with the control algorithm in the seakeeping solver used by DNV GL. The suitability should be verified. The full description of the objective and plan is given on the first page of this thesis. The vessel model created in the project thesis will also be assessed further with a numerical convergence study of the mesh. To complete the study, the following steps were identified:

1. Major findings from the project thesis should be presented, and the literature study and state-of-the-art of the problem should be supplemented.
2. The software package from DNV GL selected as research tool should be described, and relevant assumptions should be presented.

3. The numerical vessel model should be further assessed by a numerical convergence study.
4. The foil loads are to be implemented in the selected seakeeping solver. Hydrodynamic seakeeping analyses should be executed on the catamaran with steady forward speed and with zero flap angle to investigate whether the foils influence trim and sinkage. In addition, the influence of the foils on the motions in waves should be investigated.
5. The control strategy is to be implemented in the seakeeping solver. The behavior of the high-speed catamaran with foil motion control should be investigated in relevant wave conditions. The rigid body motions and global loads should be inspected as well as the occurrence of undesired phenomena such as slamming, cavitation of ventilation.
6. Conclusions should be drawn, and possible further steps should be discussed.

1.3 Flow of work

The work is executed following the chart presented in Figure 1.12.

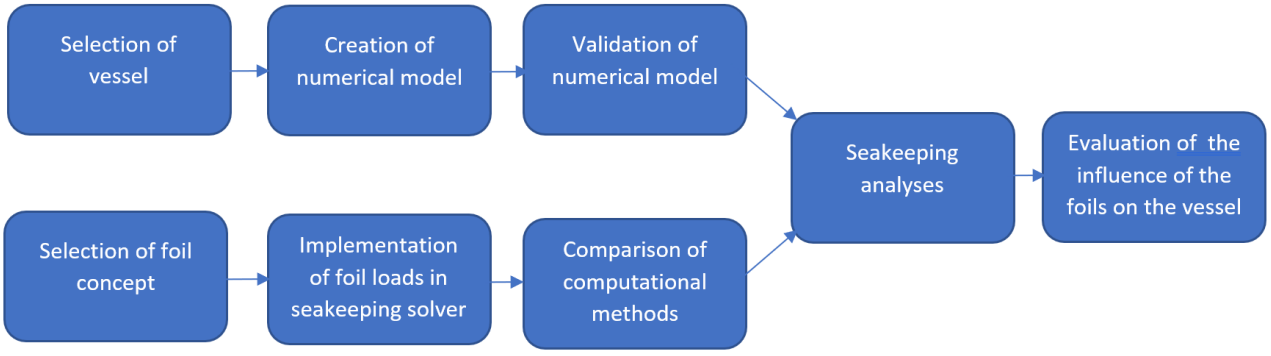

Figure 1.12: Flow diagram of work flow

1.4 Structure of report

The remaining part of the report is structured as follows.

Chapter 2 describes the software used during the thesis.

Chapter 3 presents foil theory and discusses simplifications and assumptions made. This chapter creates a theoretical foundation for the theory implemented in the source code.

Chapter 4 discusses the theory used in the seakeeping solver and compares the traditional computational techniques in hydrodynamic and control theory.

Chapter 5 discusses the control theory used for the foil motion control in this study. Assumptions and simplifications are described.

Chapter 6 presents the environmental conditions of the study and discusses the statistical analysis of the weather.

Chapter 7 presents the method followed in the selection of vessel geometry and foil concept, in addition to the creation of the numerical model.

Chapter 8 describes the selections done with regards to the solver and describes the various analyses executed.

Chapter 9 presents and discusses the results. In addition, the method followed in the study is discussed.

Chapter 10 concludes on the work of the thesis.

Chapter 11 presents suggestions for further work.

Some sections are based on the work executed in the project thesis. This holds, for instance, for parts of the sections describing theory, in addition to the presentation of the methodology regarding the selection of the vessel geometry.

Chapter 2

Software

In this chapter, the software utilized in the study is presented. First, the chronological usage of the different software is shown, then each program is described in the following sections.

2.1 Work flow: software

Figure 2.1 shows the chronological order of the software used in the study.

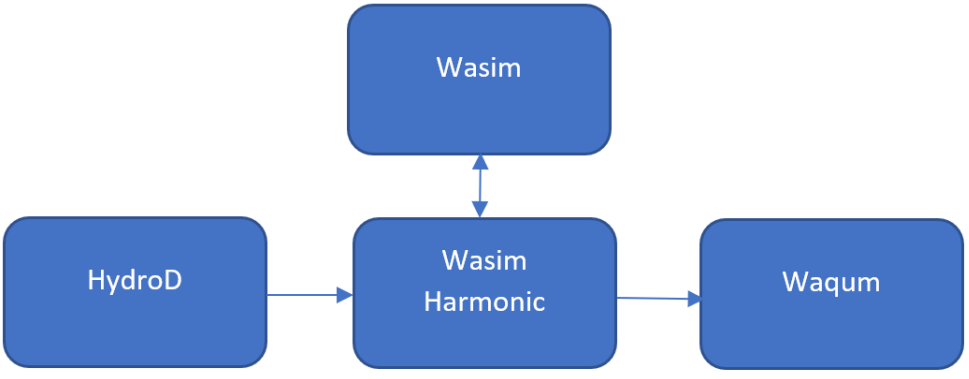

Figure 2.1: Flow chart of software usage

2.2 HydroD

HydroD is a software for hydrostatic and hydrodynamic analysis, including fully automated load transfer to FEA, DNV GL (2018b). The software is part of the DNV GL software package *SESAM* and can execute stability analyses and hydrodynamic analyses in both frequency and time domain. For time domain and frequency domain analyses of structures with a steady forward motion, *HydroD* is coupled with *Wasim*.

In this study, *HydroD* was used as a preprocessor to assess the modeled geometry and to establish the data needed for hydrodynamic simulation in *Wasim*. For instance, it was used to establish the body mass matrix and sectional mass matrix to be used in *Wasim*.

2.3 Wasim

Wasim is a time simulation tool which, like *HydroD*, is a part of the software package *SESAM* by DNV GL. The software is used for computing the local wave loading and global responses of vessels with any forward speed, as long as the vessel is not planing. The simulations are executed in the time domain. The results are, in addition, transformed to the frequency domain by the use of Fourier transforms, DNV GL (2014a).

In this study, *Wasim* is used to obtain frequency domain response amplitude operators from linear analyses for the vessel without a foil system. The program transfers rigid body accelerations and gravity loads in structural analyses automatically. The fully three-dimensional radiation/diffraction problem is solved by a Rankine panel method that uses panels both on the hull and on the free surface. When linear analysis is selected, transfer functions are calculated to represent the results. The software is based on potential flow theory, so viscous effects are not taken into consideration.

2.4 Wasim Harmonic

Wasim Harmonic is a pre- and post processor for *Wasim* to generate harmonic coefficients. In this study, *Wasim Harmonic* is used to perform equilibrium iterations to check the stability of the created model geometry, and as a tool to run the simulations to obtain the response amplitude operators.

2.5 Waqum

Waqum is a time domain hydrodynamic analysis tool part of the DNV GL software package *SESAM*. The linear equation of motion is solved for non-linear excitation forces in the time domain using the Runge Kutta 4 method. Waqum uses retardation functions to simulate the motions of a floating body and can handle arbitrary and time-dependent excitation forces. The inputs to the program are mass, added mass, damping, and stiffness coefficients from linear analysis in the frequency domain, which are transformed into the time domain using retardation functions.

In this study, the hydrodynamic loads and forces are implemented as additional functionality in *Waqum*, and the software is then used to execute the hydrodynamic analyses for evaluation of the influence of the foil loads.

Chapter 3

Foil theory

The hydrodynamic equations describing the foils and foil loads are presented and discussed in this section. First, a general introduction to foil theory is presented, then the simplifications and assumptions relevant are discussed in further detail. The theory in Section 3.2 is based on the paper *Ship pitch-roll stabilization by active fins using a controller based on onboard hydrodynamic prediction* by Huang et al. (2018), while the remaining sections are based on the work by Faltinsen (2006) unless otherwise is stated.

3.1 Foil geometry

The geometrical parameters used to define a foil are presented in Figure 3.1. This figure shows the cross-section of a typical foil.

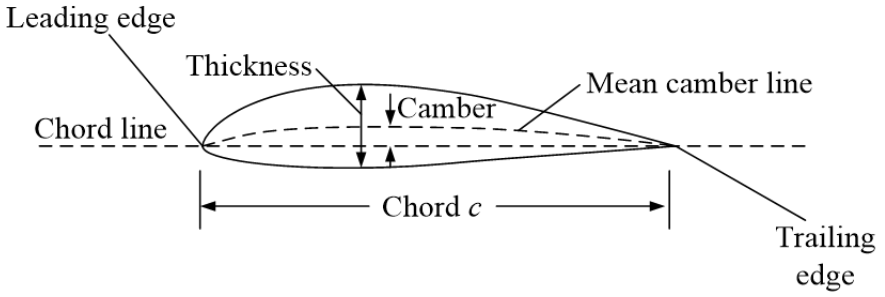

Figure 3.1: Foil geometrical parameters, from Faltinsen (2006)

The aspect ratio Λ is defined as the ratio of the square of the foil span s^2 to the projected area A as in Equation 3.1. The aspect ratio is an important parameter used when discussing foils.

$$\Lambda = \frac{s^2}{A} \tag{3.1}$$

Λ = aspect ratio, s = foil span to the projected area, A = projected area

3.2 Foil loads

Foils generate lift from the incoming flow with velocity $\boldsymbol{V}$ presented in Equation 3.2 and effective angle of attack $\alpha_t(t)$ between the flow and the foil, as described in Equation 3.4. The vessel propagates in the x-direction with forward speed $\boldsymbol{U}$, which results in a relative velocity. Each foil i is seen independently from one another, and the effects between the forward and aft foil system are neglected as it results in very complex downwash, which is not viewed in this study. This is discussed further in Section 3.7.

The hydrodynamic forces acting on foils and struts are far easier to model than the hydrodynamic forces acting on the hull as they can be expressed as point forces opposed to distributed forces, Fossen (1996). The actuating arms of the foil loads are defined as the distance from the motion reference point of the vessel to the quarter-point of foil i and are given as $x_f(i)$, $y_f(i)$ and $z_f(i)$ in x, y, and z-direction, respectively. The motion reference point is in this case defined in the seakeeping solver. $u_w(t)$ and $v_w(t)$ are the horizontal and vertical fluid particle velocities, and $\alpha_f(i)$ is the operational angle of foil i.

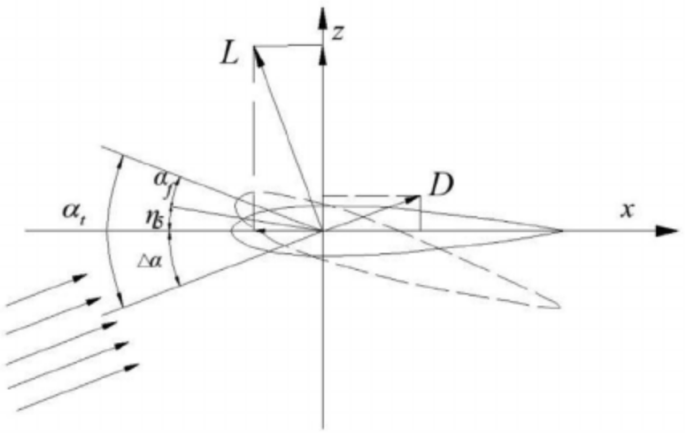

Figure 3.2: Foil geometry for foil load computations, from Huang et al. (2018)

$$\boldsymbol{V} = [V_x, V_y] = [U - u_w(t), \dot{\eta}_3(t) + y_f(i)\dot{\eta}_4(t) - x_f(i)\dot{\eta}_5(t) - v_w(t)] \tag{3.2}$$

$$\Delta\alpha(i) = -arctan\left(\frac{\dot{\eta}_3(t) + y_f(i)\dot{\eta}_4(t) - x_f(i)\dot{\eta}_5(t) - v_w(t)}{U - u_w(t)}\right) \tag{3.3}$$

$$\alpha_t(i) = \alpha_f(i) + \eta_5 + \Delta\alpha(i) \tag{3.4}$$

The lift and drag forces resulting from the foils are presented in Equation 3.5 and 3.6.

$$L_f = \frac{1}{2}\rho V^2 S \frac{\partial C_L}{\partial \alpha_t}\alpha_t(i) \tag{3.5}$$

$$D_f = \frac{1}{2}\rho V^2 S C_D \tag{3.6}$$

V = incoming flow velocity, S = surface, ρ = water density, C_L=lift coefficient, C_D=drag coefficient, α_t=effective foil angle

From the forces, the moments can be expressed as follows:

$$F_4^f = \sum_{i=1}^{4} y_f(i)[L_f(i)cos\Delta\alpha + D_f(i)sin\Delta\alpha] \tag{3.7}$$

$$F_5^f = \sum_{i=1}^{4} -x_f(i)[L_f(i)cos\Delta\alpha + D_f(i)sin\Delta\alpha] \tag{3.8}$$

From Equation 3.5, it can be seen that the lift force is quadratically proportional to the incoming flow velocity V, and just linearly proportional to the projected area of the surface S. Therefore, to obtain the same lift force from a foil on a vessel when the speed is lowered, the surface of the foil needs to be increased considerably. As a result, foil motion control systems are mainly applicable for high-speed craft. A large aspect ratio is required for efficient foils, Loveday (2006), but limitations occur due to increased bending moments for increased ratio. Therefore, the increase of the foil thickness must be taken into consideration when increasing the aspect ratio, and since a large thickness ratio reduces the efficiency and maximum speed allowed without cavitation occurring, compromises must often be made.

3.3 Coefficients

3.3.1 Lift coefficient

The lift coefficient for an individual foil depends on many parameters. The angle of attack α of the incident flow, the flap angle, camber, thickness-to-chord ratio, aspect ratio, submergence Froude number $Fn_h = U/\sqrt{gh}$, Reynold number, and cavitation number are

all important aspects in addition to the geometry of the foil surface.

The mathematical expression for the lift coefficient C_L is a function of the angle of attack, α. Figure 3.3 presents an example for C_L given by Faltinsen (2006) when steady flow past a 2D foil in infinite fluid with turbulent boundary layer flow conditions is assumed. The fluid is considered incompressible as the incoming flow velocity is assumed small relative to the speed of sound.

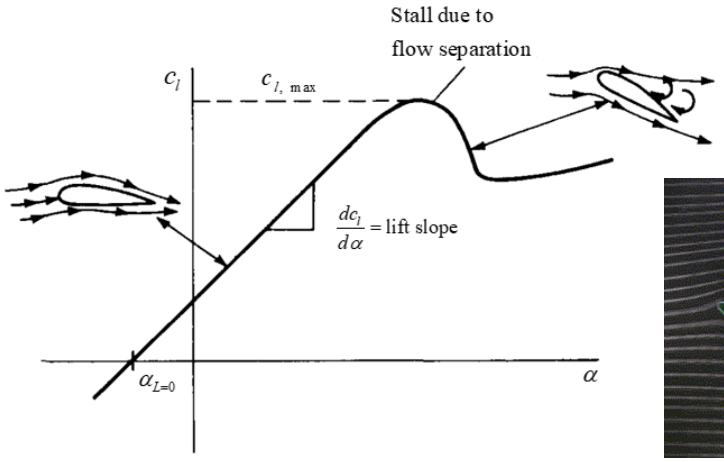

Figure 3.3: Lift coefficient to foil angle, from Faltinsen (2006)

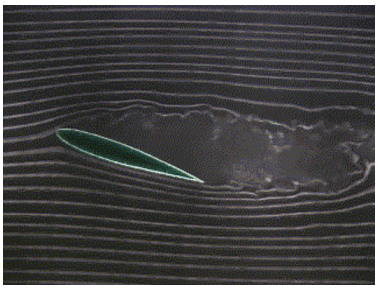

Figure 3.4: Vizualization of stall, from Faltinsen (2006)

The 2D lift coefficient can be defined as $C_L = 2\pi(\alpha - \alpha_0)$ from the linear region of the graph when the fluid is assumed inviscid and linear theory is utilized. α_0 is a parameter describing the presence of camber of flaps. The derivative of the lift coefficient is accordingly given as $\frac{dC_L}{d\alpha} = 2\pi(\frac{\pi}{180}) = 0.11$, when α is given in degrees, which has shown to be a satisfactory estimation with less than 5% deviation from experiments where a large number of angles of attack α's and foil geometries were viewed. However, the estimation of the derivative of the lift coefficient may be less fitting when the thickness-to-chord ratio is large, as for instance $\frac{t}{c} > 0.14$. For the NACA 0015 foil, the comparison between experimental and numerical data is shown in Figure 3.5.

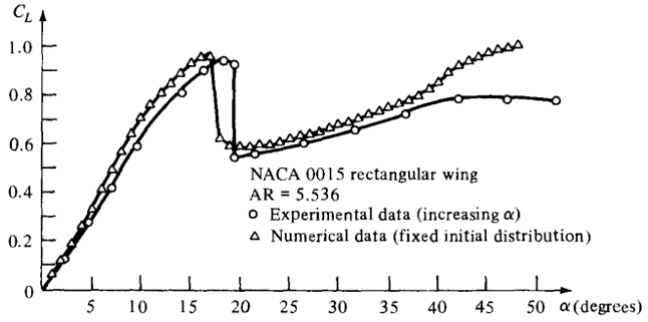

Figure 3.5: C_L, numerical and experimental results from Faltinsen (2006)

The sudden decrease in lift outside of the linear region is due to stall, which occurs when flow separation happens as the critical angle of attack is exceeded. This phenomenon is depicted in Figure 3.4. The critical angle of attack is typically $\approx 20°$, SKYbrary (2019). In this study, the effect of stall is not taken into account, and the limit of the angle of the flaps is therefore set to +- 20°. Huang et al. (2018) supports the selection of this constraint.

If the aspect ratio is considerably high, α is small, and the incident flow is assumed infinite, Prandtl's lifting line theory can be utilized to account for three-dimensional effects. A considerably high aspect ratio is defined as when the span is much larger than the chord length. Prandtl's lifting line theory calculates the lift coefficient as Equation 3.9.

$$C_L = \frac{2\pi\alpha}{1 + 2/\Lambda} \tag{3.9}$$

For the foil dimensions selected in this study, the aspect ratio is on the border of being high enough to utilize Prandtl's lifting line theory. However, Søding presented a modification of Prandtl's lifting line theory giving improved predictions for low aspect ratio wings and agreeing better with 3D-results, which is presented in Equation 3.10. This is the equation used for the lift coefficient in this study.

$$C_L = \frac{\Lambda(\Lambda + 1)}{(\Lambda + 2)^2} 2\pi\alpha \tag{3.10}$$

3.3.2 Drag coefficient

When a 2D foil in steady flow in an infinite and incompressible fluid is considered, D'Alambert's paradox states that no drag forces will be induced, Faltinsen (2006). However, in reality, a drag force is induced as flow moves past a foil due to viscous effects. The drag coefficient C_D is, like the lift coefficient, a function of the angle of attack, and

also a function of the Reynold number. This is shown in Figure 3.6 which shows C_D from a NACA 0012-foil for different Reynolds numbers.

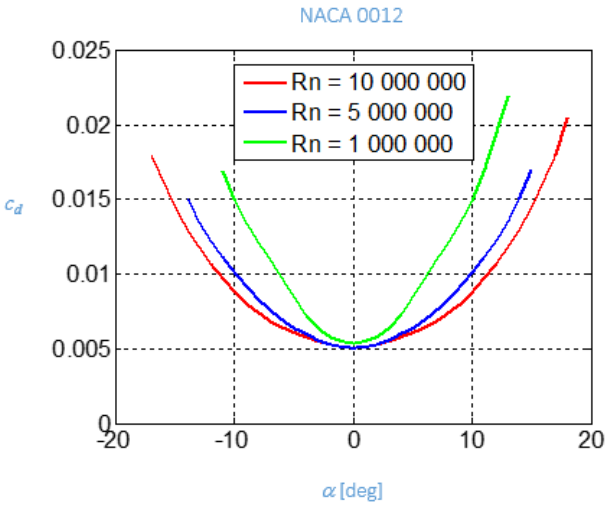

Figure 3.6: Drag coefficient as a function of Rn, from Faltinsen (2006)

From Figure 3.6, it can be seen that the drag coefficient has a bucket shape with a minimum for α=0 degrees. The resulting drag force depends on the viscous resistance, which depends on the pressure distribution, which again depends on the angle of attack. The viscous resistance corresponds to the lift force in the sense that the dominant contribution to the lift force is the pressure difference between the suction and pressure side of the foil, where the viscous boundary layer flow affects the pressure distribution. When the aspect ratio is large, the viscous drag force can be obtained by using strip theory where the foil geometry is divided into strips, and two-dimensional flow is assumed. The mathematical expression for the total drag force coefficient, Equation 3.11, is then composed of two parts: the viscous resistance found on a 2D foils $C_{D,v}$ and the lift induced contribution $C_{D,i}$. Equation 3.11 and 3.12 are implemented in the seakeeping solver for the drag coefficients.

$$C_D = C_{D,v} + C_{D,i} \tag{3.11}$$

$$C_{D,v} = 2C_F \left[1 + 2\left(\frac{t}{c}\right) + 60\left(\frac{t}{c}\right)^4\right] \qquad C_{D,i} = \frac{4\pi\alpha^2\Lambda}{(\Lambda+2)^2} \tag{3.12}$$

t = foil thickness, c = foil chord

The lift induced contribution $C_{D,i}$ occurs due to the trailing vortex sheet, where the strongest effect is caused by tip vortices and is a 3D effect that increases in importance

with decreasing aspect ratio. Winglets, which are the upward facing fins positioned at the edge of a foil, are frequently used to force the flow to become more two-dimensional and therefore used the lift-induced drag. Due to complexity, winglets are not included in this study.

One assumption made in Equation 3.11 is that both the thickness of the boundary layer and the free shear layer is zero. Therefore, it is approximated that the pressure is constant throughout the boundary layer, which in most cases is an adequate approximation according to Faltinsen (2006). Another assumption made is that the induced drag can be calculated by potential theory. Because the vorticity occurring in the boundary layer is convected downstream and remains in a thin free shear layer without much diffusion, this assumption is assumed to be valid.

The friction coefficient C_F is given by the International Towing Tank Conference (ITTC) 1975 for a smooth surface in turbulent flow as Equation 3.13 with $Rn = \frac{UL}{\nu}$. This equation has been proven to coincide with experimental results for turbulent flow along a smooth plate, Faltinsen (2006).

$$C_F = \frac{0.075}{(log_{10}Rn - 2)^2} \tag{3.13}$$

In a real flow, if flow separation occurs, the effective surface of the foil S is reduced. This phenomenon is known as drag due to the loss of leading-edge suction. This is not taken into account in this study as the maximum angle of attack is restricted not to exceed the critical angle of attack.

3.4 Flap

For the controlling aspect, flaps can be incorporated into the foils. The flaps are in this study selected to be placed at $\frac{3}{4}$ of the chord length. General guidelines from Faltinsen (2006) were used as inspiration for this decision in combination with Figure 3.7 which shows the comparison between ratio r of the flap length and chord length and the corresponding efficiency for exact and asymptotic results. The asymptotic formula is for small r and is given by Equation 3.14.

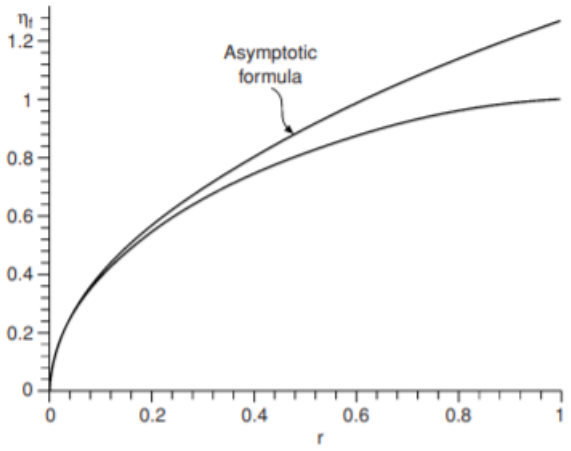

Figure 3.7: Foil efficiency as a function of flap length, from Faltinsen (2006)

The lift due to the flap can be computed from Equation 3.14 where rc is the length of the flap and α_f is the angle of the flap from the center line of the foil. From Figure 3.7 it can be seen that there is little difference between the exact computation and the asymptotic formula when the flap length is selected to be $rc = 0.25c$, which justifies the usage of the equations below.

$$L \approx 4\rho U^2 c r^{1/2} \alpha_f \tag{3.14}$$

c = chord length including flap, rc = flap length

The total lift force from the foil with flap can be calculated using the superposition principle as shown in 3.15.

$$L_{tot} = L_{foil} + L_{flap} \tag{3.15}$$

The foil efficiency can be calculated by Equation 3.16. This equation describes the capability of the foil to produce lift in contrary to a flat plate. The presented equation is valid for the asymptotic formula for small r, which is, as described, assumed to be satisfactory for r=0.25. This gives a foil efficiency of η_f=0.64. In other words, a flap with r=0.25 is quite effective for generating lift.

$$\eta_f = \frac{4}{\pi} r^{1/2} \tag{3.16}$$

For calculating the added drag due to the flap, Equation 3.11 for the drag coefficient can be altered to include the effect of a flap by substituting α with $\alpha_{flap\_effective}$ as shown in Equation 3.17, and other geometry-dependent parameters with parameters for the flap. This approach assumes that Equation 3.17 does not vary along the foil span.

$$\alpha_{flap\_effective} = \alpha_{foil} + \alpha_{flap} \tag{3.17}$$

3.5 Quasi-steady approximation

Deciding whether the quasi-steady approximation could be used was necessary with regards to validating the usage of the foil load equations. If quasi-steady conditions can be used, the linear unsteady loads from one foil can be expressed as in Section 3.2. What should be noted is that the quasi-steady approach does not include the steady lift forces that balance the vessel weight and cause zero pitch moment about the center of gravity. Whether quasi-steady conditions can be used can be decided by computing the reduced frequency k defined as in Equation 3.18.

$$k = \frac{\omega_e c}{2U} \tag{3.18}$$

ω_e=Encounter frequency, c=Foil chord, U=Vessel speed

For a quasi-steady analysis, the results correspond to k=0, which corresponds to ω_e=0. k is dependent on environmental conditions. T ranging between 4 s and 16 s were assumed relevant for the vessel, and this range is therefore evaluated. Relevant k are presented in Table 3.1. β is the angle of the incoming waves, which is head sea (β=0) in these calculations.

$$\omega_e = \omega + k_w U cos\beta \qquad k_w = \frac{\omega^2}{g} \tag{3.19}$$

$$\omega_e = \frac{2\pi}{T} + (\frac{2\pi}{T})^2 \frac{1}{g} U cos\beta \tag{3.20}$$

Fn	U [kn]	T [s]	ω [1/s]	ω_e [1/s]	k
0.934	35	4	1.57	6.09	0.15
0.934	35	6	1.57	3.05	0.07
0.934	35	16	0.39	0.67	0.017
0.5	19	4	1.57	4.02	0.19
0.5	19	6	1.57	2.13	0.10
0.5	19	16	0.39	0.54	0.014

Table 3.1: k-values for quasi-steady approximation

$|k|$ can be seen to be close to zero in the operational environmental conditions of interest, and below 0.1 in the most occurring sea states, which are discussed in Section 6.2. When

k can be assumed to be very small, $\frac{b_{33}^L}{\pi\rho U c} \approx 1$. Therefore, the quasi-steady state is assumed to be satisfactory for this study.

3.6 Foil-lift damping

For the high-speed catamaran in the study, there will be four major sources of damping:

- Wave radiation damping
- Viscous damping
- Hull-lift damping
- Foil-lift damping

The foil-lift damping is the damping provided by the T-foils due to the foil-lift in heave, roll, and pitch. This damping effect increases linearly with the speed of the vessel, and is of importance for high-speed catamarans. The size of the damping is dependent on the geometry of the foil and is, when using quasi-steady approximation, proportional to the lift.

For the approximation of the foil lift damping, it is assumed that the flow is two-dimensional and that there are no effects from boundaries as for instance free-surface effects. This implies that ventilation and cavitation are not taken into account. This is discussed further in Section 3.7. A thin, heaving foil without camber moving with forward speed U is considered. $-\frac{d\eta_3}{dt}$ is the orthogonal component of the incident flow velocity U where η_3 is the heave motion of the foil. The ambient flow velocity can then be expressed as Equation 3.21

$$V = \left(U^2 + \left(\frac{d\eta_3}{dt} \right)^2 \right)^{0.5} \approx U \tag{3.21}$$

The instantaneous angle of attack relative to the foil can then be expressed as Equation 3.22.

$$\alpha = -\frac{d\eta_3}{dt} U \tag{3.22}$$

As mentioned, Equation 3.5 for the foil lift can be used when the quasi-steady approach is assumed. Then, a 2D vertical force can be found. From this equation, the damping coefficient can be found when the expression is used in the equation of motion. b_{33} is then the two-dimensional damping coefficient in heave due to a harmonically heaving

uncambered thin foil in an infinite fluid. b_{33}^L can be decided by Figure 3.8 and Equation 3.23.

$$L = -\rho U c \pi \frac{d\eta_3}{dt}, \qquad b_{33}^L = \rho U c \pi \tag{3.23}$$

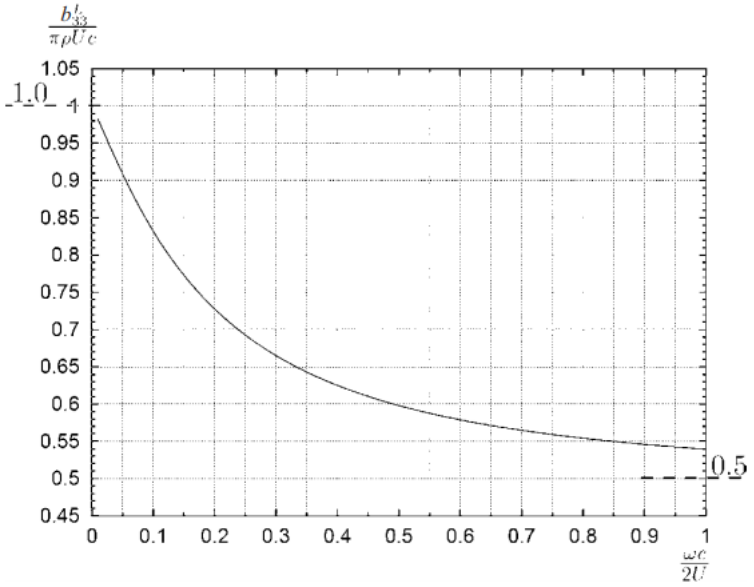

Figure 3.8: Two dimensional damping coefficient b_{33}^L, from Faltinsen (2006)

The heave damping can be generalized to other modes of motion and other orientations of the lifting surface. For instance, can pitch damping be expressed by using the expression for the local vertical motion of the foil $\eta_3 - x_F\eta_5$. Here, x_F is the average x-coordinate of the foil relative to the center of gravity of the vessel.

3.7 Simplifications and assumptions

In this section, phenomena and effects that are not included are discussed. The possible influences of the effects are viewed, and the validity of excluding the phenomena is addressed.

3.7.1 Foil interaction

As the foil configuration assessed in this study includes foils positioned both at the bow and stern, interference effects may occur in reality. Downstream of the foils at the bow,

vorticity will occur, which may influence the incoming stream, and therefore also the lift and drag forces and moments of the aft foil system. Interference resistance may also occur due to vortices generated when boundary layers of different thickness meet.

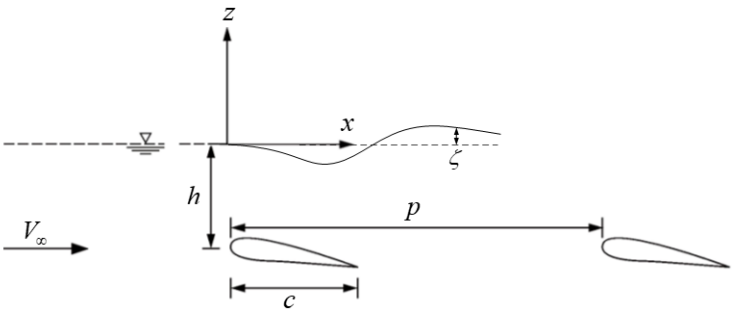

Figure 3.9: Vizualization of interference between fore and aft foil system

The effect of the transverse waves generated by the upstream foil can be evaluated by Equation 3.24 as a function of the angle of attack α_i.

$$\alpha_i = \frac{\partial\phi/\partial z|_{z=-h}}{V_\infty} = -C_L Fn^{-2} e^{-2Fn_h^{-2}} cos\left(\frac{p}{c} Fn^{-2}\right) \tag{3.24}$$

$$Fn = \frac{U}{\sqrt{gc}} \qquad Fn_h = \frac{U}{\sqrt{gh}} \tag{3.25}$$

C_L=Lift coefficient, Fn=Froude number, Fn_h=Submergence froude number, p=Distance between foils, c=Foil chord

The resulting lift on the downstream foil C_{F_2} can then be computed by Equation 3.26.

$$C_{F_2} = C_L + 2\pi\alpha_i \tag{3.26}$$

For the foil system selected in this study, the value of α_i is computed to be $-C_L \times 0.015$. Accordingly, not taking the interference effects between the fore and aft foil system is assumed to be acceptable in this study.

3.7.2 Free surface effects

The presence of the free surface may lead to several phenomena effecting the efficiency of the foil. A thin, flat, two-dimensional foil at submergence h below the mean free surface is considered. Steady flow and infinite depth is assumed. The lift force due to the presence of the foil is dependent on the circulation Γ which is influenced by the presence

of the free surface. The lift coefficient C_L increases with increasing h/c-ratio where h is the submergence and c is the chord length, so generally the presence of free surface results in loss of lift. A contradicting effect occurs when the submergence Froude number, defined as Equation 3.27, is very small. Then, the free surface acts like a wall, and the lift coefficient increases as the distance to the surface decreases. This effect is known as the wing-in-ground (WIG) effect and can be calculated from Equation 3.28. The lift when $Fn_h > 10\sqrt{h/c}$ can be found from Equation 3.29. Figure 3.11 depicts these phenomena.

$$Fn_h = \frac{V_\infty}{\sqrt{gh}} \tag{3.27}$$

$$Fn_h \to 0: \quad C_L(\frac{h}{c}) = C_L(\frac{h}{c} = \infty)\left[1 + \frac{1}{16}(\frac{c}{h})^2\right] \tag{3.28}$$

$$Fn_h > \frac{10}{\sqrt{h/c}}: \quad C_L(\frac{h}{c}) = C_L(\frac{h}{c} = \infty)\left[\frac{1 + 16(h/c)^2}{2 + 16(h/c)^2}\right] \tag{3.29}$$

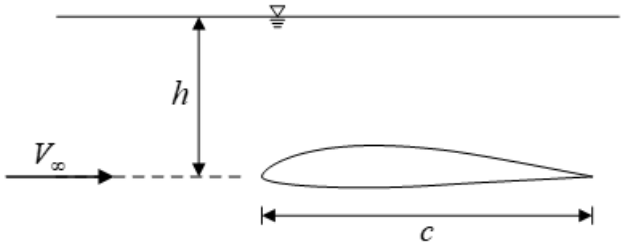

Figure 3.10: Uncambered 2D foil in steady flow, from Faltinsen (2006)

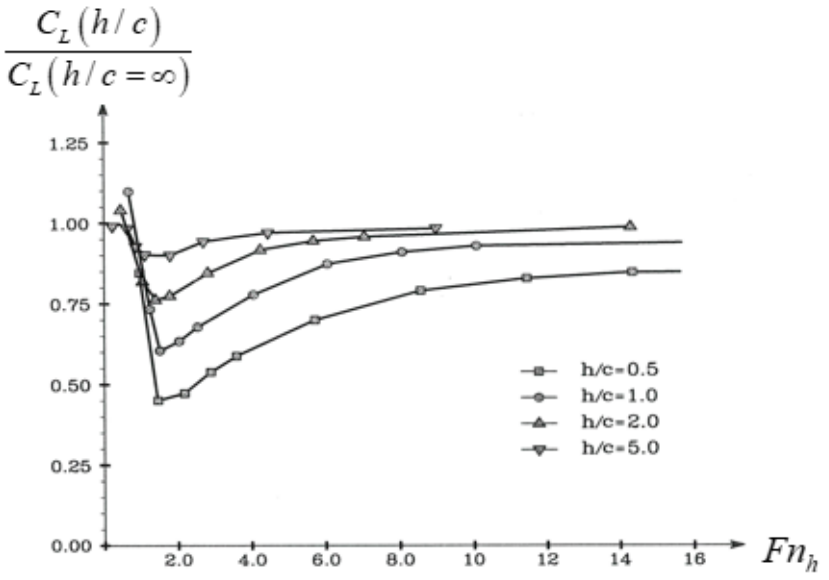

Figure 3.11: Free-surface effects for uncambered 2D foil at constant α, from Faltinsen (2006)

The submergence Froude number Fn_h is an important parameter when discussing the free surface effects. In this study, the submergence Froude number for the foils is found to be Fn_h=3.11 and the h/c-ratio to be 3.6. From Figure 3.11 it can be seen that this gives a reduction of the lift of less than 10%, which is considered to be quite little. For the catamaran and the case studied $\frac{10}{\sqrt{h/c}} = 5.25 > Fn_h$, which does not fall within the limits for Equation 3.29. For this limit to satisfied, the following would have to be fulfilled:

$$\frac{U}{\sqrt{gh}} > \frac{10}{\sqrt{h/c}} \quad \longrightarrow \quad \frac{U}{\sqrt{c}} > 10\sqrt{g} = 31.3 \quad \longrightarrow \quad c \approx 0.3 \quad or \quad U > 58kn \tag{3.30}$$

Neither fulfilling the chord length or the velocity, or another combination of the two, are considered realistic options for the catamaran viewed in this study. Nevertheless, as using the selected foil values only results in less than 10% loss of lift, neglecting the free surface effects is assumed to not give a too large deviance as it is the conceptual effect of foils that is the focus of this thesis and not the exact numerical results. However, in further studies, including the free surface effects would lead to more realistic results, and should be considered.

Due to the lift force being dependent on the circulation, an additional resistance can also occur. This resistance can be divided into two components resulting from a thickness and a lifting problem. The wave resistance due to lift can be found from Equation 3.31. $C_{DW\Gamma}$ is the drag coefficient due to circulation, and C_L is the lift coefficient $C_L = \frac{\Gamma^2}{0.25U^2c^2}$.

$$\frac{C_{DW\Gamma}}{C_L^2} = \frac{1}{2}\frac{1}{Fn_h^2}\left(\frac{c}{h}\right) exp\left(\frac{-2}{Fn_h^2}\right) \tag{3.31}$$

The thickness resistance component R_{WS} can be found from Equation 3.32. J_1 is the Bessel function of the first kind.

$$\frac{R_{WS}}{\rho g t^2} = \pi^2 \frac{c+t}{c-t} exp\left(\frac{-2}{Fn_h^2}\right) J_1^2\left(\frac{c}{2h}\frac{1}{Fn_h^2}\sqrt{1-\left(\frac{t}{c}\right)^2}\right) \tag{3.32}$$

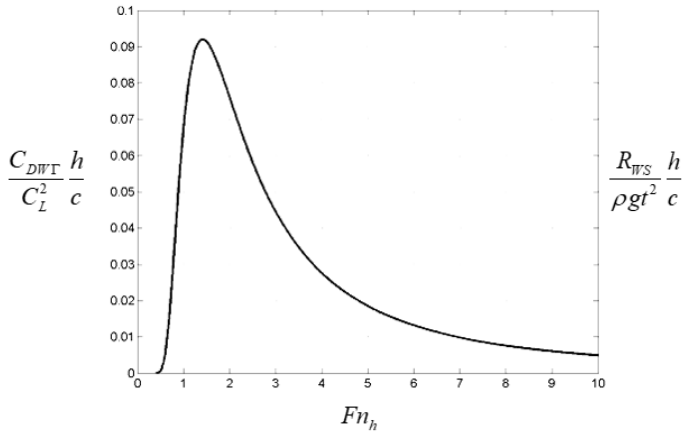

Figure 3.12: Wave resistance due to lift effects, from Faltinsen (2006)

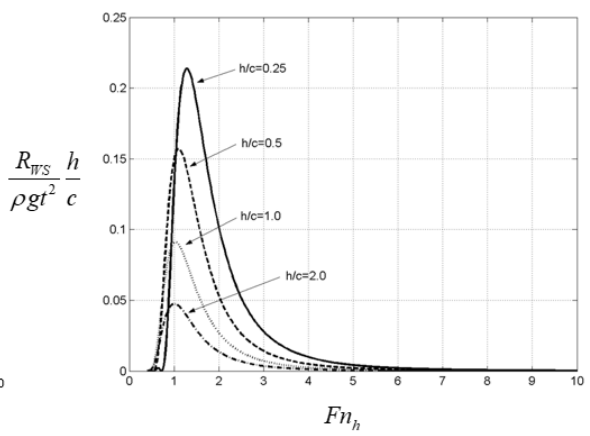

Figure 3.13: Wave resistance due to thickness effects, from Faltinsen (2006)

From Figure 3.13 it can be seen that for the relevant submergence Froude number $Fn_h = 3.11$, the wave resistance due to thickness effects is very low. The importance of the resistance due to thickness effects has also been quantified by Faltinsen (2006) by comparison with the viscous resistance. It was found that the resistance due to the thickness effect was small, and that not accounting for this resistance is assumed to be satisfactory in most cases. Figure 3.12 shows that the wave resistance for the relevant submergence Froude number is also seen to be very small. Hence, not accounting for the added resistance components due to the free surface is assumed satisfactory.

3.7.3 Cavitation

Cavitation is an effect which leads to unsteady, or a loss of, lift. The risk of cavitation is dependent on the speed of the craft. The risk depends on the ambient pressure at the position of the foil; as the pressure is increased, the risk of cavitation is decreased.

For vessels operating at speeds of 40-50 knots and up, the risk of cavitation is difficult to avoid. The vessel in this study operates at speeds a little lower than this, and the foil system used is fully submerged, which is an advantage regarding cavitation. For the vessel in this thesis, the effect of cavitation is not viewed, but the risk should be assessed in further studies.

3.7.4 Ventilation

Ventilation is an effect where air enters from the atmosphere at low-pressure areas on the strut, which results in a significant drop in lift. This effect is dependent on the Froude number, flow separation from the leading-edge area, cavitation and the trailing vortex developed at the lower strut tip. As the foil system is located below the submerged hull, ventilation is not assumed a likely risk in this study, and effects are not included.

3.7.5 Effect of strut

The foils in the study will, in reality, be connected to struts, connecting the foils to the vessel in a foil-strut system. However, the effect of the struts is not accounted for in the simulations. In this study, struts without lifting effects are considered as a relevant concept, as the struts are assumed only to have connection purposes, and therefore to be symmetric around the z-axis with no yaw. In addition to ventilation, the struts may experience steady free-surface effects, which may cause a significant drop in the lift of the foil. This drop in lift depends on the yaw-angle of the strut, and should, if relevant, be considered in further studies.

One relevant issue not accounted for due to the struts is the added resistance. The resistance caused by the struts will consist mainly of friction, and the friction coefficient can be calculated similarly to the friction coefficient of the foils, using Equation 3.13.

Chapter 4

Mathematical model

The purpose of this chapter is to give insight into the theory the numerical models used in the thesis are based on. Understanding the theory behind the mathematical model is necessary for understanding how the problem is solved and for providing a basis for addressing simplifications and assumptions.

In this thesis, traditional hydrodynamic theory is united with control theory. Usually, hydrodynamic equations are described with one set of coordinate systems, while control theory traditionally is described with another set of systems. This can, for instance, be seen clearly in the works of Faltinsen (2006), where the hydrodynamic system is used, and in the works of Fossen (2011), which focuses on control theory. The different systems also result in different ways of expressing the equations of motion. *Waqum*, the program where the foil motion control part was implemented, is written according to the control theory system, whereas the foil loads to be implemented were expressed according to hydrodynamic theory. Therefore, caution had to be taken when implementing the hydrodynamic equations in *Waqum*.

In this chapter, the equation of motion expressed in the traditional hydrodynamic way is presented, and the equation of motion used in both *Wasim* and *Waqum* are described. In addition, a study was executed comparing the foil loads computed with hydrodynamic equations and *Waqum* equations.

4.1 Hydrodynamic mathematical model

4.1.1 The potential flow problem

The theory discussed in this section presents the theory behind the software *Wasim*, and is based on DNV GL (2014a). As mentioned in Section 2.3, *Wasim* bases its computations on a potential flow solver where first order potential theory is used. According to potential theory, water is assumed to be irrotational and incompressible at all times. In addition, according to the regular wave theory, waves are assumed to be linear, including the waves on the free surface. Therefore, nonlinear effects occurring from, for instance, breaking or steep waves are not accounted for.

An initial boundary value problem is used to describe the physics of the problem. The boundary conditions used in the initial boundary value problem are the kinematic and dynamic free surface conditions. The kinematic equation requires the motion on the free surface to be preserved in the sense that a fluid particle on the surface must remain at the surface at all times. For the dynamic boundary condition, it is required that the pressure on the surface is constantly equal to the atmospheric pressure. When z is zero or less, this holds to be true. When z is larger than 0, however, the pressure becomes greater than the atmospheric pressure. This error increases in significance with increasing wave height. However, the effects of the errors occurring because linear potential theory is used are assumed to be negligible, and a potential flow solver is assumed to give satisfactory results for the cause.

In the potential flow solver used, submerged, linear wave sources are used in the computation. The initial boundary value problem for the resulting velocity potential of a submerged linear wave source moving with constant speed is given in Equation 4.1. The depth is d=-z, the forward speed is U, and the direction of the movement is along the x-axis. $\sigma(t)$ is the time-varying strength of the source and η is the free surface elevation. Equation 4.2 presents the initial condition, and Equation 4.3 and 4.4 presents the dynamic and kinematic boundary conditions, respectively.

$$\phi(\vec{x},t) - \int\int_F \frac{\partial\phi}{\partial z}(\vec{\xi},t)G(\vec{x}-\vec{\xi})d\xi = \sigma(t)R(\vec{x}) \tag{4.1}$$

$$\phi(\vec{x},0) = \eta(\vec{x},0) = 0 \tag{4.2}$$

$$\frac{\partial\phi}{\partial t} + U\frac{\partial\phi}{\partial x} = -g\eta \tag{4.3}$$

$$\frac{\partial\eta}{\partial t} + U\frac{\partial\eta}{\partial x} = -\frac{\partial\phi}{\partial z} \tag{4.4}$$

$$R(x,y) = \frac{1}{2\pi\sqrt{x^2+y^2+z^2}} \tag{4.5}$$

$G(\vec{x}-\vec{\xi})$ refers to the Green's function, which is used in most potential flow solvers. The Green's function generally satisfies the free surface boundary conditions. In *Wasim*, however, the Green's function used as a simple Rankine source $\frac{1}{r}$ which does not satisfy the boundary conditions, so additional boundary conditions are necessary. The ship hull is modeled as a sum of Rankine sources where the vessel is built up by plane panels where each panel is assigned a Rankine source. The unknowns in the problem are ϕ, $\frac{\partial\phi}{\partial z}$ and η modelled using quadratic splines, shown in Equation 4.6 and 4.7. $a_j(t)$, $b_j(t)$ and $c_j(t)$ are unknowns, and $B_j(x,y)$ is known.

$$\phi(x,y,t) = \Sigma_{j=1}^{N} a_j(t)B_j(x,y) \qquad \frac{\partial\phi}{\partial t}(x,y,t) = \Sigma_{j=1}^{N} b_j(t)B_j(x,y) \tag{4.6}$$

$$\eta(x,y,t) = \Sigma_{j=1}^{N} c_j(t)B_j(x,y) \tag{4.7}$$

The procedure used to solve the initial boundary value problem iteratively is as follows:

- ϕ_n is found on the hull from the equation of motion.
- η is found from the kinematic free surface condition
- ϕ is found on the free surface from the dynamic free boundary condition
- ϕ is found on the hull and ϕ_n on the free surface with Green's theorem and Laplace.

The equation of motion can be expressed as $M\ddot{y} = F(\ddot{y}, \dot{y}, y, t)$ where y is the position vector, M is the mass matrix of the ship, and F are the external forces. The equation of motion studied here is described in further detail in Section 4.1.4. For the calculation of ϕ_n^{n+1} on the hull, 4^{th}-order Runge Kutta is used for the four first time steps. Then the twice as fast Adam-Bashfourth-Moulton scheme is used.

The Explicit Euler-scheme is used to find η from the kinematic free surface boundary condition:

$$\frac{1}{\Delta t}\left(\eta^{n+1} - \eta^n\right) = \left(\frac{\partial\phi}{\partial z}\right) - \left(U - \frac{\partial\eta}{\partial x}\right)^n \tag{4.8}$$

The Implicit Euler-scheme is used to find ϕ from the dynamic free surface condition:

$$\frac{1}{\Delta t}\left(\phi^{n+1} - \eta^n\right) = -g\eta^{n+1} - \left(-U\frac{\partial\phi}{\partial x}\right)^{n+1} \tag{4.9}$$

ϕ is found on the hull and ϕ_n on the free surface with the use of the integral equation:

$$2\pi\phi + \int_{S_B} \phi \frac{\partial G}{\partial n} + \int_{S_F} \phi_n G = \int_{S_B} \phi_n G + \int_{S_F} \phi \frac{\partial G}{\partial n} \tag{4.10}$$

When evaluated on the hull, ϕ is the unknown, while when evaluated on the surface, ϕ_n is unknown. The solution can be expressed on the form $\boldsymbol{Lx} = \boldsymbol{R}$ where $\boldsymbol{L}$ is related to the Green's function and is pre-computed by *Wasim*, $\boldsymbol{x}$ represents the unknowns $a_j(t)$ and $b_j(t)$, and $\boldsymbol{R}$ contains ϕ and ϕ_n.
In the computation, the superposition principle is used on the potential ϕ to obtain a stable solution. Each contribution contains different effects.

$$\phi = \phi_B + \phi_I + \phi_m + \phi_l \tag{4.11}$$

- ϕ_B is the base flow accounting for the presence of the hull. Only the hull below the waterline is taken into consideration. In *Wasim*, the hull is fixed relative to surface elevation.
- ϕ_I is the incident wave potential representing the incoming sinusoidal wave.
- ϕ_m is the memory flow and describes the wave reflection due to the hull.
- ϕ_l is the local flow satisfying the boundary conditions on the hull. The response of the ship is represented.

At the end of the mesh, a numerical wave absorbing layer called a beach is implemented to damp the wave motions. This is implemented by altering the kinematic boundary condition, as shown in Equation 4.12. ρ is the radial distance from the source, and ρ_0 is the inner limit of the beach.

$$\frac{\partial \eta}{\partial t} + U\frac{\partial \eta}{\partial x} = \frac{\partial \phi}{\partial z} - 2\nu\eta + \frac{\nu^2}{g}, \phi \qquad \nu(\rho) = 3\frac{C_s}{C_W^3}(\rho - \rho_0)^2 \tag{4.12}$$

4.1.2 Definition of waves

In this section, the theory of how the waves are modeled in *Wasim* is presented. The theory is taken from DNV GL (2014a).

In *Wasim*, the incoming wave ζ is defined as a sum of harmonic waves as in Equation 4.13, or in complex form as Equation 4.14.

$$\zeta(x,y,t) = \sum_{i=1}^{I}\sum_{j=1}^{J} \zeta_{A_{ij}} cos[(k_i cos\beta_j)x + (k_i sin\beta_j)y - \omega_i t + \gamma_{ij}] \tag{4.13}$$

$$\zeta(x,y,t) = \sum_{i=1}^{I}\sum_{j=1}^{J} \zeta_{A_{ij}} exp[i(k_i cos\beta_j)x + (k_i sin\beta_j)y - \omega_i t + \gamma_{ij}] \tag{4.14}$$

k_i is the wave number defined by the dispersion relation for infinite water depths as equation 4.15, ω_i is the circular frequency, and g is the gravitational acceleration.

$$k = \frac{\omega^2}{g} \tag{4.15}$$

$\zeta_{A_{ij}}$ are the wave amplitudes, and γ_{ij} are the phase angles. β_j are the wave directions defined as the angle between the positive x-axis and the direction the wave is propagating towards. As a result, head sea is defined as 180° whereas 90° is beam seas with port side as the lee side.

The wave elevation in Equation 4.13 and 4.14 describes short-crested irregular waves. The irregularity is due to the various amplitudes, frequencies, wave numbers, and phase angles. The wave is short-crested as it propagates in both x- and y-direction. For the waves to be represented in the frequency domain, the connection between the wave spectrum $S(\omega_j)$ and the wave amplitude in Equation 4.16 can be used.

$$\frac{1}{2}\zeta^2 = S(\omega_j)\Delta\omega \tag{4.16}$$

For short-crested seas, the wave spectrum is two-dimensional and a function of both ω and θ. In this equation, a frequency dependent wave spectrum is combined with a unidirectional distribution to form a two-dimensional spectrum, Faltinsen (1990).

$$S(\omega,\theta) = S(\omega)f(\theta) \tag{4.17}$$

This results in expression 4.18 for the incoming wave.

$$\zeta(x,y,t) = \sum_{i=1}^{I}\sum_{j=1}^{J} \sqrt{2S(\omega_i\theta_j)\Delta\omega\Delta\theta} cos[(k_i cos\beta_j)x + (k_i sin\beta_j)y - \omega_i t + \gamma_{ij}] \tag{4.18}$$

4.1.3 Wave response

When in the frequency domain, the wave responses are given as transfer functions, which are defined as the relation between the input and output signal. The incoming wave at the origin of the global coordinate system is the input signal, and the output signal is the response. T is the ratio between the response amplitude and the wave amplitude. δ is the phase lag.

- Input signal: $Acos(\gamma - \omega t)$
- Output signal: $ATcos(\gamma - \omega t - \delta)$

When the phase lag is positive, the response peak occurs after the wave peak. Figure 4.1 depicts this.

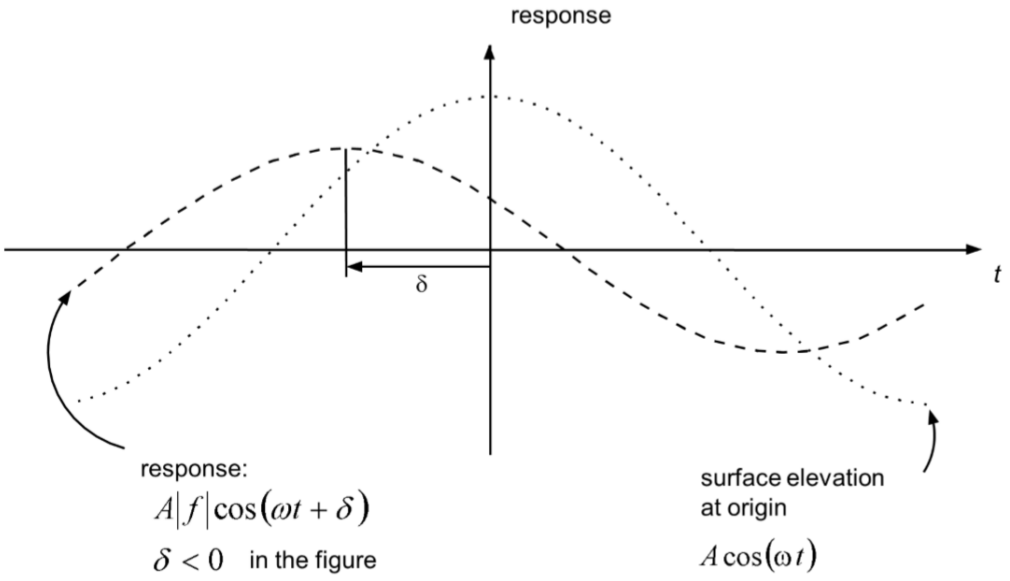

Figure 4.1: Definition of phase lag for wave responses, from DNV GL (2014a)

4.1.4 Hydrodynamic equation of motion

For a large-volume body in regular waves, it is hypothesized that the motions of the body are linear with respect to an incident wave. This has been proven to be a reasonable assumption, Ogilvie (1964). Therefore, the superposition principle can be used so that the responses initiated from multiple waves can be added together to obtain the total response of a vessel in waves. The rigid body motions with respect to the body-fixed coordinate system are shown in Figure 4.2.

Hydrodynamic problems are commonly divided into two sub-problems as defined by Faltinsen (1990):

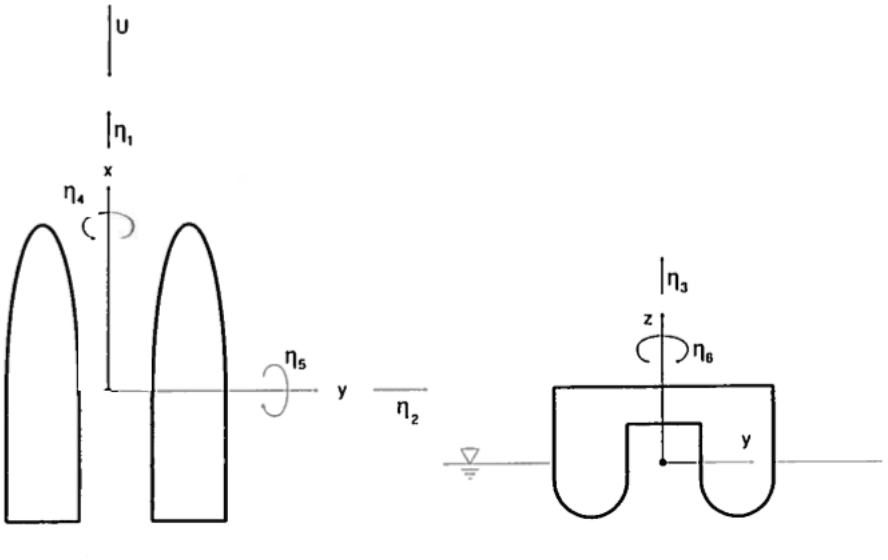

Figure 4.2: Rigid body motions of vessel

- **Excitational forces and loads** - The body is restrained from oscillating and exposed to incident regular waves. The hydrodynamic loads are composed of Froude-Krylov and diffraction forces and moments and are functions of the pressure distribution on the body.
- **Radiaton forces and loads** - The body is oscillated with the wave excitation frequency in calm water. No incident waves occur. The hydrodynamic loads are composed of the added mass, damping, and restoring terms.

The hydrodynamic problem can then be expressed by the equation of motion as Equation 4.19 with the solution given as Equation 4.20. These expressions are taken from DNV GL (2014b). Equation 4.20 is the linear motion transfer function, commonly referred to as response amplitude operators. The motion coefficients are unique for each case consisting of a vessel and an environment.

$$[M + A(\omega)]\ddot{x} + [B(\omega) + B_{if}]\dot{x} + Cx + G(\omega|\beta)x = F(\omega|\beta) \tag{4.19}$$

$$RAO(\omega|\beta) = \frac{x}{\zeta_a} = \frac{F_0(\omega|\beta)}{C - (M + A(\omega))\omega^2 + iB(\omega)\omega + G(\omega)} \tag{4.20}$$

ω = Wave frequency

β = Wave direction/ship heading

$$\zeta_a = \text{Incident wave amplitude}$$

$$x = x = x(\omega|\beta) = (A_r + A_i)\zeta_a e^{i\omega t} = RAO(\omega|\beta)\zeta_a e^{i\omega t} = \text{Motion}$$

$$M = \text{Mass}$$

$$A(\omega) = \text{Frequency dependent added mass coefficient from potential theory}$$

$$B(\omega) = \text{Frequency dependent linear damping coefficient from potential theory}$$

$$B_{if} = \text{Frequency independent linear damping coefficient}$$

$$C = \text{Restoring coefficient}$$

$$F(\omega|\beta) = (F_{0r} + iF_{0i})\zeta_a e^{i\omega t} = \text{Complex Excitation force}$$

$$G(\omega|\beta) = \text{Complex general left side force coefficient}$$

$G(\omega|\beta)$ is used for establishing retardation functions to keep the frequency dependent added mass and damping coefficients pure with respect to linear potential theory.

Retardation functions

In the above chapter, the equation of motion and the excitation force are harmonic functions. A retardation function $h(t)$ can be used to find an expression for the equation of motion when the excitation force $f(t)$ is no longer harmonic as shown in Equation 4.21.

$$(M + A^\infty)\ddot{x} + B^\infty\dot{x} + Cx + \dot{x} \times h = f(t) \tag{4.21}$$

The frequency dependent coefficients from linear potential theory are included in $h(t)$, while the other frequency dependent coefficients are in included in the excitation force $f(t)$ through $G(\omega)$.

$$f_G(t) = -G(\omega)x(\omega) \tag{4.22}$$

The retardation functions are given as Equation 4.23, and the added mass and damping are divided as in Equation 4.24.

$$h(t) = \frac{2}{\pi} = \int_0^\infty b(\omega)cos\omega t d\omega \qquad h(t) = -\frac{2}{\pi} = \int_0^\infty \omega a(\omega)sin\omega t d\omega \tag{4.23}$$

$$A(\omega) = a(\omega) + A^\infty \qquad B(\omega) = b(\omega) + B^\infty \tag{4.24}$$

4.1.5 Rigid body motions

The rigid body motions of the vessel are coupled and can be transformed from one motion reference point to another. s_i is the translational movement along axis i. When the body experiences accelerations, the gravity term given in the parenthesis should be included.

$$s_x = \eta_1 + z\eta_5 - y\eta_6(-g\eta_5) \tag{4.25}$$

$$s_y = \eta_2 - z\eta_4 + x\eta_6(+g\eta_4) \tag{4.26}$$

$$s_z = \eta_3 + y\eta_4 - x\eta_5 \tag{4.27}$$

4.2 Coordinate systems

In addition to the equations of motion being expressed differently in hydrodynamic and control theory, the software *Wasim* and *Waqum* use a number of coordinate systems for the simulations. To describe the work, four coordinate systems S1, S2, S3, and S4 will be presented. These coordinate systems are all right-handed coordinate systems.

- S_1 **-** Earth-fixed coordinate system (x_1, y_1, z_1). This system is defined relative to the Earth's reference ellipsoid, which means it is defined as the tangent plane to the Earth surface moving with the vessel, World Geodetic System (1984). x_1 points true north, y_1 points east, and z_1 is downwards normal to the earth's surface. The calm water surface is at z_1=0. This system is, for instance, used for describing the incident waves. This system will also be referred to as the $\{n\}$ or NED system.
- S_2 **-** Reference system (x_2, y_2, z_2) moving with the horizontal motions with the calm water surface at z_2=0. The rigid body motions of the vessel are defined relative to this system.
- S_3 **-** Body fixed coordinate system (x_3, y_3, z_3), fixed to the craft and with respect to the strain-free deformation of the body. This system is used for computation of the equations of motion. The system coincides with S2 when the motion state vector $\eta = \mathbf{0}$. This system will also be referred to as the $\{b\}$ or BODY system.
- S_4 **-** Body fixed coordinate system (x_4, y_4, z_4), fixed to the craft and with respect to the strain free deformation of the body. This coordinate system is used for the description of geometry when using *HydroD* and *Wasim*, for instance when creating the model geometry.

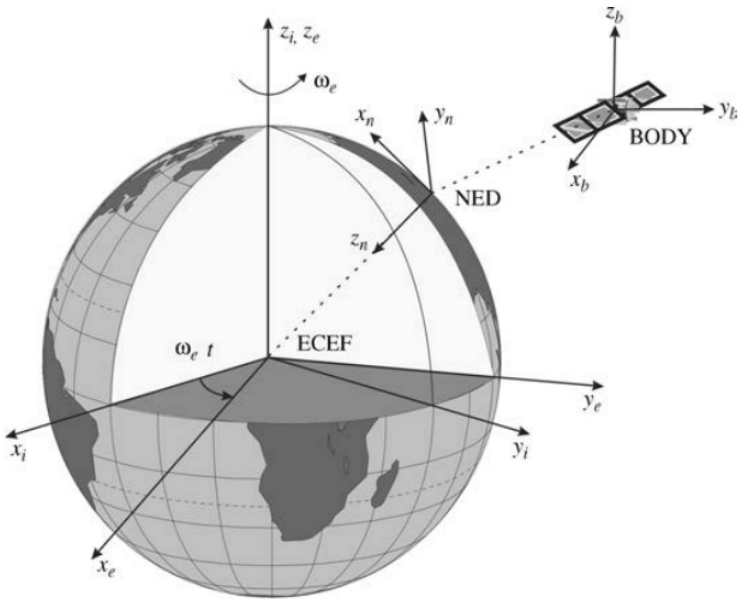

Figure 4.3: Coordinate systems visualized, from Fossen (2011). NED corresponds to S_1, BODY corresponds to S_3

4.3 Equataion of motion in Waqum

The following vectors and equations are used in *Waqum*, which is the same arrangement as the control theory system described in detail by Fossen (2011). The subscript nb means between the $\{n\}$ and $\{b\}$ coordinate system. The superscript means it is expressed in the respective coordinate system.

The position of the vessel is defined in S_1: $\mathbf{p^n} = \begin{bmatrix} x \\ y \\ z \end{bmatrix}$

The attitude, or Euler angles: $\boldsymbol{\theta_{nb}} = \begin{bmatrix} \phi \\ \theta \\ \psi \end{bmatrix}$

The body-fixed linear velocity is defined in S_3: $\boldsymbol{v^b} = \begin{bmatrix} u \\ v \\ w \end{bmatrix}$

The body-fixed angular velocity in S_3: $\boldsymbol{\omega^b_{nb}} = \begin{bmatrix} p \\ q \\ r \end{bmatrix}$

The following vectors can be used to describe the general equation of motion of a marine craft in six degrees of freedom using the following notations:

The position and Euler angels: $\boldsymbol{\eta} = \begin{bmatrix} \boldsymbol{p^n} \\ \boldsymbol{\theta_{nb}} \end{bmatrix}$

The linear and angular velocities: $\boldsymbol{\nu} = \begin{bmatrix} \boldsymbol{v^b} \\ \boldsymbol{\omega^b_{nb}} \end{bmatrix}$

The body fixed forces and moments: $\boldsymbol{\tau} = \begin{bmatrix} \boldsymbol{f^b_b} \\ \boldsymbol{m^b_b} \end{bmatrix} = \begin{bmatrix} \mathrm{X} \\ \mathrm{Y} \\ \mathrm{Z} \\ \mathrm{K} \\ \mathrm{M} \\ \mathrm{N} \end{bmatrix}$

Followingly, the relation between the velocity $\dot{\boldsymbol{\eta}}$ in S_1 and $\boldsymbol{\nu}$ in S_3 is given in Equation 4.28 and 4.29.

$$\dot{\boldsymbol{\eta}} = \boldsymbol{J}(\boldsymbol{\eta})\boldsymbol{\nu} \tag{4.28}$$

$$\begin{bmatrix} \boldsymbol{p^n} \\ \boldsymbol{\theta_{nb}} \end{bmatrix} = \begin{bmatrix} \boldsymbol{R^n_b}(\boldsymbol{\theta}) & \boldsymbol{0_{3x3}} \\ \boldsymbol{0_{3x3}} & \boldsymbol{T_\theta}(\boldsymbol{\theta}) \end{bmatrix} \begin{bmatrix} \boldsymbol{\nu^b_b} \\ \boldsymbol{\omega^b_b} \end{bmatrix} \tag{4.29}$$

$$\boldsymbol{R^n_b}(\boldsymbol{\theta}) = \begin{bmatrix} c\psi c\theta & -s\psi c\phi + c\psi s\theta s\phi & s\psi s\phi + c\psi c\phi s\theta \\ s\psi c\theta & c\psi c\phi + s\phi s\theta s\psi & -c\psi s\phi + s\theta s\psi c\phi \\ -s\theta & c\theta s\phi & c\theta c\phi \end{bmatrix} \quad \boldsymbol{T_\theta}(\boldsymbol{\theta}) = \begin{bmatrix} 1 & s\phi t\theta & c\phi t\theta \\ 0 & c\phi & -s\phi \\ 0 & s\phi/c\theta & c\phi/c\theta \end{bmatrix} \tag{4.30}$$

The non-linear equation of motion is then expressed in S_3 as Equation 4.31 including the rigid body dynamics expressed as Equation 4.32.

$$\boldsymbol{M}\dot{\boldsymbol{\nu}} + \boldsymbol{C}(\boldsymbol{\nu})\boldsymbol{\nu} + \boldsymbol{D}(\boldsymbol{\nu})\boldsymbol{\nu} + \boldsymbol{g}(\boldsymbol{\eta}) = \boldsymbol{\tau} \tag{4.31}$$

$$\boldsymbol{M_{RB}}\dot{\boldsymbol{\nu}} + \boldsymbol{C_{RB}}(\boldsymbol{\nu})\boldsymbol{\nu} = \boldsymbol{\tau_{RB}} \tag{4.32}$$

$\boldsymbol{M}$ is the mass matrix, $\boldsymbol{D}$ is the damping matrix, and $\boldsymbol{C}$ covers the centripetal effect $\omega \times r$ and the coriolis effect $\boldsymbol{\omega} \times \boldsymbol{\nu}$.

The relation between the acceleration in S_1 and S_3 can, through differentiation, be expressed as in Equation 4.33 or 4.34.

$$\ddot{\boldsymbol{\eta}} = \dot{\boldsymbol{J}}(\boldsymbol{\eta})\boldsymbol{\nu} + \boldsymbol{J}(\boldsymbol{\eta})\dot{\boldsymbol{\nu}} \tag{4.33}$$

$$\ddot{\boldsymbol{p}}^{\boldsymbol{n}} = \dot{\boldsymbol{R}}_{\boldsymbol{b}}^{\boldsymbol{n}}(\boldsymbol{\theta})\boldsymbol{\nu} + \boldsymbol{R}_{\boldsymbol{n}}^{\boldsymbol{n}}(\boldsymbol{\theta})\dot{\boldsymbol{\nu}} \qquad \ddot{\boldsymbol{\theta}} = \dot{\boldsymbol{T}}_{\boldsymbol{\theta}}(\boldsymbol{\theta})\boldsymbol{\omega} + \boldsymbol{T}_{\boldsymbol{\theta}}(\boldsymbol{\theta})\dot{\boldsymbol{\omega}} \tag{4.34}$$

4.4 Equation of motion in Wasim

Wasim shares the definition for both the positions and velocities in both S_1 and S_3 with *Waqum*. However, the accelerations are defined differently, as shown in Equation 4.35.

$$\ddot{\boldsymbol{p}}^{\boldsymbol{n}} = \boldsymbol{R}_{\boldsymbol{b}}^{\boldsymbol{n}}(\boldsymbol{\theta})\boldsymbol{a_3} \qquad \ddot{\boldsymbol{\theta}} = \dot{\boldsymbol{T}}_{\boldsymbol{\theta}}(\boldsymbol{\theta})\boldsymbol{\omega} + \boldsymbol{T}_{\boldsymbol{\theta}}(\boldsymbol{\theta})\dot{\boldsymbol{\omega}} \tag{4.35}$$

4.5 From Wasim to Waqum

When Equation 4.31 is written out according to the Waqum-notations, the three first components are shown in Equation 4.36. When Equation 4.31 is written out according to the Wasim-notations, the three first components are shown in Equation 4.37.

$$\begin{aligned} m[\dot{u} - vr + \omega q - x_g(q^2 + r^2) + y_g(pq - \dot{r}) + z_g(pr + \dot{q})] &= X_{waqum} \\ m[\dot{v} - \omega p + ur - y_g(r^2 + p^2) + z_g(qr - \dot{p}) + x_g(qp + \dot{r})] &= Y_{waqum} \\ m[\dot{\omega} - uq + vp - z_g(p^2 + q^2) + x_g(rp - \dot{q}) + y_g(rq + \dot{q})] &= Z_{waqum} \end{aligned} \tag{4.36}$$

$$\begin{aligned} m[a_1 - x_g(q^2 + r^2) + y_g(pq - \dot{r}) + z_g(pr + \dot{q})] &= X_{wasim} \\ m[a_2 - y_g(r^2 + p^2) + z_g(qr - \dot{p}) + x_g(qp + \dot{r})] &= Y_{wasim} \\ m[a_3 - z_g(p^2 + q^2) + x_g(rp - \dot{q}) + y_g(rq + \dot{q})] &= Z_{wasim} \end{aligned} \tag{4.37}$$

The terms with translational and angular speed $\boldsymbol{\omega} \times \boldsymbol{\nu}$ is the difference between these equations. However, the acceleration in the earth-fixed coordinate system has to be the same in both Waqum and Wasim. This can be achieved by setting the accelerations in Equation 4.34 and 4.35 equal to each other.

$$\begin{aligned} &\dot{\boldsymbol{R}}_{\boldsymbol{b}}^{\boldsymbol{n}}(\boldsymbol{\theta})\boldsymbol{\nu}^{\boldsymbol{b}} + \boldsymbol{R}_{\boldsymbol{b}}^{\boldsymbol{n}}(\boldsymbol{\theta})\dot{\boldsymbol{\nu}}^{\boldsymbol{b}} = \boldsymbol{R}_{\boldsymbol{b}}^{\boldsymbol{n}}(\boldsymbol{\theta})\boldsymbol{a_3} \\ &\dot{\boldsymbol{\nu}}^{\boldsymbol{b}} = \boldsymbol{R}_{\boldsymbol{b}}^{\boldsymbol{n-1}}(\boldsymbol{\theta})[\boldsymbol{R}_{\boldsymbol{b}}^{\boldsymbol{n}}[\boldsymbol{\theta})\boldsymbol{a_3} - \dot{\boldsymbol{R}}_{\boldsymbol{b}}^{\boldsymbol{n}}(\boldsymbol{\theta})\boldsymbol{\nu}^{\boldsymbol{b}} = \boldsymbol{a_3} - \boldsymbol{R}_{\boldsymbol{b}}^{\boldsymbol{n-1}}(\boldsymbol{\theta})\dot{\boldsymbol{R}}_{\boldsymbol{b}}^{\boldsymbol{n}}(\boldsymbol{\theta})\boldsymbol{\nu}^{\boldsymbol{b}} \end{aligned} \tag{4.38}$$

For any vector x, the following identity is valid:

$$\begin{aligned} \dot{\boldsymbol{R}}_{\boldsymbol{b}}^{\boldsymbol{n}}\boldsymbol{x} &= \boldsymbol{R}_{\boldsymbol{b}}^{\boldsymbol{n}}(\boldsymbol{\omega} \times \boldsymbol{x}) \\ \dot{\boldsymbol{R}}_{\boldsymbol{b}}^{\boldsymbol{n}} &= \boldsymbol{R}_{\boldsymbol{b}}^{\boldsymbol{n}}\boldsymbol{S}(\boldsymbol{\omega}) \end{aligned} \tag{4.39}$$

By inserting 4.39 into Equation 4.38, the relation in Equation 4.40 can be obtained.

$$\dot{\boldsymbol{\nu}}^{\boldsymbol{b}} = \boldsymbol{a_3} - \boldsymbol{\omega} \times \boldsymbol{\nu}^{\boldsymbol{b}} \tag{4.40}$$

Then, when Equation 4.38 is substituted into 4.37, the forces in *Wasim* and *Waqum* are equal.

$$\boldsymbol{F_{waqum}} = \boldsymbol{F_{wasim}} \tag{4.41}$$

Conclusively, the forces in *Wasim* and *Waqum* are found to be equal when the velocities in the body frame are defined relative to S_1, and are decomposed into S_3. This also holds for S_2 (for S_1).

4.6 Comparison of foil loads

As mentioned, hydrodynamic theory and control theory is traditionally expressed in different sets of coordinate systems. In this thesis, a study was executed comparing the foil loads computed by typical hydrodynamic equations, referred to as the Faltinsen method, and the loads calculated by using a control theoretic approach, referred to as the Fossen method. The results are presented in Section 9.2.

4.6.1 Fossen method

The foil loads according to the *Waqum*-system are implemented as follows below. The superscript defines the selected coordinate system, and the subscript the physical position. "earth" corresponds to S_1 and "body" to S_3. The 0-position denotes the motion reference point of the vessel.

The position of the foil in EARTH is found:

$$\boldsymbol{p}_{\boldsymbol{foil}}^{\boldsymbol{earth}} = \boldsymbol{p}_{\boldsymbol{0}}^{\boldsymbol{earth}} + \boldsymbol{R}(\boldsymbol{\theta}_{\boldsymbol{nb}}) \cdot \vec{\boldsymbol{r}}_{\boldsymbol{foil}} \tag{4.42}$$

$\vec{\boldsymbol{r}}_{\boldsymbol{foil}}$ is the vector from the motion reference point of the vessel to the quarter point of the foil. $\boldsymbol{R}(\boldsymbol{\theta}_{\boldsymbol{nb}})$ is defined in Equation 4.30.

The velocity of the foil in BODY is found:

$$\boldsymbol{v}_{\boldsymbol{foil}}^{\boldsymbol{body}} = \boldsymbol{H}(\vec{\boldsymbol{r}}_{\boldsymbol{foil}}) \cdot \boldsymbol{v_0} \tag{4.43}$$

$$\boldsymbol{H}(\boldsymbol{r}) = \begin{bmatrix} \boldsymbol{I_{3\times3}} & \boldsymbol{S^T(r)} \\ \boldsymbol{0_{3\times3}} & \boldsymbol{I_{3\times3}} \end{bmatrix} \qquad \boldsymbol{S(r)} = -\boldsymbol{S^T(r)} = \begin{bmatrix} 0 & -r_3 & r_2 \\ r_3 & 0 & -r_1 \\ -r_2 & r_1 & 0 \end{bmatrix} \tag{4.44}$$

The wave-particle velocity at the foil is found and converted to BODY. This is the inverse of Equation 4.28. $\boldsymbol{J(\eta)}$ is defined in Equation 4.29.

$$\boldsymbol{v}_{\boldsymbol{water\_particle}}^{\boldsymbol{body}} = \boldsymbol{J^{-1}(\eta)} \cdot \dot{\boldsymbol{\eta}}_{\boldsymbol{water\_particle}}^{\boldsymbol{body}} \tag{4.45}$$

Then the relative velocity at the foil between the foil and wave can be calculated. U is the speed of the vessel.

$$\boldsymbol{v}_{\boldsymbol{rel}}^{\boldsymbol{body}} = \boldsymbol{v}_{\boldsymbol{foil}}^{\boldsymbol{body}} + \boldsymbol{U} - \boldsymbol{v}_{\boldsymbol{wave\_particle}}^{\boldsymbol{body}} \tag{4.46}$$

This relative velocity can then be used to compute the incoming flow angle $\Delta\alpha$.

$$\Delta\alpha = arctan\left(\frac{\boldsymbol{v}_{\boldsymbol{rel\_z}}^{\boldsymbol{body}}}{\boldsymbol{v}_{\boldsymbol{rel\_x}}^{\boldsymbol{body}}}\right) \tag{4.47}$$

Finally, the effective flow angle can be computed. $\alpha_{operational}$ is the controlled angle of the overall foil. In this thesis, this angle was set to zero.

$$\alpha_{effective} = \alpha_{operational} + \Delta\alpha \tag{4.48}$$

4.6.2 Faltinsen method

The hydrodynamic implementation follows the theory described in Section 3.2. For the motions and velocities of the vessel ($\boldsymbol{\eta}$ and $\dot{\boldsymbol{\eta}}$), the hydro-coordinate system in *Waqum* was used. The hydro-coordinate system is the same as the body-coordinate system except for that it does not follow the wave frequent motions of the body.

First, the horizontal and vertical relative velocity of the water at the foil is calculated.

$$\begin{aligned} V_x &= \dot{\eta}_1 + U_x - v^{earth}_{water\_particle\_x} \\ V_z &= \dot{\eta}_3 + y_{foil\_actuating\_arm} \cdot \dot{\eta}_3 - x_{foil\_actuating\_arm} \cdot \dot{\eta}_4 - v^{earth}_{water\_particle\_z} \end{aligned} \tag{4.49}$$

$\Delta\alpha$ is then computed.

$$\Delta\alpha = arctan\left(\frac{V_z}{V_x}\right) \tag{4.50}$$

The effective flow angle $\alpha_{effective}$ is then calculated.

$$\alpha_{effective} = \alpha_{operational} + \eta_5 + \Delta\alpha \tag{4.51}$$

Chapter 5

Foil Motion Control

In this section, the modeling of the control system for the controlling of the foil flaps is presented and discussed.

When developing a control system for a high-speed catamaran, stability, maneuverability, sea kindliness meaning the ride quality, and safety are key factors that should be assessed. For the high-speed catamaran viewed in this study, the motions and accelerations in the vertical plane, heave, surge, and pitch, were chosen as the objective to be controlled, whereas reduction of the pitch motion was chosen as the main control goal. The paper by Zhang et al. (2014) and the book *Guidance and Control of Ocean Vehicles* by Fossen (1996) are used for inspiration for the ride motion control system selected in this thesis. The angles of the flaps α_f on the foils are selected as control surfaces and can be controlled relative to the vertical velocities to increase the heave and pitch damping. The damping effect due to the control will then contribute in addition to the damping effect discussed in Section 3.6. The block diagram for the catamaran with foil used for controlling purposes can be visualized as in Figure 5.1.

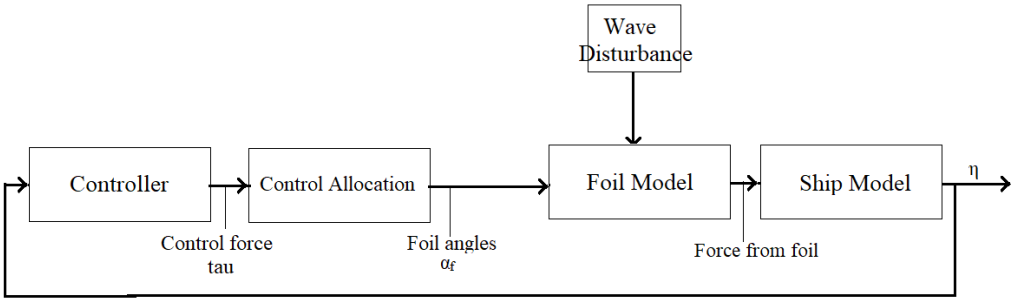

Figure 5.1: Block diagram of catamaran with controlled foils

The controller provides the desired control force $\boldsymbol{\tau}$ in order to fulfill the control goal, which in this case is to counteract pitch motions. The input to the controller is the states of the vessel $\boldsymbol{\eta}$, such as for instance vessel motions and velocities. The control allocation calculates the desired flap angle by each of the foils α_f to create the desired control force $\boldsymbol{\tau}$. The foil flaps are in this thesis set free to move independently of each other. The foil model calculates the created forces by the foils with flaps. In these calculations, the wave disturbance is taken into account. Finally, the foil forces are added to the forces of the vessel, and the system is solved in a seakeeping analysis. Then, the cycle is repeated for every time step.

5.1 Controller

When designing the controller, the Proportional-Integral-Derivative (PID) controller was considered. The mathematical equation for a PID-controller is given in Equation 5.1. K_p is the proportional gain, K_d is the derivative gain, and K_i is the integral gain. The control error e is defined by Equation 5.2. Here, $\boldsymbol{r(t)}$ is the target value while $\boldsymbol{y(t)}$ is the measured value.

When understanding how a PID-controller works, the functionality of the terms can be viewed separately. A P-controller works as a linear feedback system that uses the error to create the proportional output and can therefore not eliminate the error. The integral term is added in a PI-controller, the offset is compensated for as the cumulative error is integrated and eliminated. In this thesis, the integral term could, for instance, be used to account for a permanent, unwanted trim angle of the vessel. However, for a PI-controller, the signal may exceed the reference. This is known as overshooting and can be solved by adding a derivative term. The derivative term in a PID-controller is therefore added to achieve the desired position more effectively.

$$\boldsymbol{\tau(t)} = k_p \cdot \boldsymbol{e(t)} + k_d \cdot \frac{d\boldsymbol{e(t)}}{dt} + k_i \cdot \int_0^t \boldsymbol{e(\tau)} d\tau \tag{5.1}$$

$$\mathbf{e(t)} = \mathbf{r(t)} - \mathbf{y(t)} \tag{5.2}$$

The control goal was taken into account when selecting the final controller. As the goal was to decrease the pitch motion, increasing the damping in pitch was selected at the target. The controller chosen is a derivative (D) controller, as this was found fitting for the problem studied. A D-controller works as a control loop feedback mechanism correcting and regulating a control function automatically and accurately. The mathematical expression for D-controller is given in Equation 5.3. A derivative controller can, in general, be said to give a prediction of the future errors of the system.

$$\boldsymbol{\tau(t)} = \mathbf{k_d} \cdot \frac{d\mathbf{e(t)}}{dt} \tag{5.3}$$

The final selected controller is modeled as Equation 5.3. The input, or error, was set to be the pitch velocity of the vessel, and the gain k_d was defined as in Equation 5.4. The control error was set as in Equation 5.5.

$$\mathbf{k_d} = \begin{bmatrix} 0 & 0 & 0 & 0 & 0 & 0 \\ 0 & 0 & 0 & 0 & 0 & 0 \\ 0 & 0 & 0 & 0 & 0 & 0 \\ 0 & 0 & 0 & 0 & 0 & 0 \\ 0 & 0 & 0 & 0 & k_{55} & 0 \\ 0 & 0 & 0 & 0 & 0 & 0 \end{bmatrix} \tag{5.4}$$

$$\frac{d\mathbf{e(t)}}{dt} = \dot{\boldsymbol{\eta}} = \begin{bmatrix} \dot{\eta}_1 & \dot{\eta}_2 & \dot{\eta}_3 & \dot{\eta}_4 & \dot{\eta}_5 & \dot{\eta}_6 \end{bmatrix} \tag{5.5}$$

The value of k_{55} was decided by viewing the value of the linear damping coefficients of the vessel and an iteration process to select a coefficient both large enough to produce a desired damping effect, and within the range of the force the flaps were able to produce. This iteration process included adding the control force to the right-hand side of the equation of motion, and solving the equation of motion for different values of k_{55}. The final vale is presented in Table 5.1. A saturation element was included to keep α_f between the maximum and minimum limits, and a maximum rate of change restriction was added for mechanical realism.

Gain	Value
k_{55}	-4 $\cdot 10^8$

Table 5.1: Controller gain

Even though a pure derivative controller was selected in this study, such a controller is not always desirable or realizable in reality. One possible issue is that when the error is constant, the derivative controller will receive the message that the rate of change of the error is zero, and therefore not have anything to control on, and as a result produce zero control force. As the catamaran in the study is exposed to unsteady forces from waves for the time periods relevant for control, this should not be an issue.

Another issue is that a derivative controller operates to "slow down" the rate of change of the error. This may result in the controller slowing down the rate of change towards zero pitch motion, rather than enabling the process to go as fast as possible. In this study, the rate of change of the error is the pitch velocity of the vessel. This is a value desired to

stay low, and the "slowing down" effect of a derivative controller is rather preferred than unwanted. A derivative controller may therefore not be suitable in several applications, but in the one studied in the thesis, it should be acceptable. On the contrary, some issues arise when using a pure derivative controller in reality. One is that derivative controllers are very sensitive to noise, and another is that they are very sensitive to set point changes. This should be taken into account in a realization.

The vessel in the study has a very stiff dynamical system with eigenfrequencies in heave, pitch, and surge around 3 seconds. It was tried to develop a controller that would make the dynamical system "softer", and therefore shift the peak of the RAOs to higher periods. This would be advantages with regards to seasickness, as the acceleration of the vessel, which is the cause of seasickness, is proportional to the square of the frequency, as shown in Equation 5.6. Shifting the peak to higher periods, which means lower frequencies, will then result in lower accelerations.

$$\ddot{\eta} \approx \eta\omega^2 \tag{5.6}$$

However, the dimensioned foils and flaps were not able to produce large enough forces to give a desirable result. In addition, the final selected controller was found to reduce the accelerations significantly giving satisfactory results.

5.2 Control allocation

A control allocation algorithm was implemented so that the generalized control force $\boldsymbol{\tau}$ is distributed optimally to the actuators. The control allocation algorithm implemented is presented in this section.

The forces and moments $\boldsymbol{f}$ created by the foils are expressed in Equation 5.7.

$$\boldsymbol{f} = \boldsymbol{K}\boldsymbol{u} \tag{5.7}$$

$\boldsymbol{u}$ is the control input, which is the flap angles in this case. $\boldsymbol{K}$ is a diagonal force coefficient matrix defined as in Equation 5.8. K_i is then the force coefficient of the force produced by the flap of foil i. V is the relative inflow velocity at the foil, cr is the flap length, and ρ is the density of the water.

$$\boldsymbol{K} = \begin{bmatrix} K_1 & 0 & 0 & 0 \\ 0 & K_2 & 0 & 0 \\ 0 & 0 & K_3 & 0 \\ 0 & 0 & 0 & K_4 \end{bmatrix} = \begin{bmatrix} 4\rho V^2 cr^{1/2} & 0 & 0 & 0 \\ 0 & 4\rho V^2 cr^{1/2} & 0 & 0 \\ 0 & 0 & 4\rho V^2 cr^{1/2} & 0 \\ 0 & 0 & 0 & 4\rho V^2 cr^{1/2} \end{bmatrix} \tag{5.8}$$

The control force $\boldsymbol{\tau}$ is the forces and moments in the relevant degrees of freedom corresponding to $\boldsymbol{f}$ as shown in Equation 5.9. The flap is assumed to create a vertical force F_z as well as moments due to this force. Horizontal forces due to flap F_x and F_y are assumed negligible in the control allocation, Fossen (2011), but including them would most likely result in improved control.

$$\boldsymbol{\tau} = \begin{bmatrix} \boldsymbol{f} \\ \boldsymbol{r} \times \boldsymbol{f} \end{bmatrix} = \begin{bmatrix} F_z \\ F_z l_y \\ F_z l_x \end{bmatrix} \tag{5.9}$$

The actuator forces and moments relate to the control forces and moments as shown in Equation 5.10.

$$\boldsymbol{\tau} = \boldsymbol{T}\boldsymbol{f} = \boldsymbol{T}\boldsymbol{K}\boldsymbol{\alpha_f} \tag{5.10}$$

$\boldsymbol{T}$ is the thrust configuration matrix. The thrust configuration matrix describes the geometry of the actuators or foils in this case.

$$\boldsymbol{T} = \begin{bmatrix} 1 & 1 & 1 & 1 \\ l_{y1} & l_{y2} & l_{y3} & l_{y4} \\ l_{x1} & l_{x2} & l_{x3} & l_{x4} \end{bmatrix} \tag{5.11}$$

When Equation 5.12 is solved, the flap angles of each foil is found. The flap angles are then fed to the calculation of the foil forces.

$$\boldsymbol{\alpha_f} = [\boldsymbol{T}\boldsymbol{K}]^{-1}\boldsymbol{\tau} = \boldsymbol{K}^{-1}\boldsymbol{T}^{-1}\boldsymbol{\tau} \tag{5.12}$$

$\boldsymbol{T}$ is a non-square, non-invertible matrix. Therefore, it was necessary to use the pseudoinverse in place of the inverse.

$$\boldsymbol{K^{-1}} = diag\left[\frac{1}{K_1}, ..., \frac{1}{K_4}\right], \qquad \boldsymbol{T^{-1}} \approx \boldsymbol{T^{+}} = \boldsymbol{T^{T}}(\boldsymbol{T} \cdot \boldsymbol{T^{T}})^{-1} \tag{5.13}$$

In the simulation model, $\alpha_{flap\_effective} = \alpha_{foil} + \alpha_{flap}$. In the control allocation, the additional force due to $\alpha_{effective}$ is not taken into account. Accounting for this force in the control allocation algorithm could lead to a more accurate flap control with and a more effective reduction of the motions and loads.

5.3 Sensors

In control systems, sensors can be said to be a control system's window to the real world. It is through the sensors the control system can obtain readable data about the needed physical information. In this study, no effects of sensors are taken into account. In a real-life application, it would be necessary to consider the sensor accuracy, signal-to-noise ratio, and dynamic range, among other things. However, as this is first and foremost considered a theoretical study, sensor effects were not considered of high importance and were not prioritized.

Chapter 6

Environment

An important aspect of deciding the boundary conditions of the study was to define a possible location and environment, as this would contribute to the foundation of the dimensioning of the vessel. In this chapter, the location selected is presented, and the weather data obtained is discussed.

6.1 Location

It was desirable to select a realistic location that could be relevant for the actual implementation of the study executed. Research was done mapping the locations where high-speed catamarans within the relevant size range operate, and a selection was made with regards to geographical proximity. High-speed catamarans operate in several countries, including Scandinavia, the United States, Russia, Germany, Japan, Africa, Australia, and New Zealand. The high-speed ferry Stena Carisma - Express by Stena Line Scandinavia (2019) shown in Figure 6.1 was selected as fitting inspiration with the route Gøteborg - Fredrikshavn, a maximum velocity of 40 knots and an overall length of 89.75 m.

Figure 6.1: Stena Carisma Express

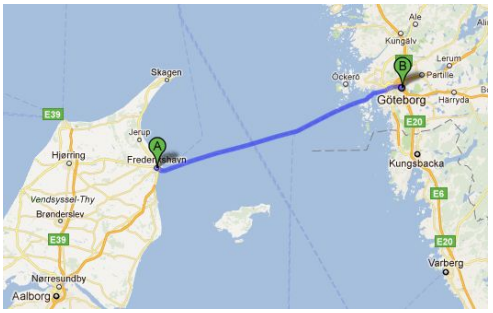

Figure 6.2: Route for the study

6.2 Weather

In a seakeeping analysis, the waves the vessel is exposed to must be defined. Therefore, a study was executed finding the relevant wave conditions for the work. A point in the middle of the route, with the coordinates 57°33'21.6"N 11°09'36.0"E, was selected. Wave data for 365 days was extracted from DNV GL's database. The occurrence of the significant wave height H_s, the mean up-crossing period T_z and the wave direction for the time period is shown in Figure 6.3, 6.4 and 6.5. For this study, it was desired to select the most often occurring sea state as the problem viewed is control of the wave-induced loads and motions over a period of time. Therefore, the waves occurring often are of considered to be of higher relevance than waves initiating extreme responses.

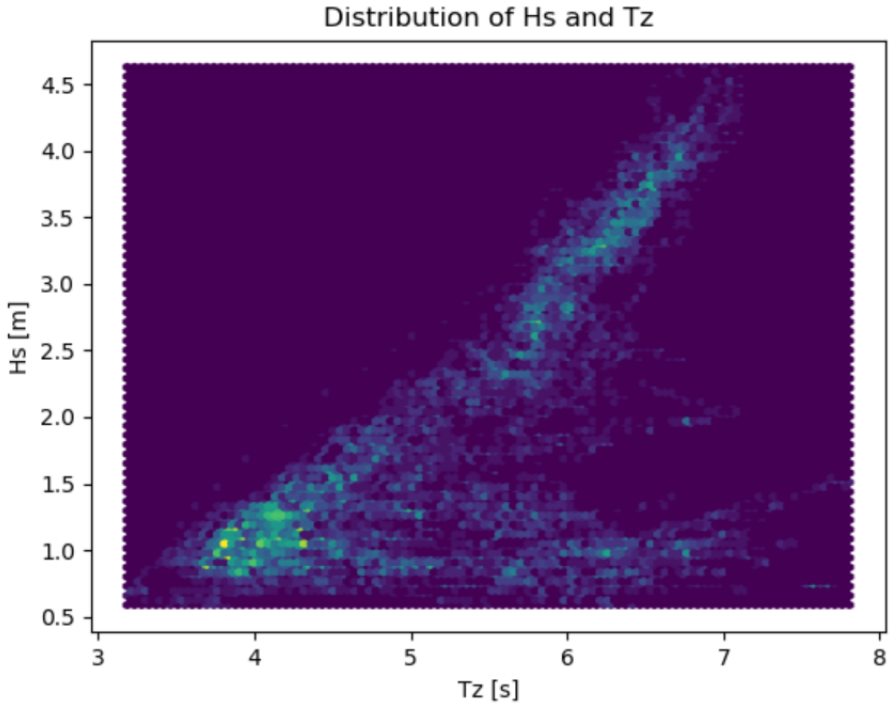

Figure 6.3: Overall occurence of H_s and T_z

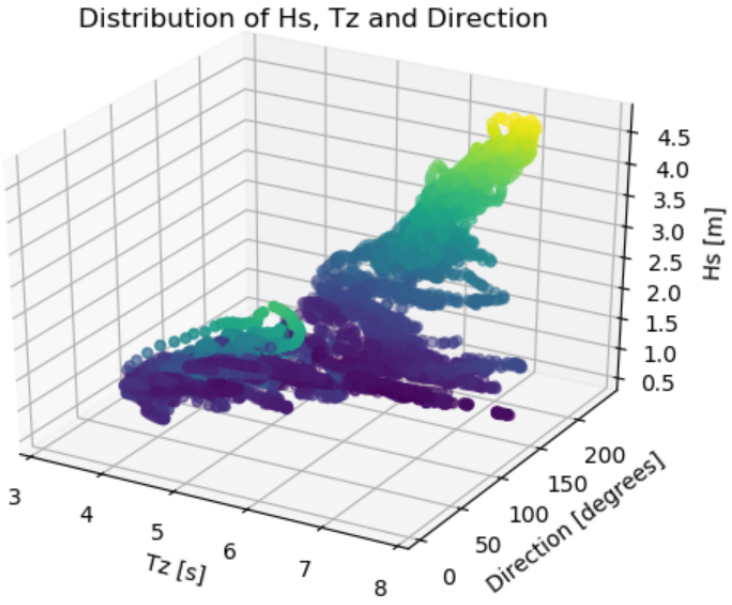

Figure 6.4: Overall occurence of H_s, T_z and direction

The lighter the color is, the more often the combination occurs. From Figure 6.3 it can be seen that the most common combination of H_s and T_z is $H_s \approx 4$ m and $T_z \approx 1$ s. Another combination occurring often is $H_s \approx 3.5$ m and $T_z \approx 6.5$ s. The most common wave direction overall can be seen from Figure 6.5 and is $\approx 200°$.

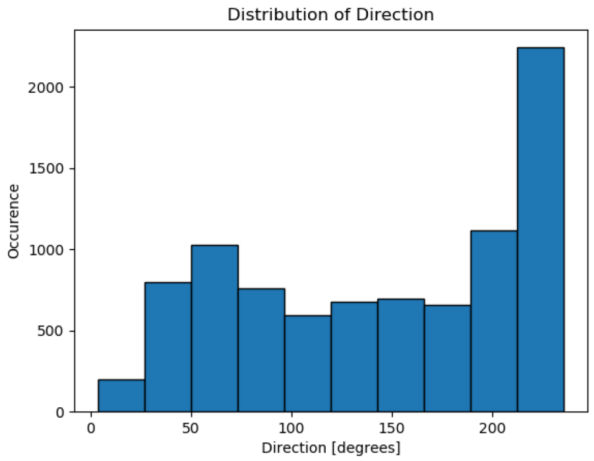

Figure 6.5: Overall occurrence of wave directions

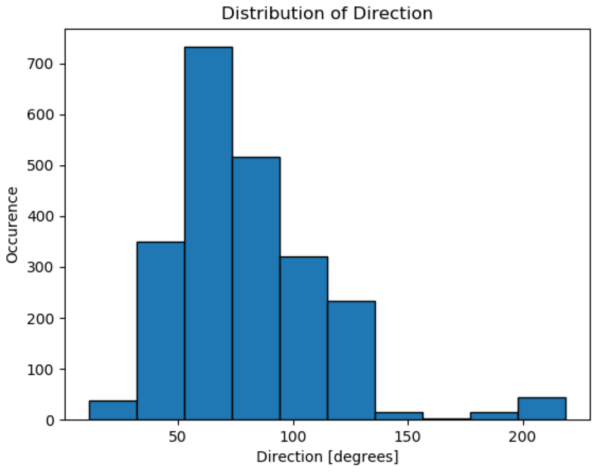

Figure 6.6: Occurence of direction for 3.5 s< T_z > 4.5 s and 0.75 m< H_s >1.5 m

An important point is that not all combinations of T_z, H_s are distributed equally over all wave directions. The occurrence of wave directions for 3.5 s< T_z >4.5 s and 0.75 m

$< H_s >$1.5 m is shown in Figure 6.6. From this, sea state 1 can be concluded. In Figure 6.7 the occurrence of H_s and T_z for wave directions $> 200°$ are plotted. This plot is interpreted to have two prominent "peaks", one for $Hs \approx 2.5$ m and $T_z \approx 6$ s, and one for $Hs \approx 3.5$ m and $Tz \approx 6.5$ s. The 3D-plot in Figure 6.4 supports these observations. The said combinations were selected as sea state 2 and 3. Conclusively, the sea states selected as most relevant for the simulations are displayed in Table 6.1.

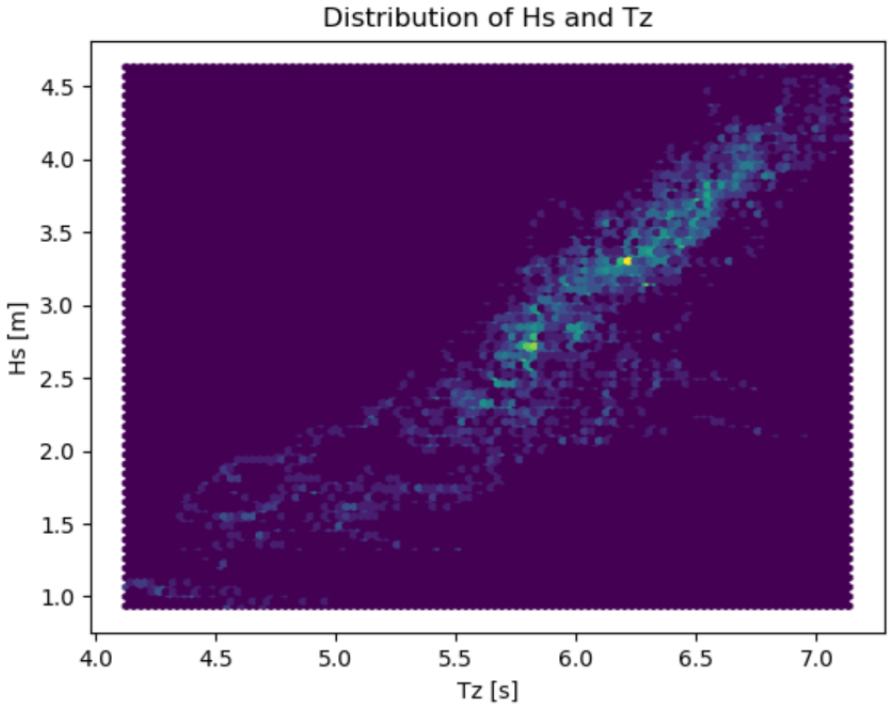

Figure 6.7: Occurence of T_z and H_s for directions>200°

Sea state	H_s [m]	T_z [s]	*Direction* [°]
1	1	4	65
2	2.5	6	225
3	3.5	6.5	225

Table 6.1: Most relevant sea states

The wave directions were compared to the direction of the vessel in the earth coordinate system to investigate the resulting wave direction on the vessel. For the wave directions from the wave data, 0° is defined as waves coming from north, and 90° is defined as waves coming from east. The approximate angle of the vessel route in the earth system is shown in Figure 6.8.

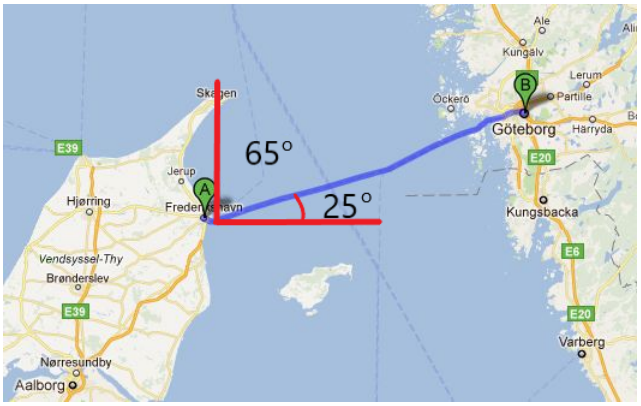

Figure 6.8: Angle of vessel route

When the approximate angle of the vessel route is compared to the wave directions from the wave data, it is evident that 65° is equal to head sea, and that 225° has a 20° deviation off head seas. That is when the vessel travels one way. On the return, the incoming wave angle will, of course, be 180° to this. Conclusively, head seas is considered relevant regarding the environmental conditions, and is kept as the heading of interest.

Chapter 7

Model and concept

In this chapter, the method of creating the numerical vessel model is described. Decisions and assumptions are discussed as well as corrections and challenges. In summary, a 3.778 m catamaran model was scaled to the full size of 37.78 m and modeled for numerical simulations. In addition, a foil concept was chosen including positioning and dimensioning.

This thesis was not considered an optimization study, so the decisions done with regards to geometry are not necessarily optimal. However, comprehensive research was done regarding the decisions, and the final concept is considered satisfactory for the thesis.

7.1 Vessel geometry

As part of the study, the vessel geometry was decided. After discussion with Odd Faltinsen, the semi-submerged catamaran model used in the work *Global Loads on High-speed Catamarans*, Faltinsen (1992), by the Division of Hydrodynamics at NTNU was selected as fitting. The line sketch of the geometry shown in Figure 7.1 and a table of the model parameters is attached in appendix A.2. The model was scaled with the scale 1:10. The dimensions of the full-scale vessel are given in Table 7.1. The radii of gyration are taken with respect to the axis through the center of gravity.

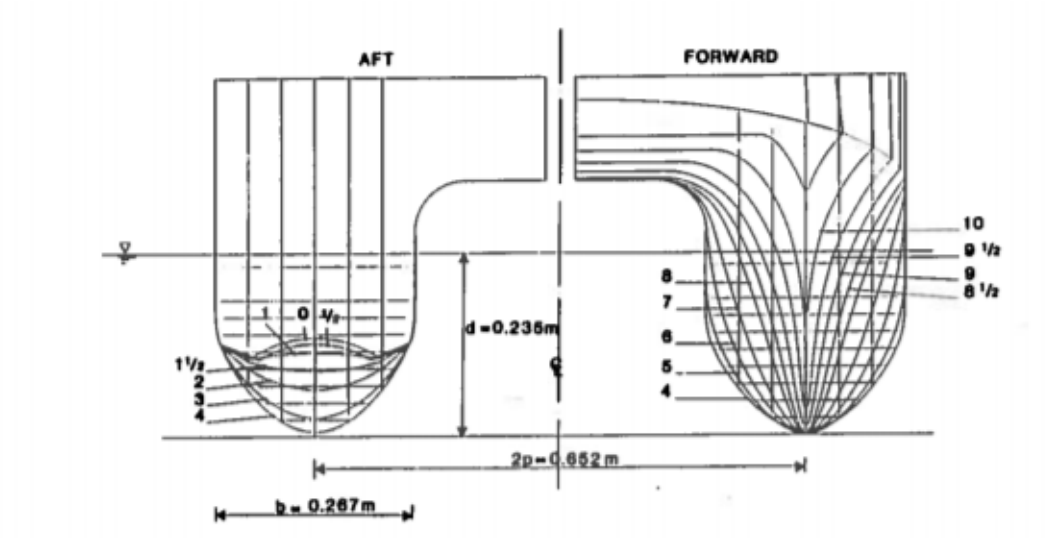

Figure 7.1: Line sketch of catamaran model, taken from Faltinsen (1992)

Designation	Symbol	Unit	Value
Length between perpendiculars	L	$[m]$	37.78
Beam at waterline amidships	B	$[m]$	9.18
Draft, even keel	d	$[m]$	2.35
Displacement	∇	$[m^3]$	257
Block coefficient	C_b	-	0.542
Breadth of one hull at waterline amidships	b	$[m]$	2.67
Distance between centre of hulls	$2p$	$[m]$	6.52
Transverse metacentric height	GM	$[m]$	5.56
Centre of gravity above keel	KG	$[m]$	3.32
Centre of gravity aft of amidships	LCG	$[m]$	2.96
Pitch radius of gyration	r_{55}	$[m]$	9.81
Roll radius of gyration	r_{44}	$[m]$	3.34
Yaw radius of gyration	r_{66}	$[m]$	10.22
Distance from centerline to COG of one half	y_A	$[m]$	2.98

Table 7.1: Dimensions of vessel geometry, full scale

An electronic geometry of the catamaran was created using *HydroD*. The coordinates of the curves in x-, y- and z-direction describing the geometry were taken from an old *.hul*-file which did not include bow and stern coordinates. It was assumed that the bow and stern could be modeled freely from sight as mainly the geometry above the waterline was missing since the simulation tools only take the geometry below the waterline into consideration. The modelled geometry is shown in Figure 7.2 and 7.3, and the dimensions of the final vessel model is presented in Table 7.2.

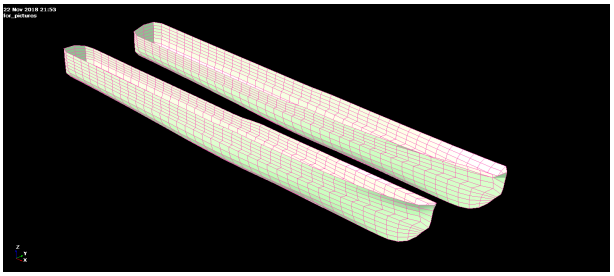

Figure 7.2: Geometry below waterline

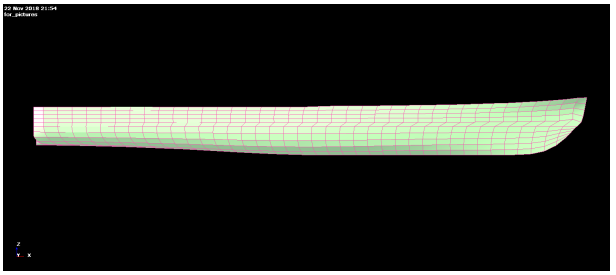

Figure 7.3: Geometry, side view

Designation	Symbol	Unit	Value
Trim	-	$[deg]$	0.00675
Heel	-	$[deg]$	0
Draft AP	d_{AP}	$[m]$	2.3669
Draft FP	d_{FP}	$[m]$	2.3713
Mass	M	$[kg]$	$2.6345 * 10^5$
Metacentric height in roll	GM	$[m]$	5.82
Centre of gravity z-axis (from origin)	VCG	$[m]$	3.32
Centre of gravity x-axis (from origin)	LCG	$[m]$	16.7
Center of gravity y-axis (from origin)	TCG	$[m]$	0

Table 7.2: Parameters of vessel model, full scale

7.1.1 Meshing

A requirement in *Wasim* is that all patches below the waterline must have a minimum of 5x5 elements. Each hull consists of two patches. All patches were meshed equally with a regular grid. Another rule of thumb is that there should be at least 10 elements per wavelength. The wavelengths can be found from the dispersion relation for deep water and the equation for the wave number k. The wavelengths for a range of the relevant wave periods are shown in Table 7.3.

$$\omega^2 = kg \qquad \lambda = \frac{2\pi}{k} \qquad \omega = \frac{2\pi}{T} \qquad \longrightarrow \qquad \lambda = \frac{gT^2}{2\pi} \tag{7.1}$$

Wave period [s]	Wave length [m]
3	14
6.5	66
6.9	74
16	400

Table 7.3: Wave lengths for selected wave periods

For 40 elements lengthwise, the condition of minimum 10 elements per wavelength is fulfilled for all relevant wave periods. Growth ratio of the element size was not applied as it is stated in the user interface of *HydroD* that growth ratio is not considered important for *Wasim* analyses. A mesh convergence study was executed for further assessment of the grid. This is described in further detail in Section 8.1. The final mesh parameters are presented in Table 7.4. Close-ups of the mesh are presented in Figure 7.4 and 7.5.

	Elements longitudinally	Elements girthwise	Growth ratio
Per patch	40	5	1

Table 7.4: Final grid parameters

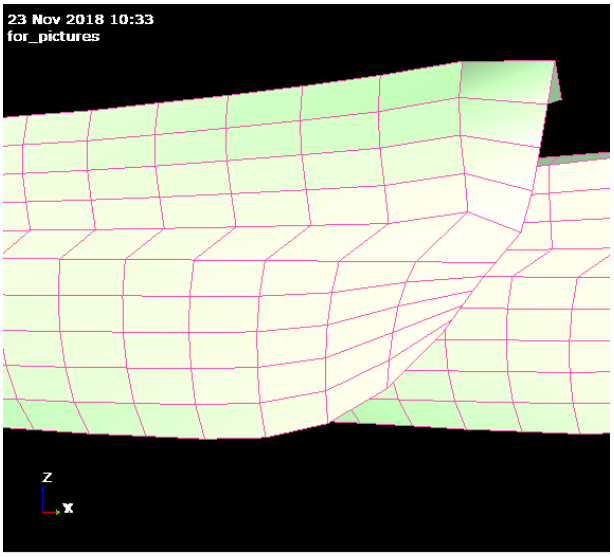

Figure 7.4: Grid on bow

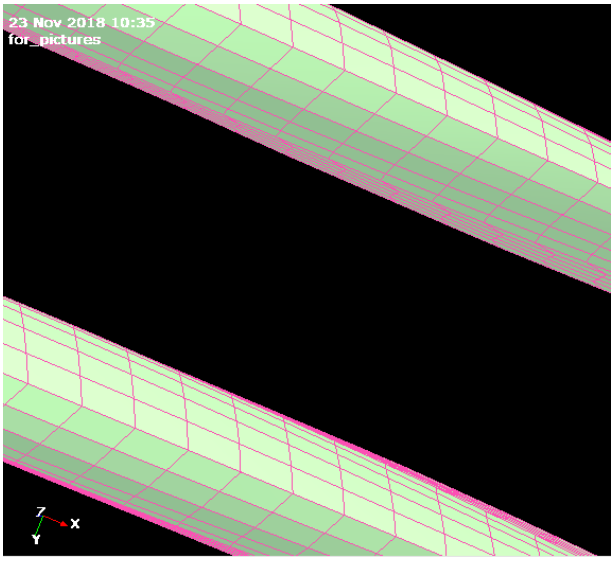

Figure 7.5: Grid on hulls, from below

7.2 Froude number

In hydrodynamics, a high-speed vessel is defined by Faltinsen (2006) as a vessel operating with Froude numbers, Fn, larger than 0.4 when viewing fast vessels with submerged hulls, whereas Baird (1998) categorizes high-speed vessels as crafts operating with speeds higher than 30 knots. In this study, 35 knots, corresponding to a Froude number Fn=0.934, was selected as the maximum operational speed. The Froude number is defined in Equation 7.2 where U is the velocity, g is the gravity, and L is the characteristic length.

$$Fn = \frac{U}{\sqrt{gL}} \tag{7.2}$$

7.3 Foil system

7.3.1 Foil concept

T-foils, flaps (trim tabs) and interceptors are all devices utilized as parts of foil motion control systems for high-speed catamarans. T-foils are commonly positioned at the bow of the vessel, as the vertical motions are largest there, while trim tabs and interceptors, in general, are positioned at the transom stern. T-foils are considered the most effective when it comes to damping of the vertical motions, both passively and actively, and can reduce the dive-in of the bow in following sea conditions. Therefore, T-foils were chosen as the device of choice in this study.

Fully submerged foils are advantageous with regards to slamming, cavitation, and ventilation. Since the foils viewed in this study were chosen to be fully submerged, the effects mentioned are not taken into account. The assumption of neglecting these effects is discussed further in Section 3.7. The presence of a T-foil adds drag and resistance to the system. Therefore, a retractable foil, that could be retracted in calm water conditions, is an advantage. Another advantage of a retractable foil is accessibility in shallow water. Therefore, when designing and building a foil system for a catamaran in reality, retractability should be considered.

As for the number of and positioning of the foils, various possibilities were viewed. Figure 7.6 shows resistance ϵ comparisons for planing catamarans. From the figure, it can be seen that foils located at the stern, in addition to the bow, improve the characteristics of the vessel significantly. This effect can be assumed to be similar for a non-planing catamaran with lower Froude numbers. The foil system was conclusively chosen to consist of four fully submerged T-foils; two positioned at the bow and two towards the stern.

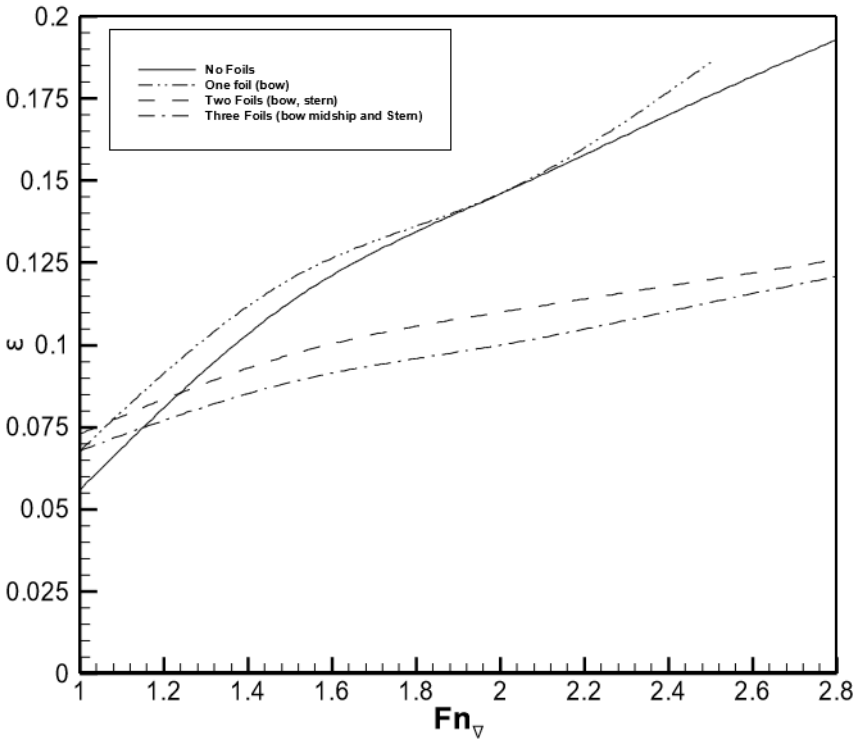

Figure 7.6: Resistance comparison for planing catamarans with tandem foils, from Migoette and Hoppe (1999)

7.3.2 Foil positioning

All four foils should be located on the hull centerlines for structural support. It is desirable to position the foils as far forward and aft as possible to maximize the damping effect due to large actuating arms. However, the foils should also be located far enough away from the bow to avoid the largest dynamic loads due to for instance slamming. Placing the aft and fore foils at equal distances from the motion reference point is desirable to avoid added pitching effect for static foils. The catamaran INCAT Natchan Rera by INCAT (2018) was used for inspiration with a fore T-foil located approximately 5/6 of the length overall from the stern. The locating of the aft foil system was based on the works of Hardwood (2006) and was chosen to be approximately 5m from the stern to give enough room for the flow effects due to the propulsion system. The final lengthwise positioning gives equal actuating arms to the motion reference point. The depth of the foil below keel was chosen to be 44% of the foil span. This decision was based on the depiction of typical T-foil positioning presented by Faltinsen (2006). The final positioning of the foils is presented in Table 7.5.

Foil number	Distance from stern, lengthwise [m]	Distance from centerline, crosswise [m]	Distance below keel [m]
Foil 1	33.83	3.26	1
Foil 2	33.83	-3.26	1
Foil 3	5.8	3.26	1
Foil 4	5.8	-3.26	1

Table 7.5: Foil positioning of each foil

7.3.3 Foil dimensions

For the dimensioning of the foils, the high-speed catamarans of INCAT Tasmania were used for inspiration. These vessels are surface piercing high-speed catamarans that use active motion control algorithms for the reduction of dynamic loads. The foil systems used by INCAT Tasmania consists of a retractable T-foil located at the bow on the center line, and two active trim fins at the stern, Alavimehr et al. (2017). The full-size T-foil prior to installation used for a 112m INCAT Tasmania high-speed wave piercing catamaran is presented in Figure 7.7. This foil was scaled to fit the catamaran in this study. The final dimensions of the foils are presented in Table 7.6. Another source used to validate the choices done with regards to the foil dimensions was the foil catamaran Foil Cat 2900 mentioned by Faltinsen (2006). This catamaran has an overall length of 29.5m and is situated with two fully submerged T-foils at the bow with the span 2.5m.

Figure 7.7: Full scale T-foil, Alavimehr et al. (2017)

T-foil parameter	INCAT Tasmania Catamaran	Catamaran in this study
Chord [m]	2.63	0.939
Span [m]	6.30	2.25

Table 7.6: T-foil parameters from INCAT Tasmania Alavimehr et al. (2017) to catamaran studied

The shape of the NACA (National Advisory Committee for Aeronautics) 64A410 foil was used for inspiration for the geometry of the foils as the modified 6-series of the NACA foils permit a relatively high lift coefficient with a minimal thickness-to-chord ratio, Hardwood (2006). The NACA 64A410 foil is shown in Figure 7.8. A low thickness-to-chord ratio is advantageous with regards to limiting drag. The foils in this series also have relatively little curvature in the back part of the body, which is desirable as the mathematical modeling does not take such effects into account. The resulting T-foil parameters used in this study are presented in Table 7.7. The maximum foil thickness is set to 10% of the chord length.

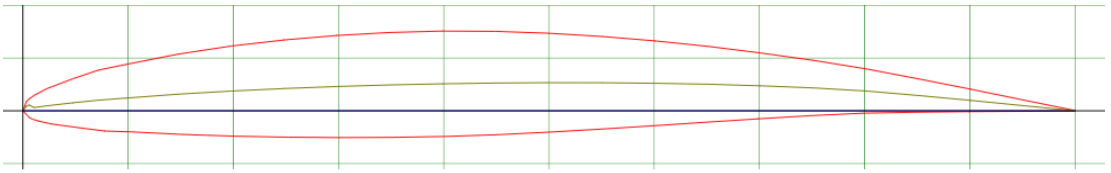

Figure 7.8: NACA 64A410 Foil, from NACA (2019)

Parameter	Unit	Value
Chord	m	0.939
Span	m	2.25
Aspect ratio	m	5.39
Thickness	m	0.0939
Thickness-to-chord ratio	m	0.1

Table 7.7: Final T-foil parameters

Chapter 8

Methodology and analyses

In this chapter, the execution of the work and the various analyses done in this thesis are described. Challenges encountered are addressed, and the choices made with regards to the seakeeping solver are discussed.

8.1 Mesh convergence study

A mesh convergence study was executed with the objective of selecting a suitable grid for the simulations. Using a suitable mesh size is crucial for obtaining reliable results, and finding the balance between computation time and desired accuracy. In the mesh convergence study, three grids were tested. The grids are presented in Table 8.1. The elements are given per patch. As mentioned, each of the hulls consists of two patches, each stretching from stern to bow. As the mesh size is decreased, the timestep also has to be decreased for the numerical computations.

Discretization	Elements horizontally	Elements vertically	Timestep	Δx [m]
Δx_1	20	2.5	0.1	1.889
Δx_2	40	5	0.01	0.9445
Δx_3	80	10	0.001	0.47225

Table 8.1: Discretizations for mesh convergence study

The convergence study executed was inspired by the paper by Colicchio et al. (2006). The evaluation is based on assuming that the error approximated for a given quantity q is proportional to Δx^{OA} where OA is the order of accuracy defined as in Equation 8.1. The order of accuracy provides information about the convergence of the numerical solution, and positive and large values are desired.

$$OA = \frac{log(\frac{|I_g(\Delta x_2) - I_g(\Delta x=0)|}{|I_g(\Delta x_1) - I_g(\Delta x=0)|})}{log(\frac{\Delta x_2}{\Delta x_1})} \tag{8.1}$$

$I_q(\Delta x_1)$ and $I_q(\Delta x_2)$ are integrated values of a given quantity which is predicted numerically for the corresponding discretization. $I_q(\Delta x = 0)$ is the exact value of the time integral of the quantity q. For the studied case, the exact integral value is not known. Therefore, Equation 8.1 is modified so that the exact solution can be computed by assuming a linear logarithmic relationship between I_q, and Δx and extrapolation from the values $I_q(\Delta x_1)$, Colicchio et al. (2006).

$$\frac{log(\frac{|I_g(\Delta x_2) - I_g(\Delta x=0)|}{|I_g(\Delta x_1) - I_g(\Delta x=0)|})}{log(\frac{\Delta x_2}{\Delta x_1})} = \frac{log(\frac{|I_g(\Delta x_3) - I_g(\Delta x=0)|}{|I_g(\Delta x_2) - I_g(\Delta x=0)|})}{log(\frac{\Delta x_3}{\Delta x_2})} \tag{8.2}$$

The heave and pitch motions were chosen as the values to be analyzed, as these were considered important parameters in the thesis. Simulations were run in *Waqum* for the vessel without foil system with the three grid sizes to obtain the exact solution. The wave H=2 m, T=6.959590 s was selected, and the time interval chosen was 100-110 s, which is when the responses were well past the transient phase. From Equation 8.2, the exact solution was computed to be $I_q(\Delta_x = 0)$=891.564 for the pitch motion and $I_q(\Delta_x = 0)$=6238.525 for the heave motion. The order of accuracy was computed for the finest, and second finest mesh. The parameters obtained for the computations are displayed in Table 8.2, while the order of accuracy is displayed in Table 8.3. The pitch and heave motions for the three grids are displayed in Figure 8.1 and 8.2.

Discretization	$I_q(\Delta_{xi})$ Heave motion [m]	$I_q(\Delta_{xi})$ Pitch motion [degree]
Δx_1	2831.52	1003.58
Δx_2	5628.36	888.23
Δx_3	6129.25	891.66

Table 8.2: Values used for the computation of order of accuracy

Quantity	Time interval [s]	OA
Heave motion	100-110	2.481
Pitch motion	100-110	5.073

Table 8.3: Order of accuracy

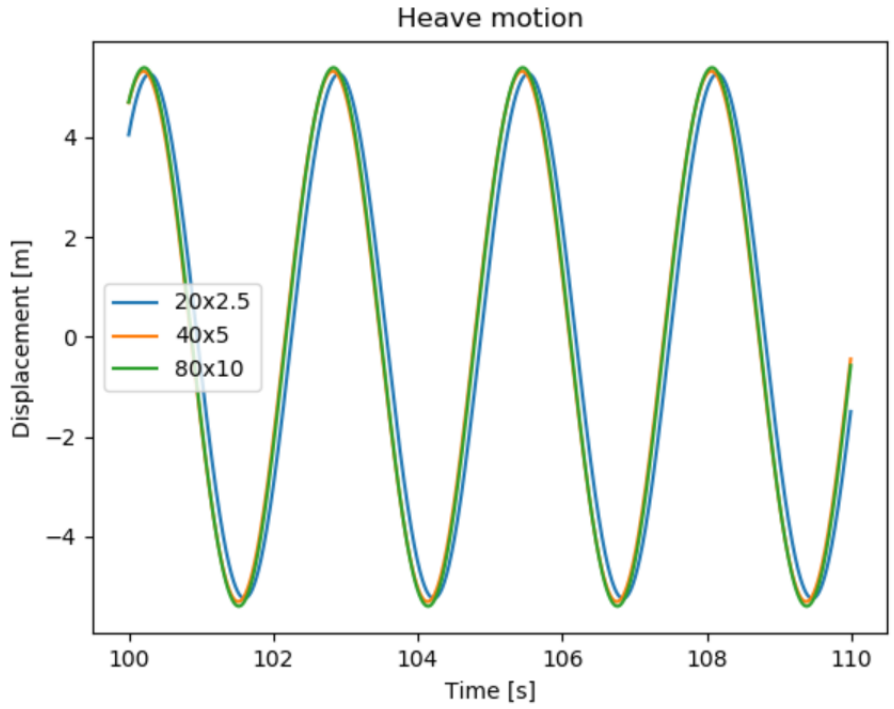

Figure 8.1: Heave motion, mesh convergence study

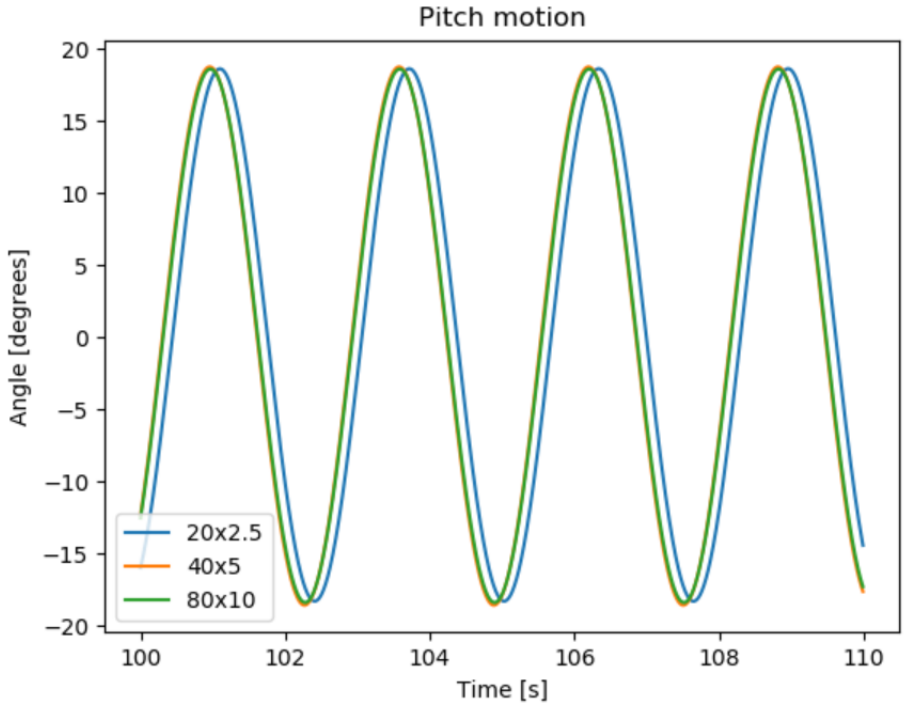

Figure 8.2: Pitch motion, mesh convergence study

The order of accuracy is found to be positive, indicating that Δx_2 and Δx_3 obtain more similar results than for Δx_1. Figure 8.1 and Figure 8.2 support this, as the lines for $40x5$ and $80x10$ can be seen to be overlapping and approximately equal, which does not hold for the line for $20x2.5$. A convergence can also be observed by the values of $I_q(\Delta_{xi})$ in Table 8.2. Using the finest mesh would result in an extensive computation time, which is not desired. As discretization Δx_2 is assumed to provide satisfactory results, the grid $40x5$ elements was chosen for proceeding with the study.

8.2 Implementation and solver

The foil loads were implemented in *Waqum* according to the theory discussed in Chapter 3. The control strategy was implemented according to Chapter 5. The software is described in further detail in Section 2.5.

A limitation of 20° was included regarding the maximum deflection of the foil flaps to avoid stall, as discussed in Section 3.3.1. In addition, the maximum rate of change for the flap angles was set. The maximum rate of change was selected to be from -20° to +20° in one second, in other words one full switch per second.

A fourth-order Runge-Kutta method was used for the solver. This solver iterates four times every time step, and the solution obtained in the fourth iteration is used. Consequently, the foil loads were computed four times per time step. The controller was only updated once every time step. Hydrodynamic analyses were followingly run on the vessel including the forces linear restoring, linear wave excitation including diffraction, rigid body coriolis and a convolution force computing the convolution integral of the velocity and retardation. The catamaran with foil system was exposed to linear wave excitation from sine waves in various wave conditions. The different analyses are described in further detail in Section 8.4.

8.3 Instability

Prior to the master thesis, simulations with the vessel model had only been executed with the software *Wasim*. In these simulations, the catamaran was found to be stable, and the results were verified as described in Section 1.1.1. From the *Wasim*-simulations, WDB-files to be used in *Waqum* were generated. A WDB (Waqum Database) is a file format for storing results from *Wasim Harmonic* where the linear hydrodynamic information about a hull is stored. When these created WDB-files were run in *Waqum*, the catamaran showed to be unstable. Much time was devoted to investigating the cause of the instability. Each of the forces contributing to the total hydrodynamic computation

was plotted separately, and the motion coefficients were investigated.

Conclusively, negative damping in surge was discovered as the source of the instability. This issue was solved by adding a spring with a spring damping of 1.8 and spring period of 40 s in surge. This period was assumed to be large enough to not have a significant influence on the results of the simulations in this study. RAO's were obtained showing similar results for *Waqum* and *Wasim* with the inclusion of this spring. This can be seen in Section 9.1. As the results were equal with the addition of this spring, the spring was assumed not to alter the characteristics of the vessel that were of importance for in this study.

Spring parameter	Value
Degree of freedom	1
Damping	1.8
Period	40

Table 8.4: Parameters of spring added for stability

8.4 Simulations

Several different simulations were executed as part of the study for the thesis. The different simulations are described below. Both time series and RAOs were produced to depict the results obtained. The RAOs were created based on a least square algorithm. Each time series shows the motions and accelerations of the vessel in detail for one regular wave, while the RAOs display the response of the vessel in multiple waves. To evaluate the influence of the passive foils and control algorithm on the vessel, a statistical analysis was executed obtaining the root-mean-square and reduction efficiency ratio in addition to the RAOs and time series.

Validation of the catamaran in Waqum

Before executing the analyses of the catamaran with the foil system in *Waqum*, it was crucial to verify that *Waqum* obtained the same simulation results as *Wasim* for the vessel. This was especially important as the results from *Wasim* were used directly in the comparisons of RAOs with and without foil loads, in addition to being important for validating the results obtained by *Waqum*. The results are presented in Section 9.1.

Comparison of foil loads

In this thesis, control theory is coupled with hydrodynamic theory. These theories are traditionally expressed in two different mathematical ways of expression. Simulations were run computing the loads created by the foils according to each of these ways, as described in Section 4.6. $\alpha_{effective}$ is shown as the final result of this comparison as the computation from there is equal in the seakeeping analysis. The results are presented in Section 9.2.

Influence of foils on the mean catamaran configuration

A study was executed regarding the influence of the foil loads on the mean catamaran configuration. A simulation was run for a steady forward speed of 35kn in calm water and with flap angles set to zero. From this test, the relevance of the foils on trim and sinkage could be found. The results can be seen in Section 9.3.

Seakeeping of catamaran with static foils, zero flap angle

A seakeeping analysis of the vessel with static foils with flap angles set to zero was executed in *Waqum*. The influence of the foils on the catamaran motions and accelerations in waves was assessed. The results are presented in Section 9.4.

Catamaran with foil motion control

The behavior of the catamaran with foil motion control was investigated in relevant wave conditions, and the influence of the controller was investigated by executing simulations in *Waqum*. The results are shown in Section 9.5.

Vertical motion at bow

The vertical motion at the bow can lead to phenomena such as slamming and deck-diving. In addition, large vertical motions are uncomfortable for the passenger. As a measure of the efficiency of the foil motion control, the vertical motion at the bow was investigated in Section 9.6.

Chapter 9

Results and discussion

In this chapter, the results for the different analyses and studies are presented and discussed. In addition, the method followed throughout the study is evaluated.

9.1 Validation of the vessel in Waqum

The results computed by *Waqum* were validated by comparing the results obtained for the catamaran without foil system with the RAOs (Response Amplitude Operators) produced by *Wasim*. The RAOs for surge, heave and pitch motion and acceleration for *Waqum* and *Wasim* are displayed in Figure 9.1 and 9.2. The simulation parameters are displayed in Table 9.2, and the waves used for obtaining the RAOs are shown in Table 9.1.

H_s [m]	2	2	2	2	2	2	2
T_z [s]	3.9798	5.9798	6.4798	6.9596	7.9596	10.5237	16.9192

Table 9.1: Wave heights and periods for RAOs, *Waqum* validation

Maximum time	500s
Δt	0.01
Wave heading	180°
Vessel speed	35kn

Table 9.2: Simulation Parameters, *Waqum* validation

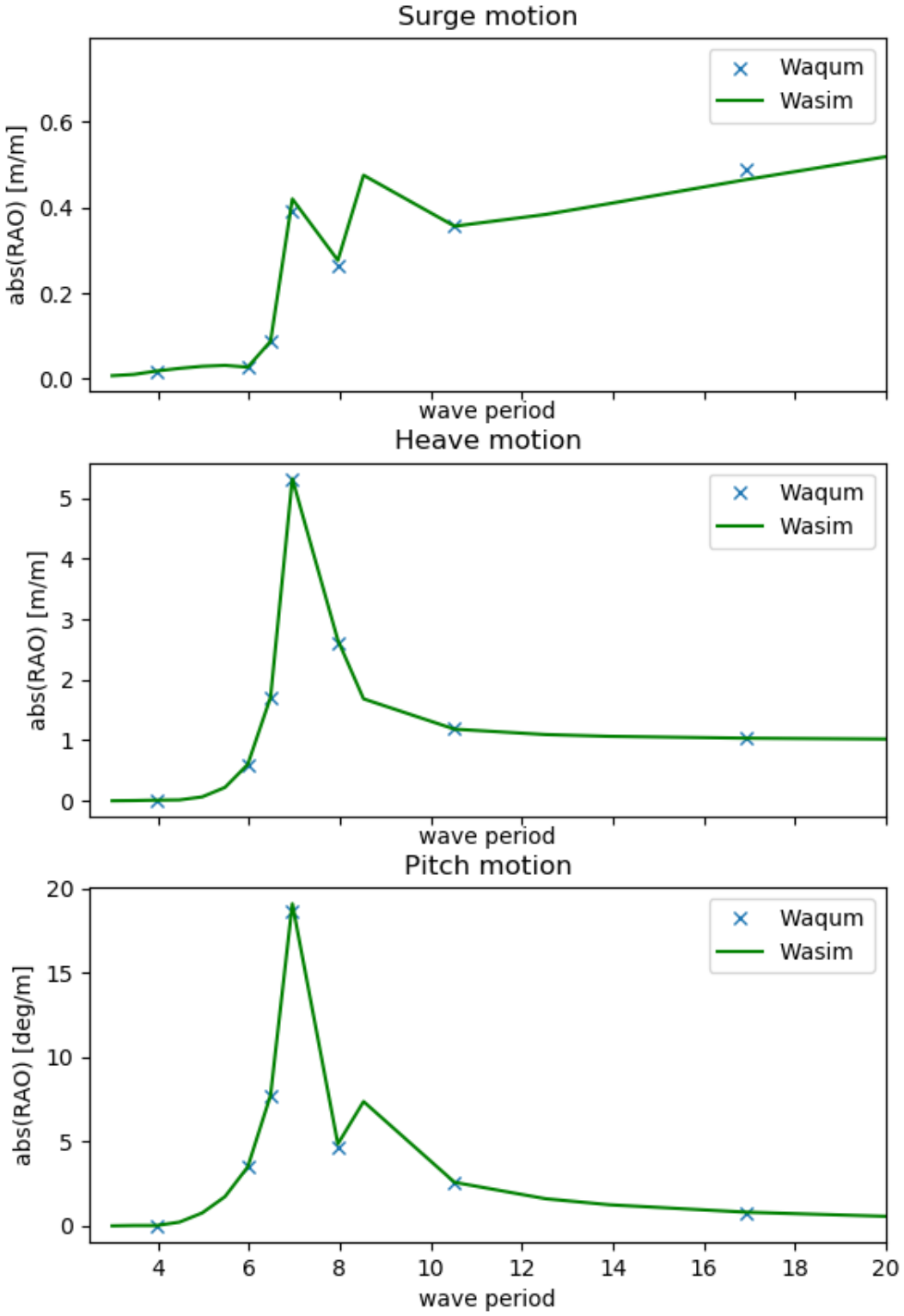

Figure 9.1: RAO for surge, heave and pitch motion, results for *Waqum* and *Wasim*

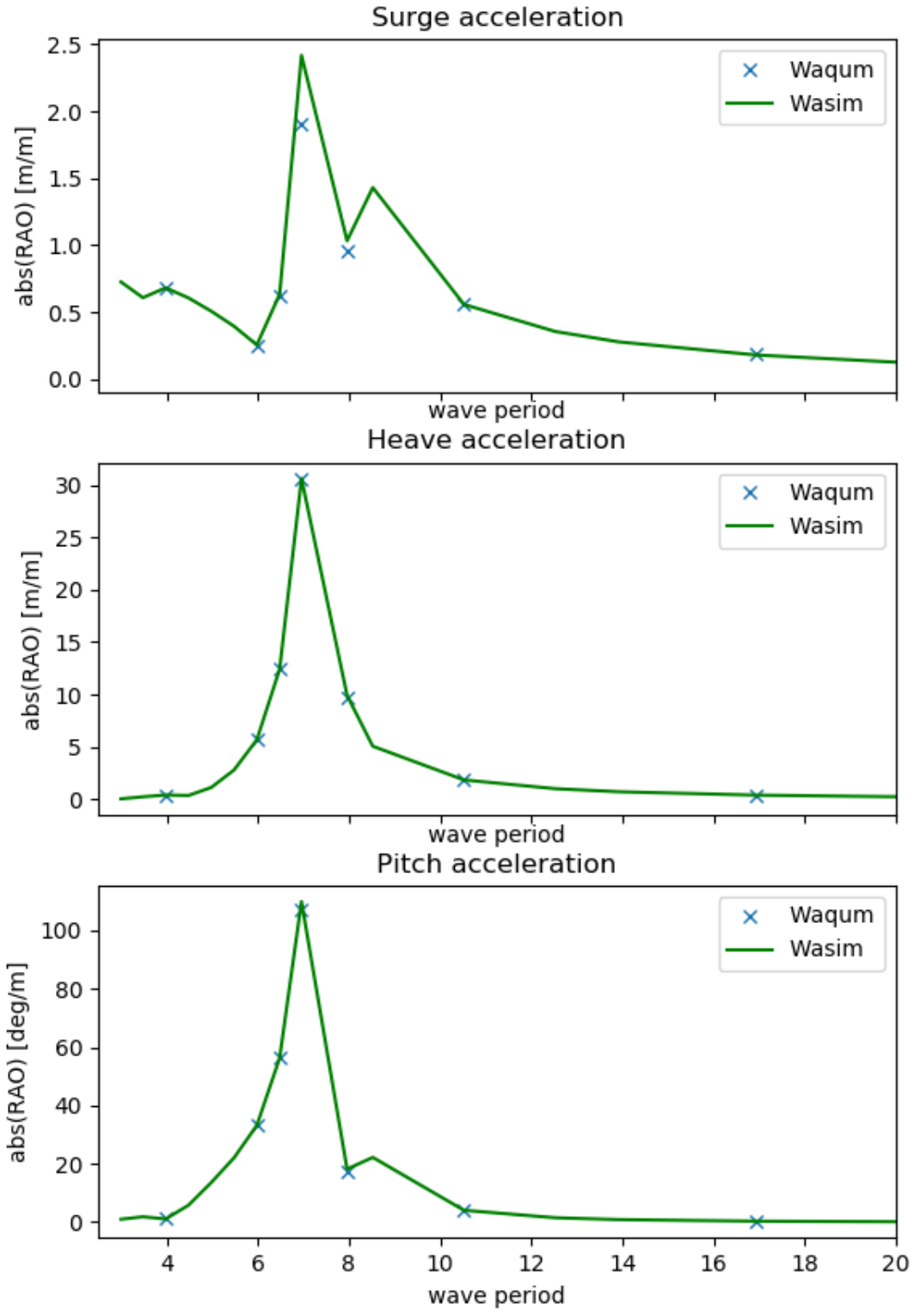

Figure 9.2: RAO for surge, heave and pitch acceleration, results for *Waqum* and *Wasim*

The RAOs showing displacements are seen to correspond well between the programs with insignificant or no deviance. The RAOs correspond well also for the accelerations. However, some deviance is seen for the acceleration in surge. The causes of this are unknown but might be due to the fact that *Waqum* is designed mainly for larger vessels operating at lower Froude numbers, which may lead to some inaccuracies for a relatively short high-speed vessel as the one studied. Overall, the comparison between *Waqum* and *Wasim* was found to be satisfactory, but the inaccuracy should be taken into account in the evaluation of the influence of the foil loads.

9.2 Comparison of foil loads

The foil loads are in the full simulation calculated from $\alpha_{effective}$ equally for both cases. Therefore, if the $\alpha_{effective}$ are equal, the foil loads will also be equal. A simulation of the vessel was run in regular waves in *Waqum* with the conditions given in Table 9.3 and the simulation parameters in Table 9.4. The wave period was chosen randomly from the *Wasim* wave periods. The result is shown in Figure 9.3.

Wave period [s]	Wave amplitude [m]	Heading [°]
10.524	2.0	180

Table 9.3: Wave parameters, foil load comparison

Maximum time	100s
Δt	0.01
Wave heading	180°
Vessel speed	35kn

Table 9.4: Simulation Parameters, foil load comparison

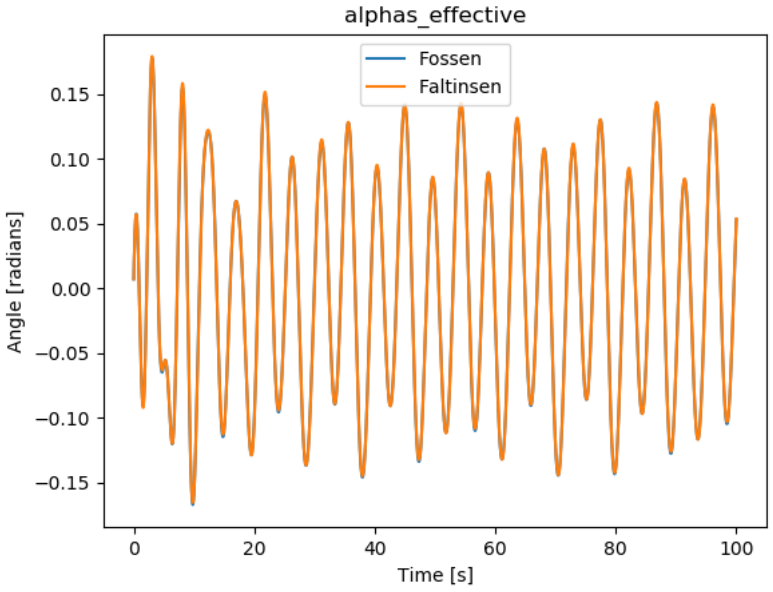

Figure 9.3: Comparison of $\alpha_{effective}$, Fossen and Faltinsen

The $\alpha_{effective}$ calculated by the two methods are seen from Figure 9.3 to be equal. Therefore, it should not matter what method is chosen when moving forward with the simulations of the vessel including the foil system. As the rest of the code in *Waqum* is written according to the control theory-system, the corresponding way of expression was selected for the final implementation. The correspondence of the computed foil loads can also be viewed as a form of validation of the equation of the effective foil angle, as the two separate computational methods result in the same results.

9.3 Influence of foil loads on mean catamaran configuration

The influence of the foil loads on the mean catamaran configuration was inspected to understand the effect of the foil loads. First, the trim angle of the vessel without foils for 0kn and 35kn was viewed. These trim angles were obtained in the stability analyses by *Wasim*. The obtained trim angles are presented in Table 9.5.

Speed [kn]	Froude Number	Trim [°]
0	0	0.0525
35	0.934	0.07545

Table 9.5: Trim angles for catamaran without foils

The trim angles were practically zero both with and without speed, only increasing to below 0.1° for 35kn. This is unexpected, as the trim angle is expected to have a significant increase for such a large increase in speed. One reason for the small increase in trim might be that *Wasim* does not execute the trim position calculations very accurately. The trim is an effect of the flow around the hull; when the flow moves around the hull, the flow velocity increases. In the stability analysis in *Wasim*, Neuman Kelvin solution is used. This means that the flow around the hull is evaluated without the presence of the hull, which may give inaccurate results. Alternatively, Double Body Flow could be used. Then the flow around the hull would be evaluated with the hull, and the trim would most probably change.

An analysis in *Waqum* was executed in still water on the vessel including the foil loads. The analysis was executed with the simulation parameters in Table 9.6. The results of the still water analyses are shown in Figure 9.4 and 9.5.

Maximum time	200s
Δt	0.01
Wave heading	180°
Vessel speed	35kn

Table 9.6: Simulation Parameters, still water analysis

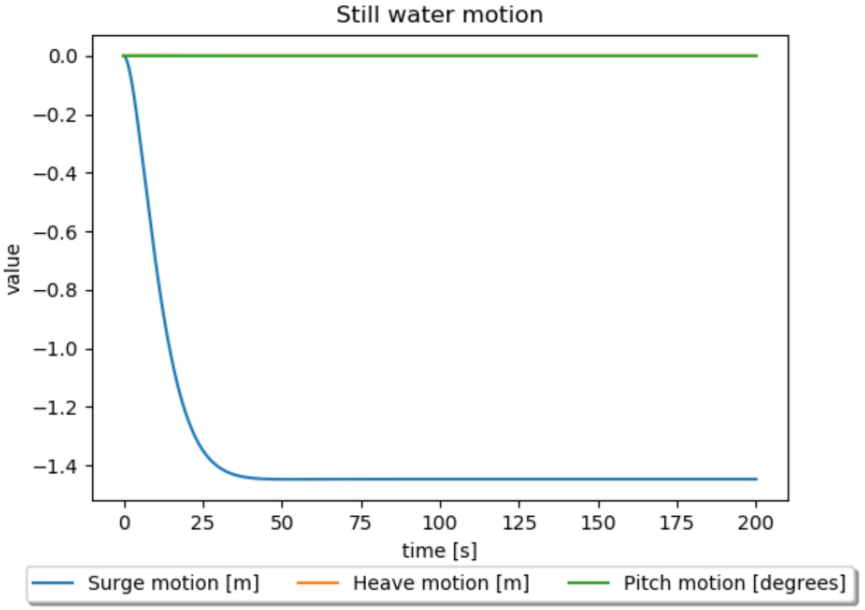

Figure 9.4: Motions in surge, heave and pitch, still water test

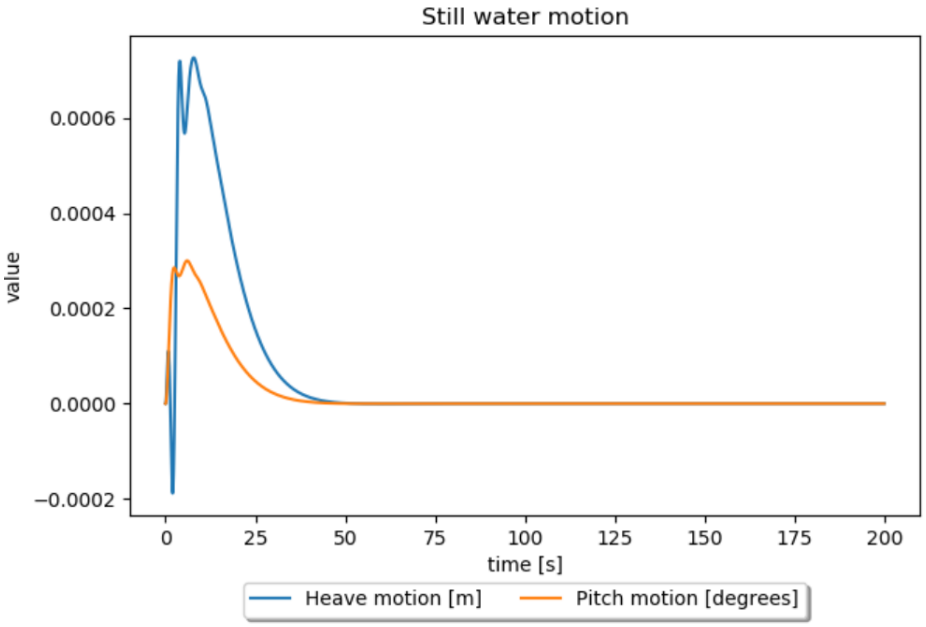

Figure 9.5: Motions in heave and pitch, still water test

Figure 9.4 and 9.5 show that the foil loads initiate practically no change in the trim angle of the vessel. This is as expected from the initially negligible trim angle, as the forces in the vertical plane are functions of the incoming flow angle. When the incoming flow angle is zero, so are the vertical forces and moments. However, this is not a very realistic result as a real high-speed vessel would experience an increase in trim, which would result in a further change of trim due to the presence of the foils. A constant drag force can be observed from Figure 9.4, as the x-position of the vessel converges to a constant negative value. This shows that the foils add a resistance component. This added resistance is not assessed in detail in this study due to limited time. However, to maximize the efficiency of the foil, minimizing the added resistance is crucial.

9.4 Seakeeping analysis with static foils

Seakeeping analyses were conducted on the catamaran with static foils using *Waqum*. RAOs, shown in Figure 9.6 and 9.7, and time series, shown in Figure 9.8 to 9.13, were obtained to evaluate the influence of the passive foil system on the vessel. The wave heights and periods used for the RAOs are displayed in Table 9.7. T denotes the wave period, and H denotes the wave height. These specific periods were selected for easier comparison as they correspond to the periods used in *Wasim*, as the continuous RAOs used for the vessel without foils are extracted from *Wasim*. The simulation parameters are given in Table 9.8. Only the motions in the vertical plane, heave, pitch, and surge, were

accounted for in the inclusion of the foil loads. Therefore, it is only considered relevant to view the effect of the foils in the said degrees of freedom.

H_s [m]	2	2	2	2	2	2	2
T_z [s]	3.9798	5.9798	6.4798	6.9596	7.9596	10.5237	16.9192

Table 9.7: Regular waves for RAOs, seakeeping analysis with static foils

Maximum time	500s
Δt	0.01
Wave heading	180°
Vessel speed	35kn

Table 9.8: Simulation Parameters, seakeeping analysis with static foils

The initial plan was to execute seakeeping analyses in irregular waves. However, trouble was encountered in the source code when an irregular wave or wave spectrum was used. Therefore, instead of running the analyses in sea states, only regular waves were used to gather further insight into the influence of the foil system. To obtain the time series, the high-speed catamaran was exposed to the regular waves presented in Table 9.9. The T-values were chosen corresponding to the ones used in *Wasim*. H=2 m, T=6.95959 s is the first wave chosen as this wave period coincides with the resonance period of the system and hence initiates the largest motions and accelerations, seen from the RAOs. H=3.5 m, T=6.5 s is the second wave chosen as this was pointed out as the parameters for one of the most often occurring sea states in the environmental area chosen, in addition to being relevant for the control purpose of this study. For a better understanding of the motions, the forces and moments created by each foil were plotted together with the motions and velocities. This is presented in Figure 9.14 to 9.23.

Wave number	H [m]	T [s]
1	2	6.95959
2	3.5	6.5

Table 9.9: Regular waves, seakeeping analysis with static foils

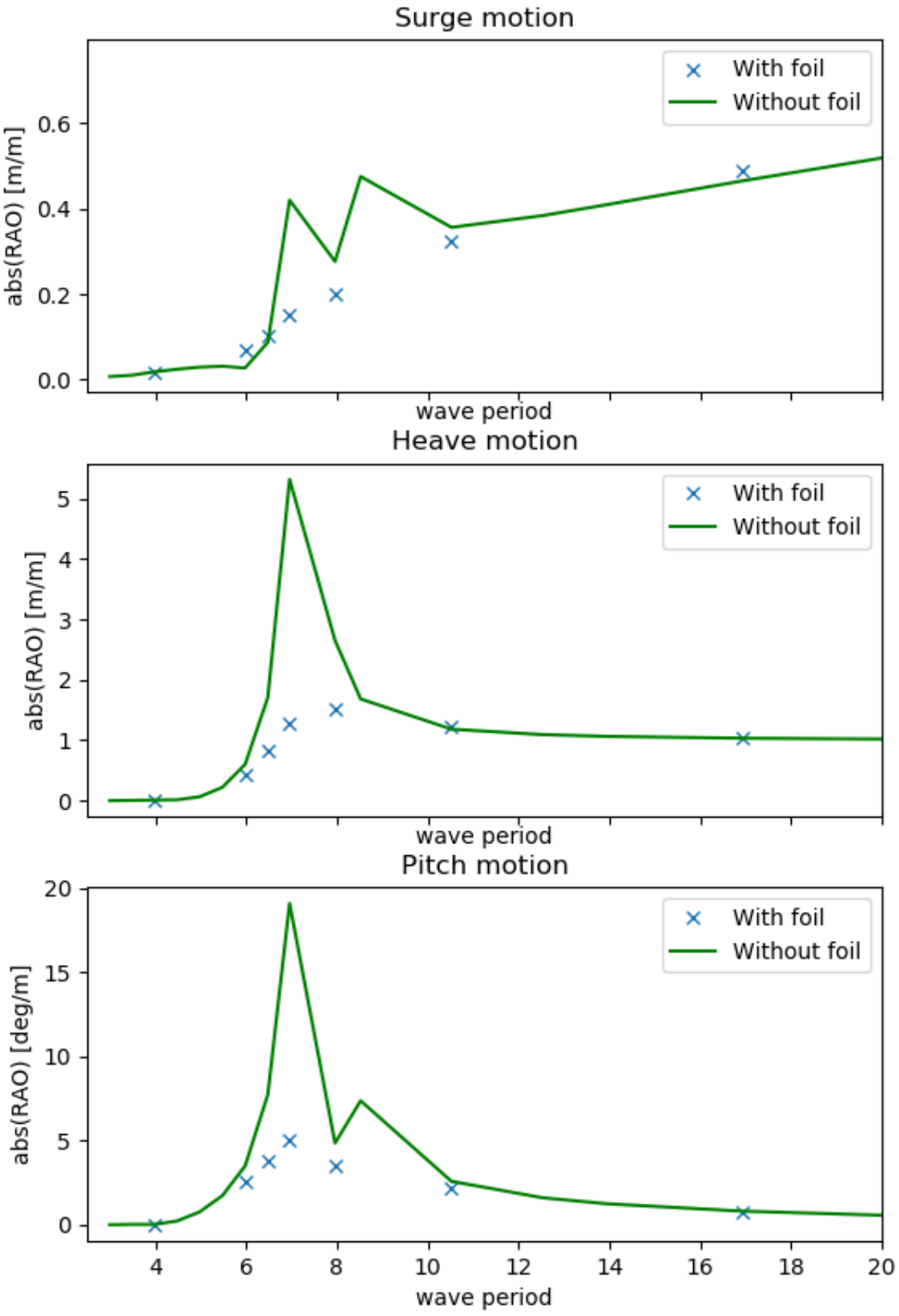

Figure 9.6: RAO for surge, heave and pitch motion, catamaran with foils, no control

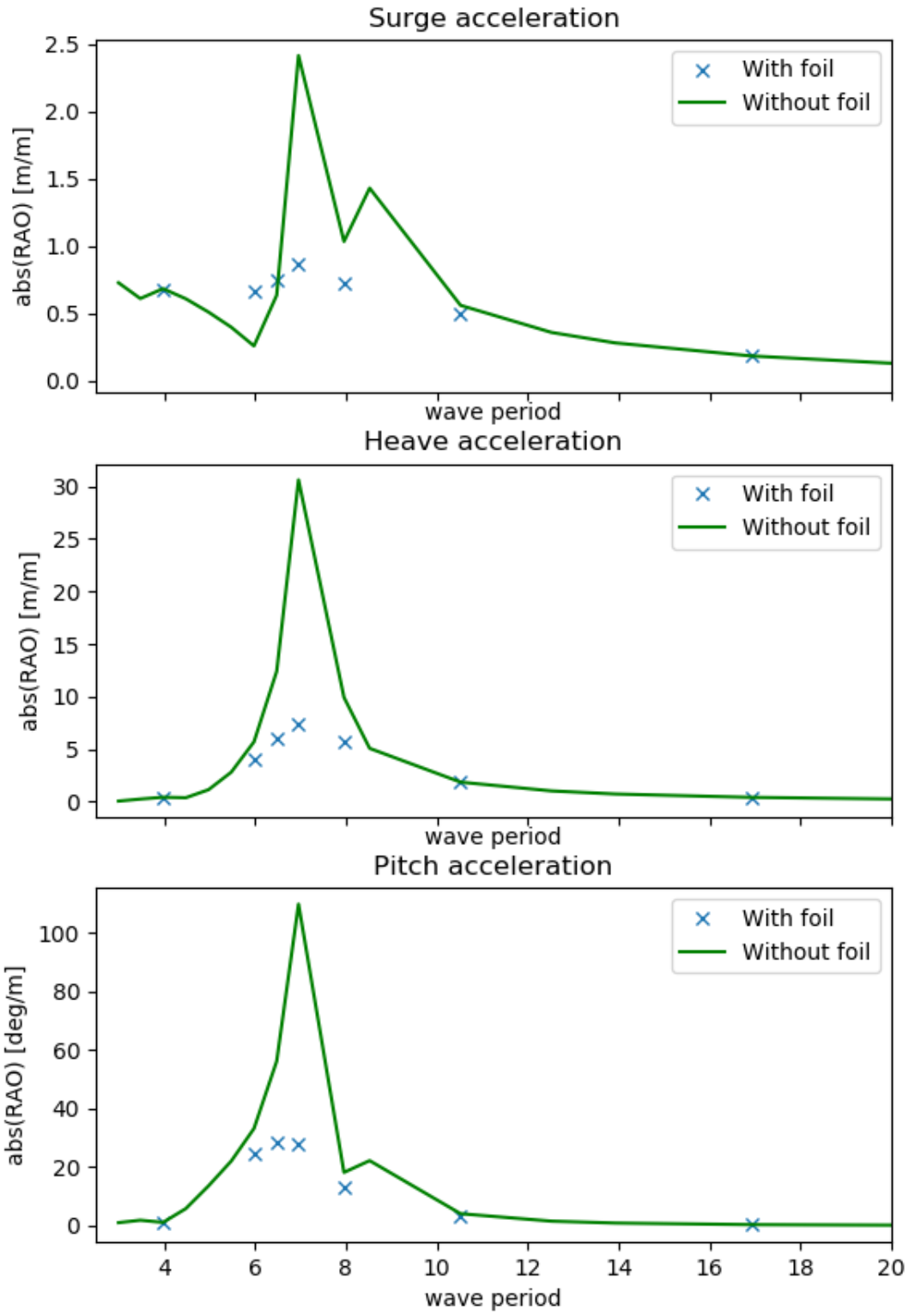

Figure 9.7: RAO for surge, heave and pitch acceleration, catamaran with foils, no control

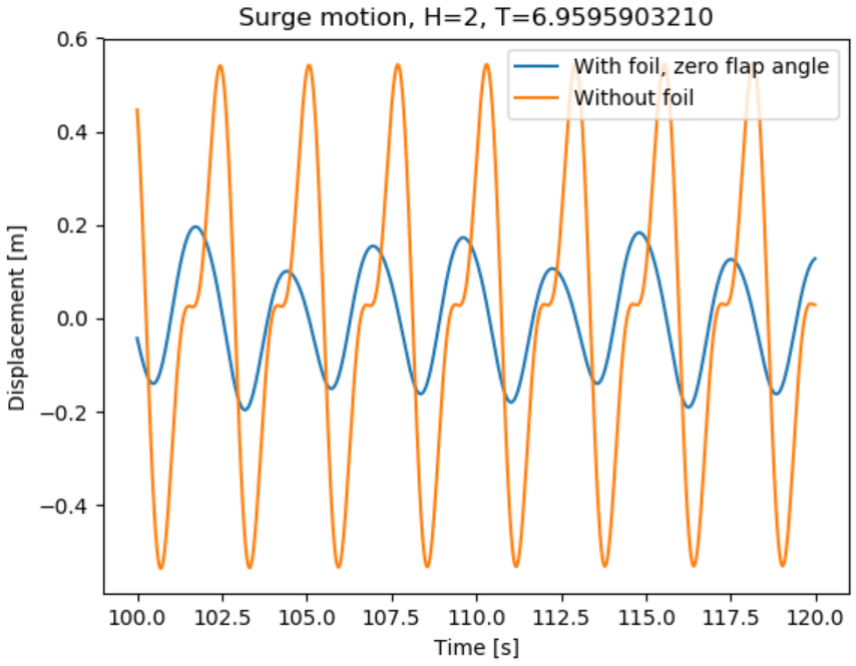

Figure 9.8: Surge motion time series, catamaran with foils, no control, H=2 m T=6.959590 s

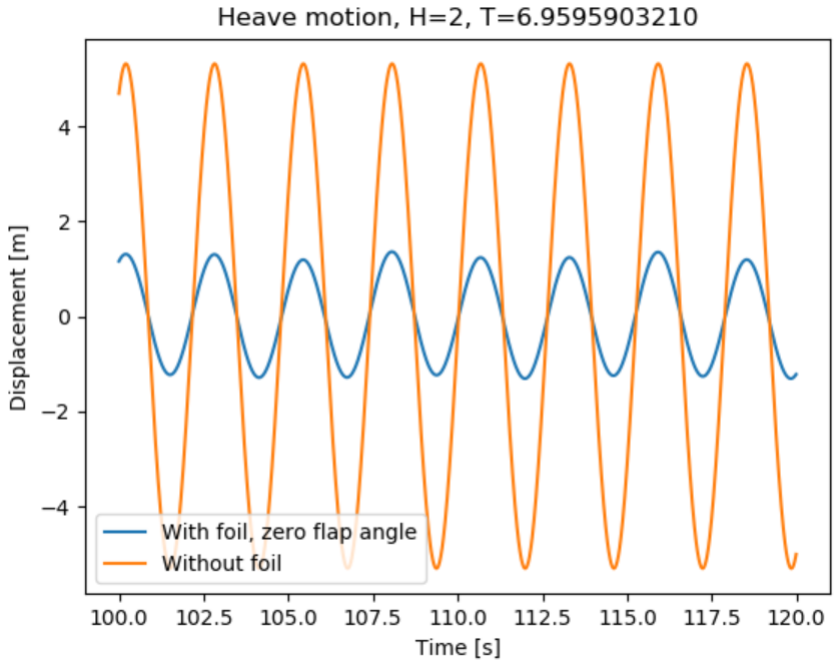

Figure 9.9: Heave motion time series, catamaran with foils, no control, H=2 m T=6.959590 s

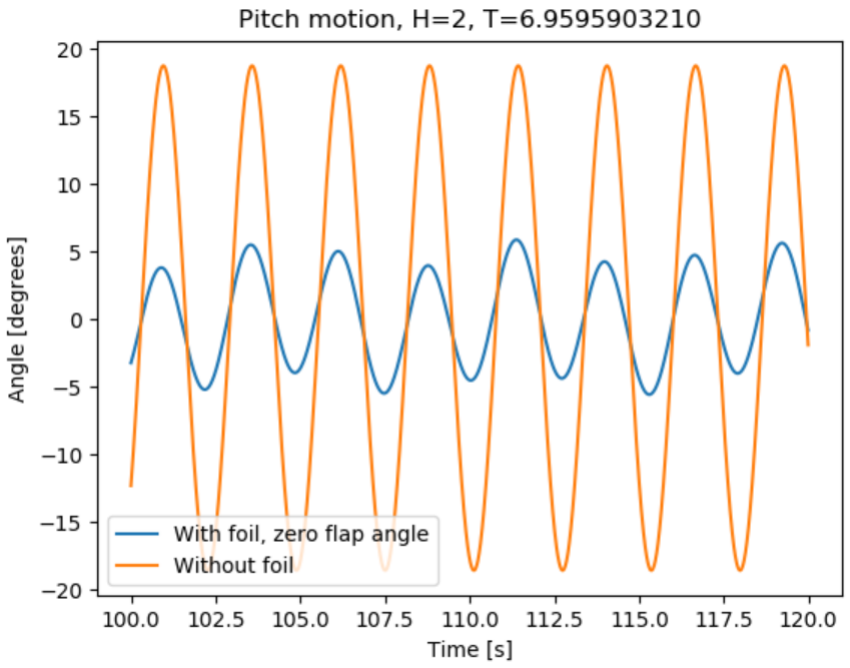

Figure 9.10: Pitch motion time series, catamaran with foils, no control, H=2 m T=6.959590 s

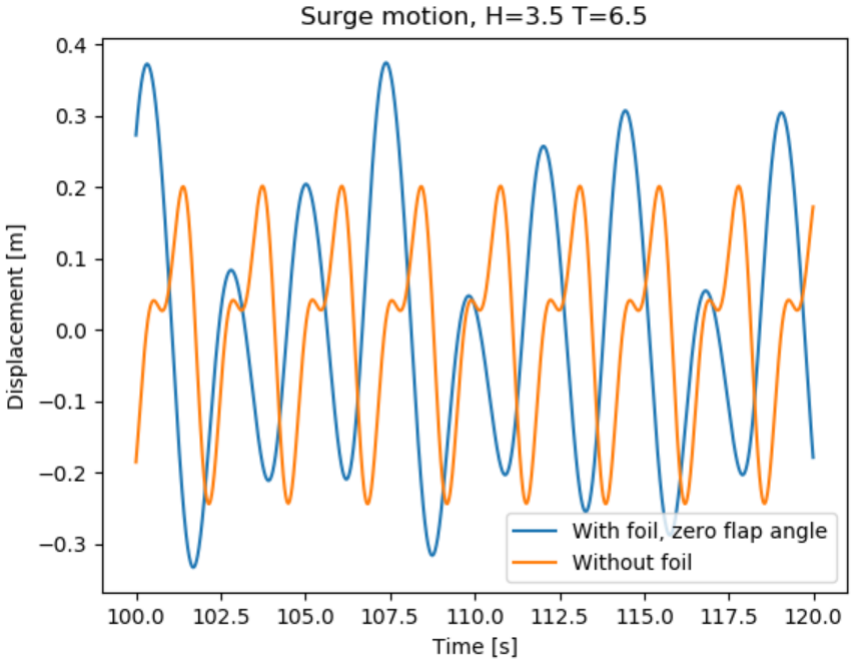

Figure 9.11: Surge motion time series, catamaran with foils, no control, H=3.5 m T=6.5 s

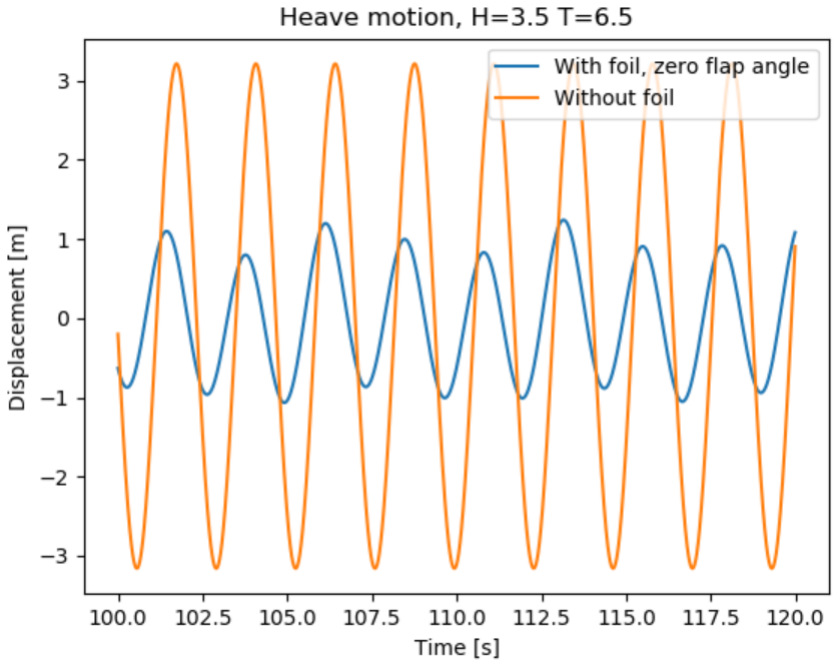

Figure 9.12: Heave motion time series, catamaran with foils, no control, H=3.5 m T=6.5 s

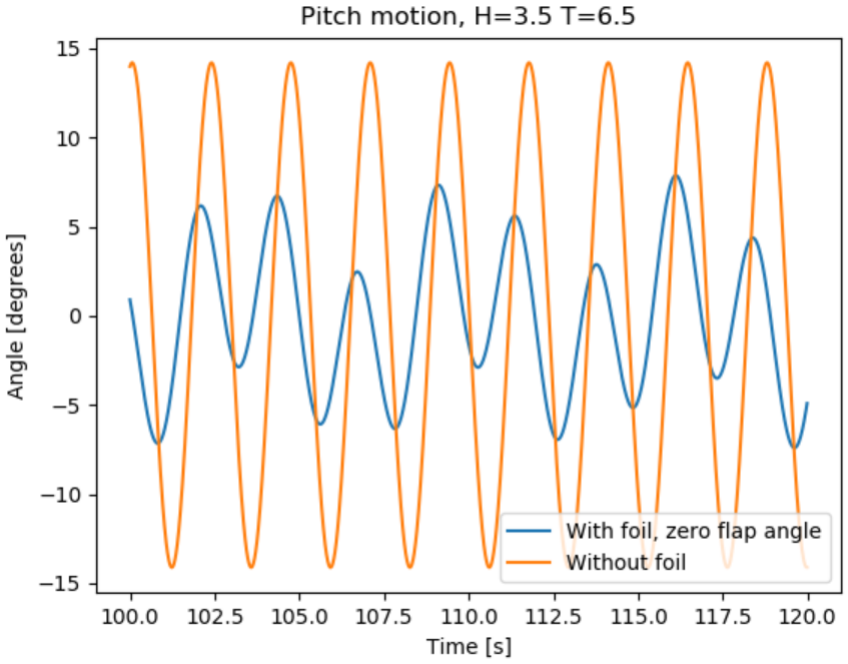

Figure 9.13: Pitch motion time series, catamaran with foils, no control, H_s=3.5 m T_z=6.5 s

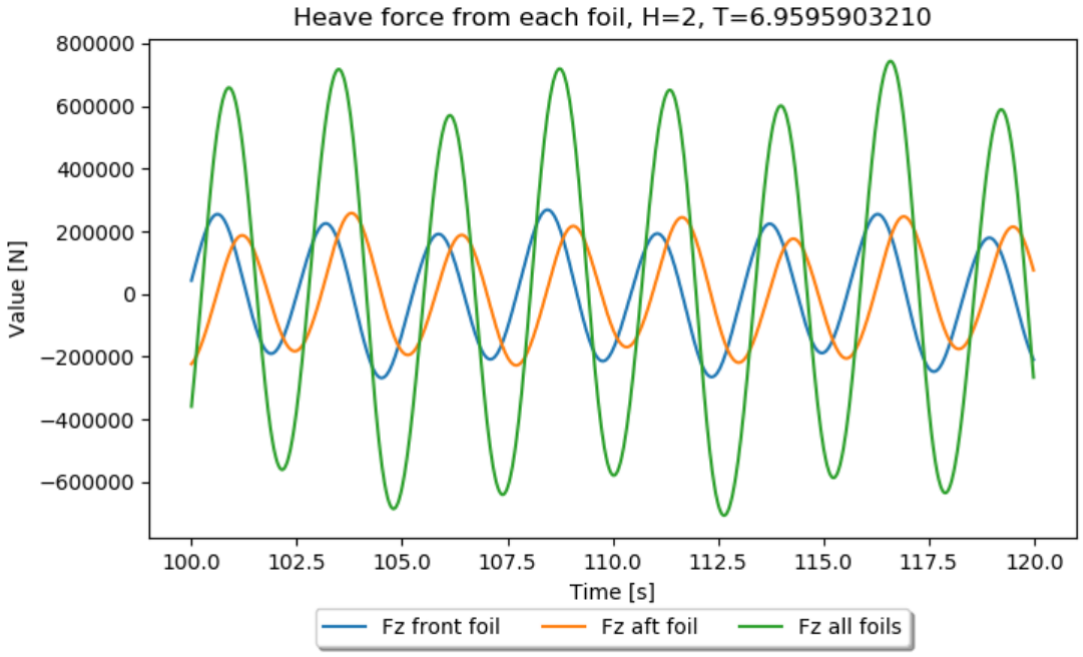

Figure 9.14: Heave force from separate foils, catamaran with foils, no control, H=2 m T=6.959590 s

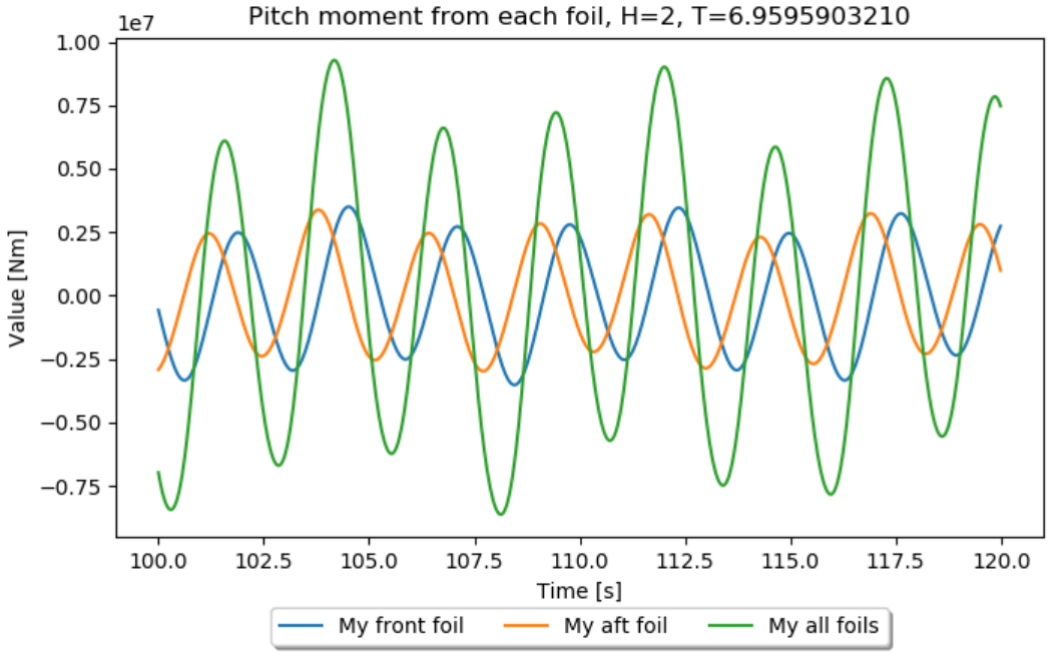

Figure 9.15: Pitch force from separate foils, catamaran with foils, no control, H=2 m T=6.959590 s

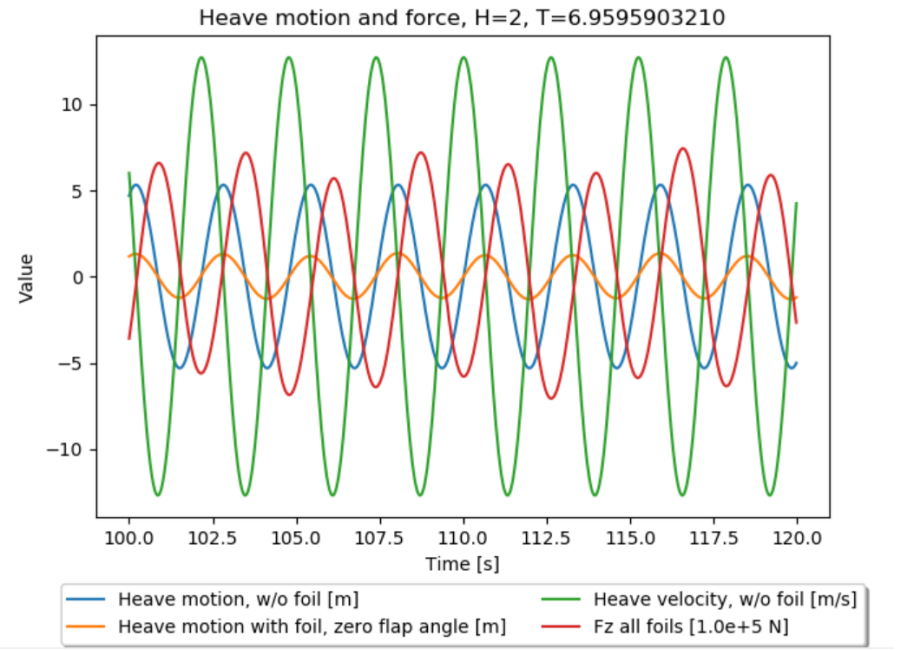

Figure 9.16: Heave motion and force, catamaran with foils, no control, H=2 m T=6.959590 s

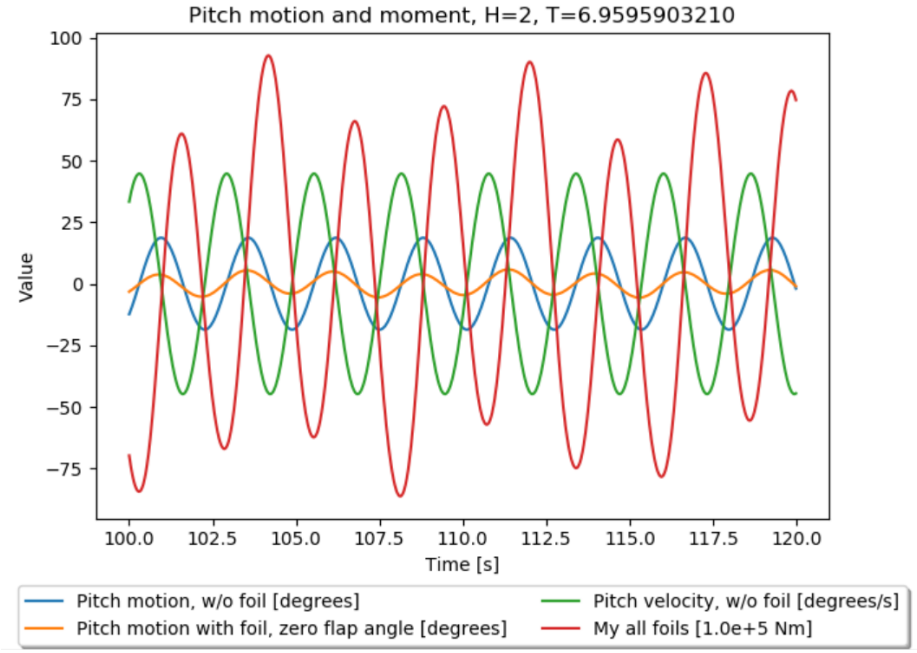

Figure 9.17: Pitch motion and force, catamaran with foils, no control, H=2 m T=6.959590 s

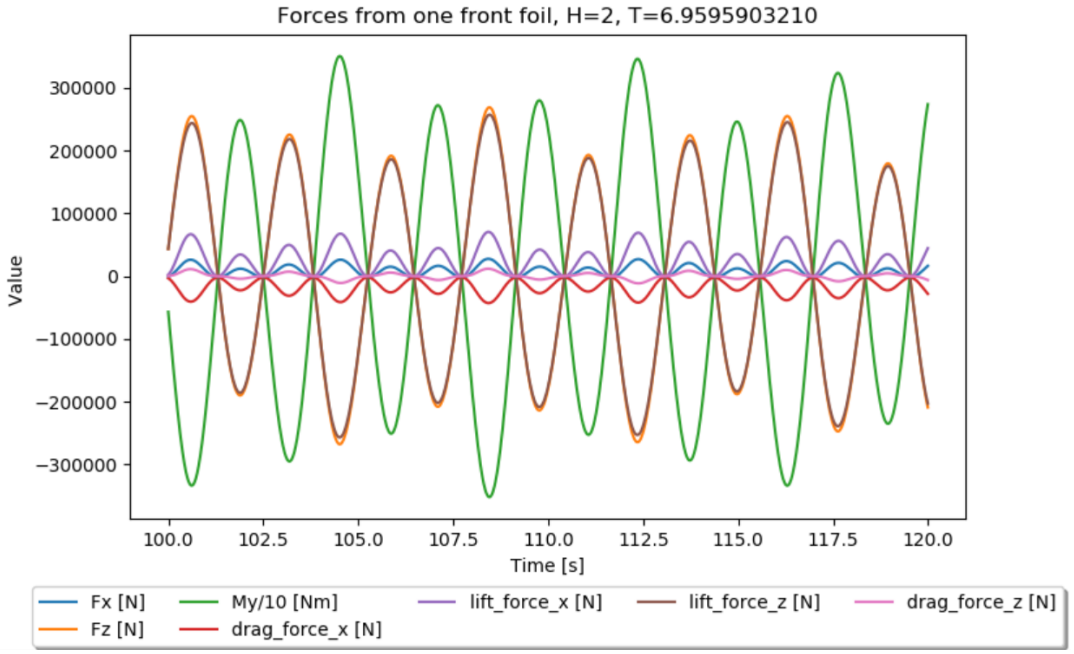

Figure 9.18: Forces from one front foil, catamaran with foils, no control, H=2 m T=6.959590 s

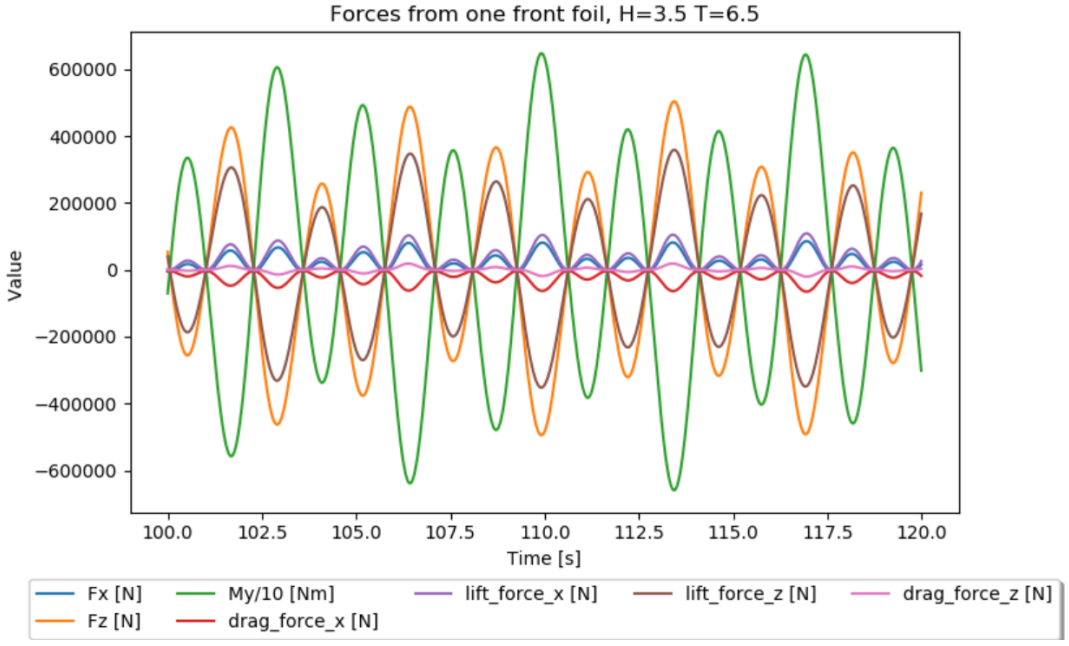

Figure 9.19: Forces from one front foil, catamaran with foils, no control, H=3.5 m T=6.5 s

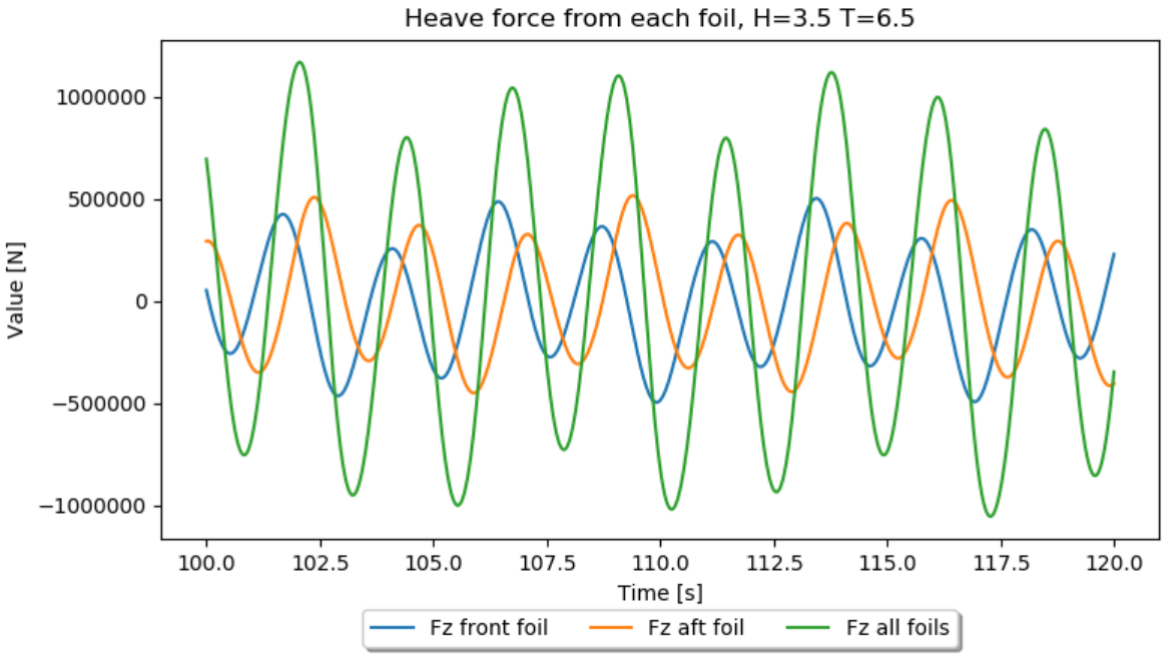

Figure 9.20: Heave force from separate foils, catamaran with foils, no control, H=3.5 m T=6.5 s

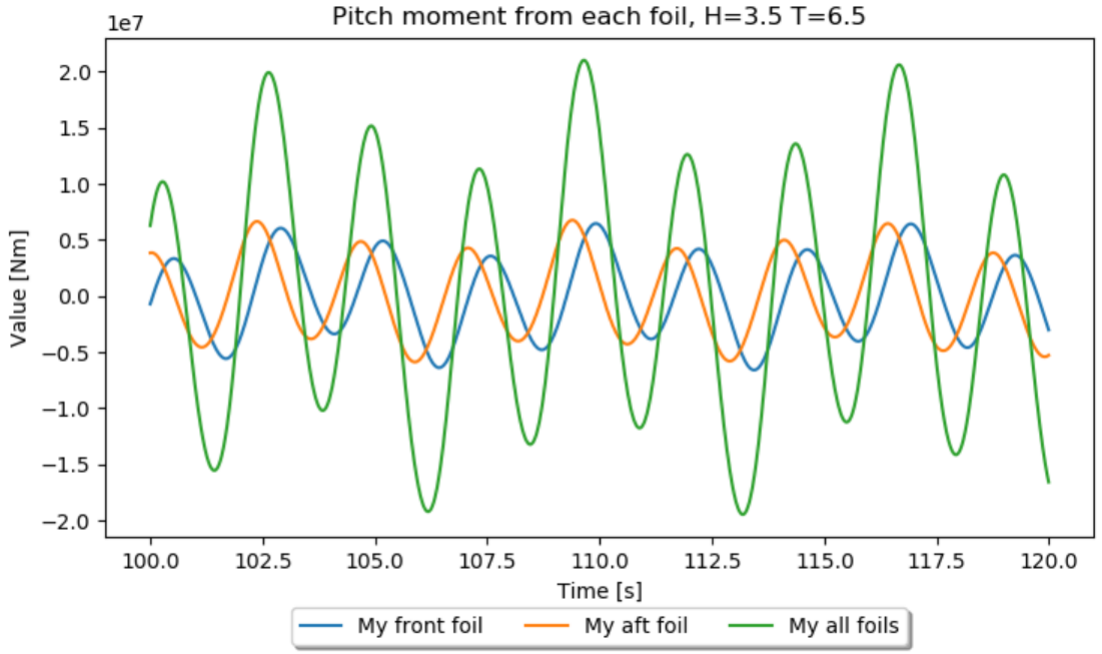

Figure 9.21: Pitch force from separate foils, catamaran with foils, no control, H=3.5 m T=6.5 s

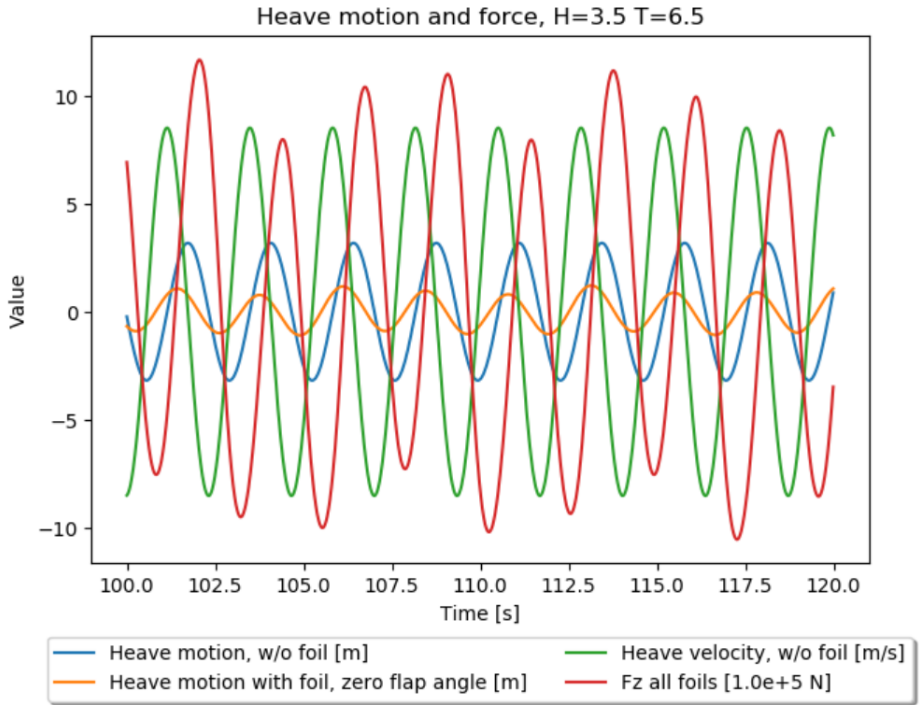

Figure 9.22: Heave motion and force, catamaran with foils, no control, H=3.5 m T=6.5 s

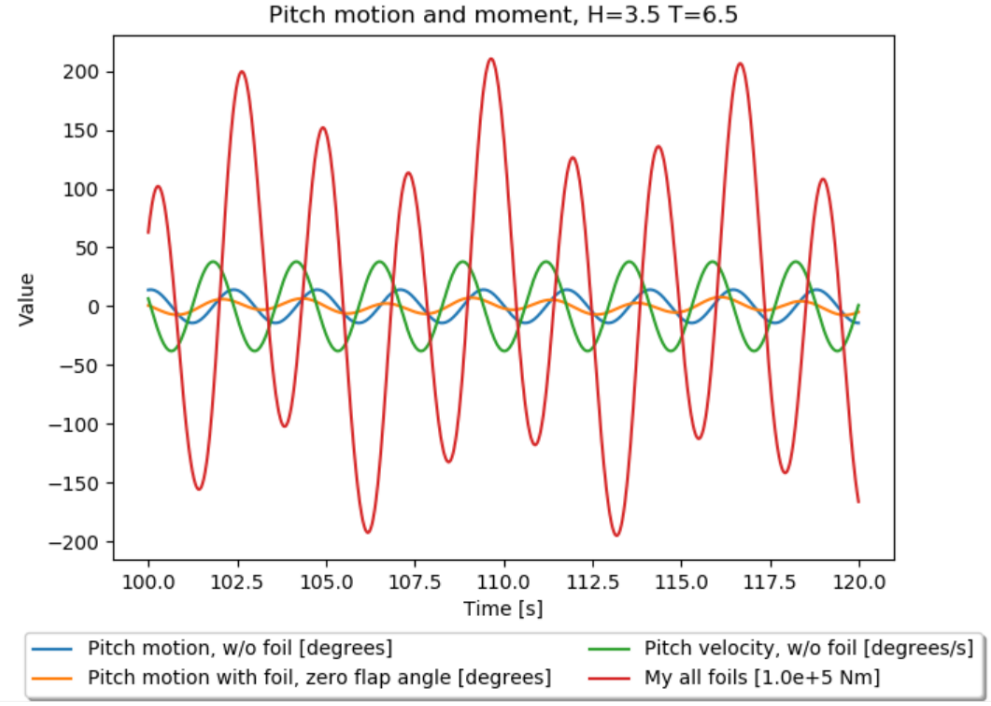

Figure 9.23: Pitch motion and force, catamaran with foils, no control, H=3.5 m T=6.5 s

The displacement RAOs in Figure 9.6 show that the passive foils provide significant damping in surge, heave and pitch for the sea states causing the most extreme displacements, meaning periods between 6 and 12. For periods below 6 and above 12, no visible damping effect was obtained from the foils. Therefore, a greater number of simulations were run for the area around the peaks. The largest damping is found for periods around the resonance frequencies of the vessel in head seas, $T \approx 7$ s. This is desirable as this is not only where the most extreme motions are initiated, but the corresponding sea states also occur frequently in the geographic area chosen. The acceleration RAOs depict the same tendency; visible damping around the resonance frequencies, and little damping outside of this area.

A foil system can induce a positive force in the x-direction functioning as added thrust. This extra thrust is a result of the quasi-steady analysis, as the lift force has a constantly positive horizontal component with the direction of the vessel speed. However, the possibility of additional viscous drag forces due to potential flow effects could influence this added thrust. These effects could cause drag due to the free vortex systems in the 3D flow and free-surface effects, which are not taken into account in this study. The thrust effect can be evaluated by analyzing the surge motions. *Waqum* had some inaccuracies regarding computing the mean surge position of the vessel, due to inconsistency in the already existing source code. Therefore, the mean value of the surge position was subtracted from the time series of the surge position in the plotting. As a result, the thrust effect could not be viewed from the change in the mean position of the surge position. However, for Figure 9.18 and 9.19, the resulting force in x-direction F_x is seen to be positive, which indicates an increase in the thrust. This effect can be seen to be larger for Wave 2. From Figure 9.8, the surge motion for Wave 1 can be seen to be damped with passive foils, while Figure 9.11 shows that the surge motion for Wave 2 is enhanced. This points to that the thrust effect may be greater for greater wave heights.

The heave motion can be seen to be reduced by approximately 2/3 for both waves from Figure 9.9 and Figure 9.12. In Figure 9.16 it can be seen that the resulting heave force from the foils is 180° out of phase with the heave velocity of the vessel without foil for Wave 1, which causes optimal damping. For Wave 2, the phase is not exactly 180°, resulting in less damping. From Figure 9.14 and 9.20 the resulting vertical foil force can be seen to have a slightly positive mean value, which indicates that the foils produce a resulting positive lifting effect in passive state. Whether this resulting lift force causes the deck to be lifted completely out of the water should be considered. However, as the resulting heave motion in whole is significantly damped by the foils, this should rather be addressed as part of the design the hull geometry than as a foil effect, as the risk is decreased regardless. However, as the draft of the vessel is 2.369 m, the risk is considered to be insignificant.

For Wave 2, the phase of the heave and pitch motion for the vessel with foil is a little shifted to the phase of heave and pitch motion of the vessel without foils. A simulation

was run changing the wave height parameter for Wave 1 to T=3.5 s, resulting in the wave T=3.5 s, H=6.959590 m, to investigate whether the cause of the shit was due to change in wave height or wave period. The heave and pitch motion time series are appended in Appendix B.1 and B.2. The figures show a tendency of a similar phase shift. However, the phase shift is not as large. This points to that it is both the increase in wave height and change in wave period causing this shift.

The time series for pitch show a reduction of the pitch motion of around 3/4 for both waves. As for heave, the resulting pitch moment from the foils is 180° out of phase with the pitch velocity, seen from Figure 9.15 and Figure 9.21. The pitch motion for the vessel with foils also has a similar effect as the lift motion regarding having a positive mean value. This is also seen from Figure 9.15 and 9.21. However, this effect can be seen to be small. This is as expected, as the foil actuating arms to the motion reference point are equal, resulting in balancing pitch moments. For both the heave and pitch time series, two frequencies are visible; one shorter with a period≈2, and the other considerably larger. To understand the frequency composition of the motions, power spectra were plotted. Figure 9.24 and 9.25 show the power spectra for the heave and pitch motion for Wave 1. A power spectrum describes the distribution of power into frequency components composing that signal. Therefore, the power spectrum depicts what frequencies a signal is made up of. Wave 2 gave similar spectra as the ones presented for Wave 1.

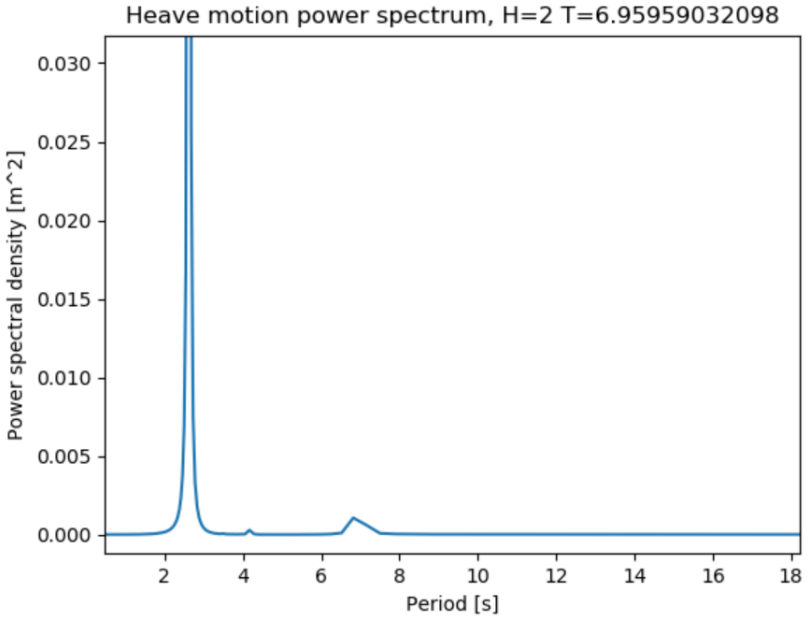

Figure 9.24: Power spectrum for heave motion, catamaran with foils, no control, H=2 m T=6.959590 s

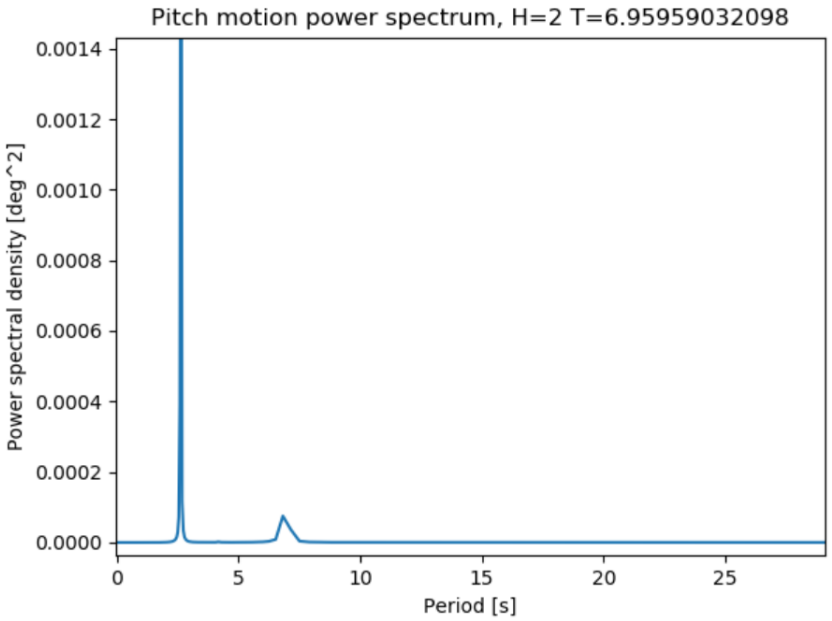

Figure 9.25: Power spectrum for pitch motion, catamaran with foils, no control, H=2 m T=6.959590 s

The motions for both heave and pitch can be seen to give very similar spectra. The main frequency component can be seen for $T \approx$2.5 s. This coincides with the encounter frequency $\omega_e \approx$2.5 1/s, computed from Equation 3.20. The other visible peak in both spectra is the peak for $T \approx$7 s. This frequency may be initiated by the angle of the inflow velocity $\Delta\alpha$, expressed in Equation 3.3, which is dependent on the heave motion. This may result in an effect corresponding to the effect of a spring with the frequency of the pitch resonance frequency. This frequency is ≈7 s, which can for instance be seen from the RAOs in Figure 9.6.

The time series for the accelerations for both waves are appended in Appendix B.3 to B.8. Overall, the trends of the acceleration results are similar to the trends of the motion time series with an overall significant reduction of acceleration, as seen in the RAO 9.7.

9.5 Seakeeping analysis with foil motion control

Seakeeping analyses were conducted on the catamaran with foils with controlled flaps using *Waqum*. RAOs, shown in Figure 9.26 and 9.27, were obtained for the vessel. The wave heights and periods in the RAOs are displayed in Table 9.10. These conditions are the same as used in Section 9.4. The simulation parameters are given in Table 9.11. The vessel with foil motion control was exposed to the regular waves in Table 9.12, the same waves as for the analysis with static foils in Section 9.4. Time series for surge, heave and pitch motions are presented in Figure 9.28 to 9.33. T are the wave periods and H the wave heights.

H_s [m]	2	2	2	2	2	2	2
T_z [s]	3.9798	5.9798	6.4798	6.9596	7.9596	10.5237	16.9192

Table 9.10: Regular waves for RAOs, seakeeping analysis with active foils

Maximum time	500s
Δt	0.01
Wave heading	180°
Vessel speed	35kn

Table 9.11: Simulation Parameters, seakeeping analysis with active foils

H [m]	T [s]
2	6.95959
3.5	6.5

Table 9.12: Regular waves, seakeeping analysis with active foils

A maximum flap angle of 20° and a maximum rate of change from -20° to +20° per seconds is included. The flap angles are presented in Figure 9.34 and 9.35. The flap forces and moments were compared to the forces and moments created by the passive part of the foils in Figure 9.36 to 9.41.

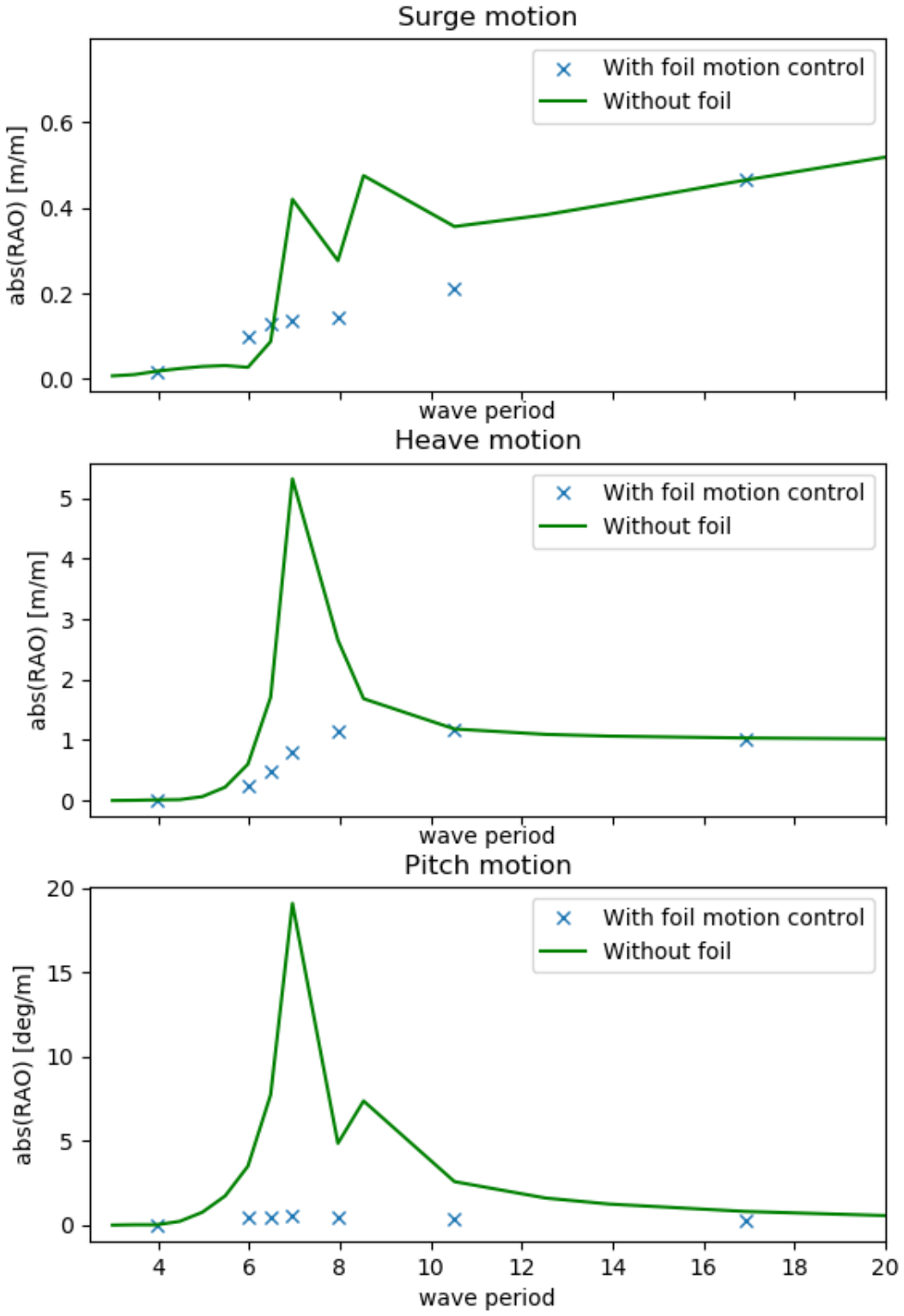

Figure 9.26: RAO for surge, heave and pitch motion, catamaran with foils, with control

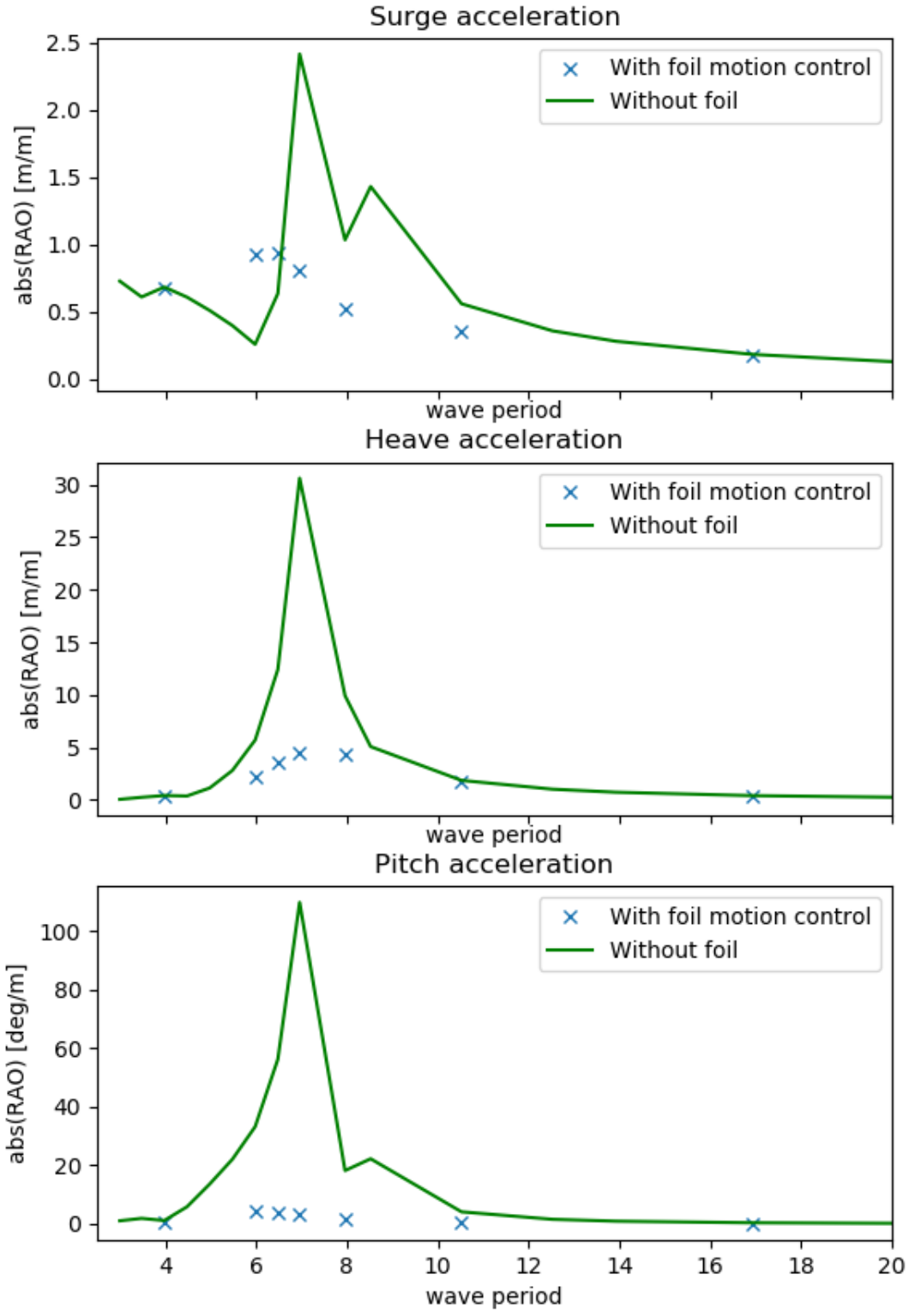

Figure 9.27: RAO for surge, heave and pitch acceleration, catamaran with foils, with control

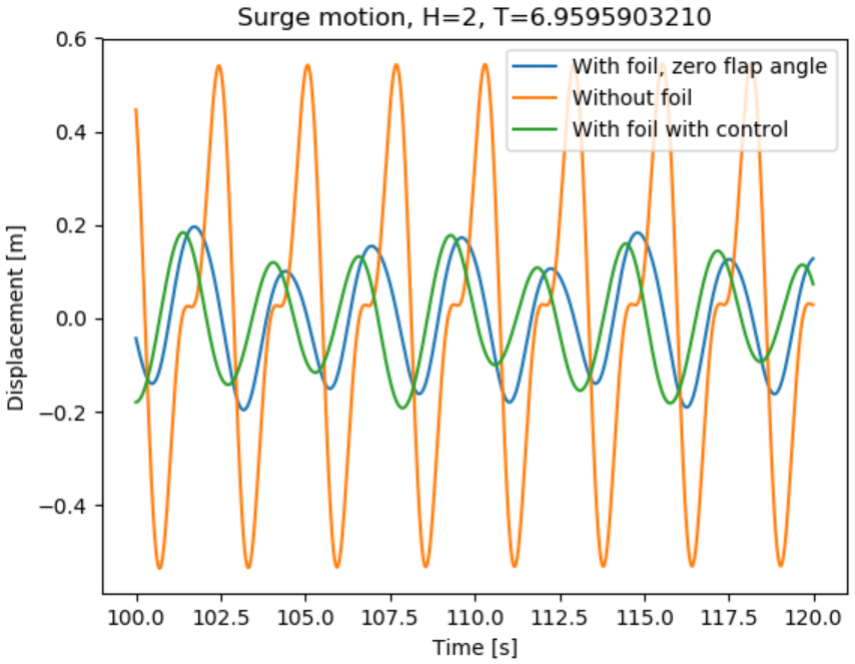

Figure 9.28: Surge motion time series, catamaran with foils, with control, H=2 m T=6.959590 s

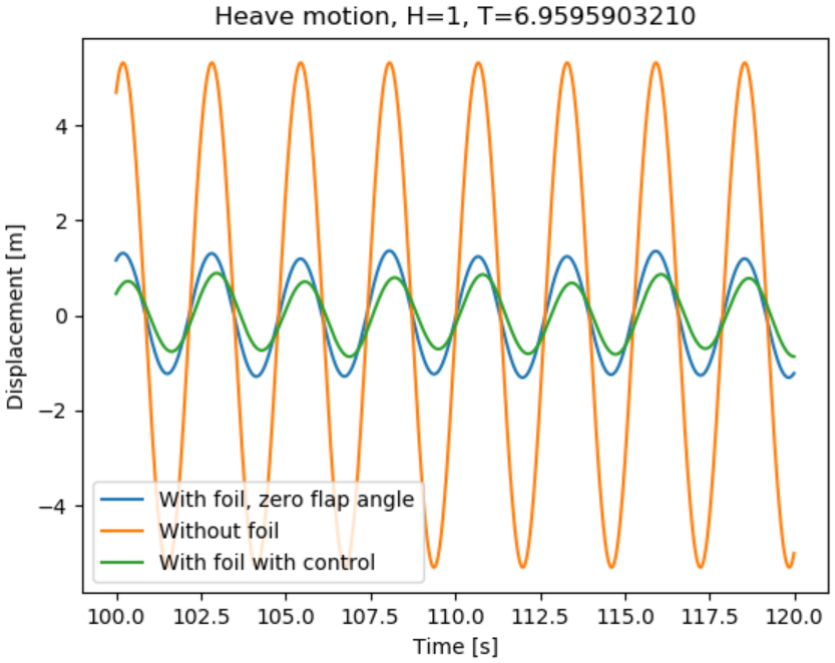

Figure 9.29: Heave motion time series, catamaran with foils, with control, H=2 m T=6.959590 s

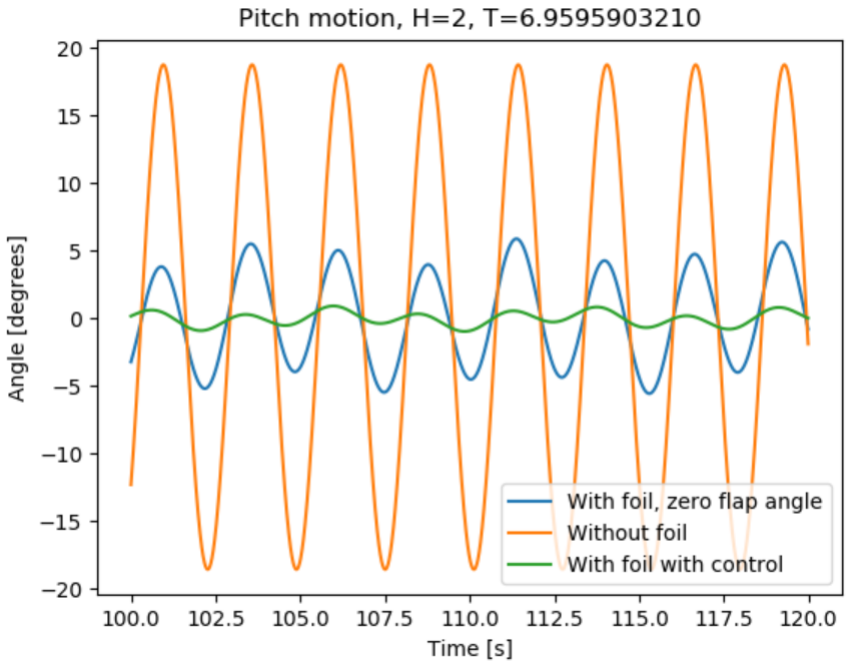

Figure 9.30: Pitch motion time series, catamaran with foils, with control, H=2 m T=6.959590 s

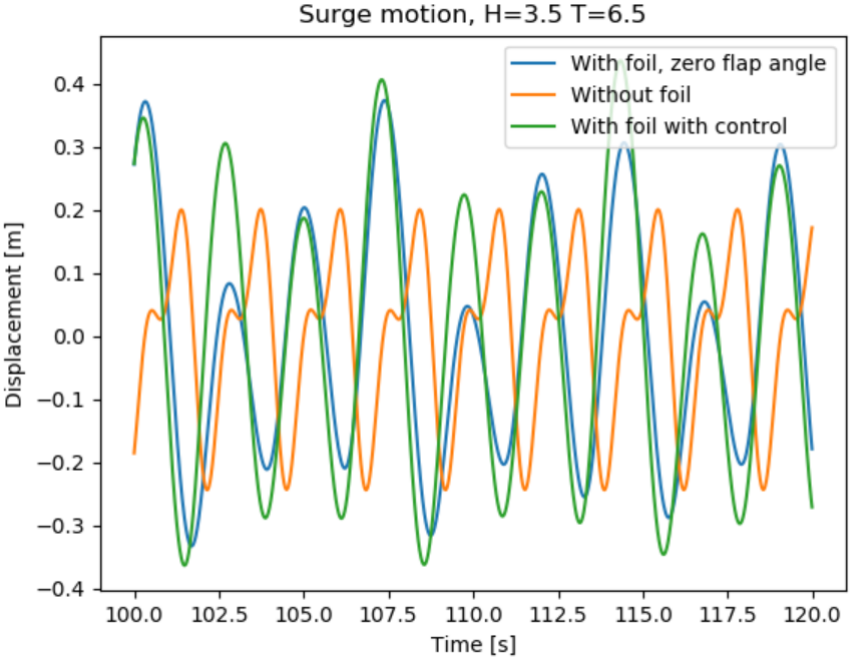

Figure 9.31: Surge motion time series, catamaran with foils, with control, H=3.5 m T=6.5 s

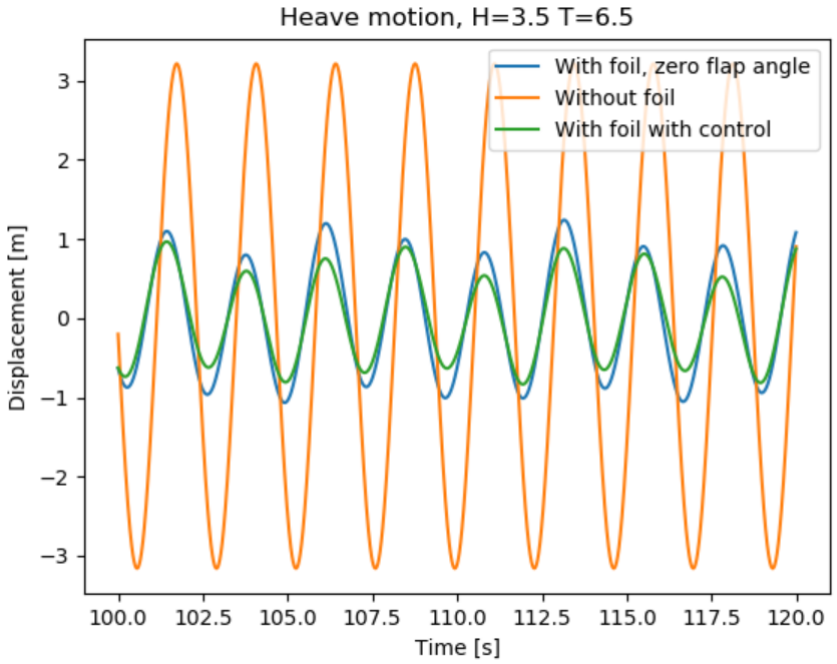

Figure 9.32: Heave motion time series, catamaran with foils, with control, H=3.5 m T=6.5 s

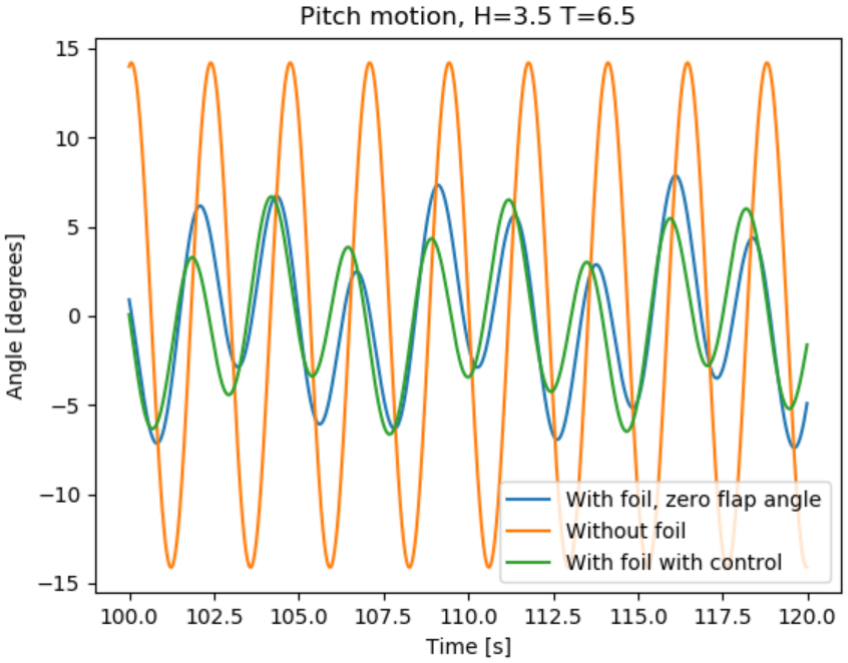

Figure 9.33: Pitch motion time series, catamaran with foils, with control, H=3.5 m T=6.5 s

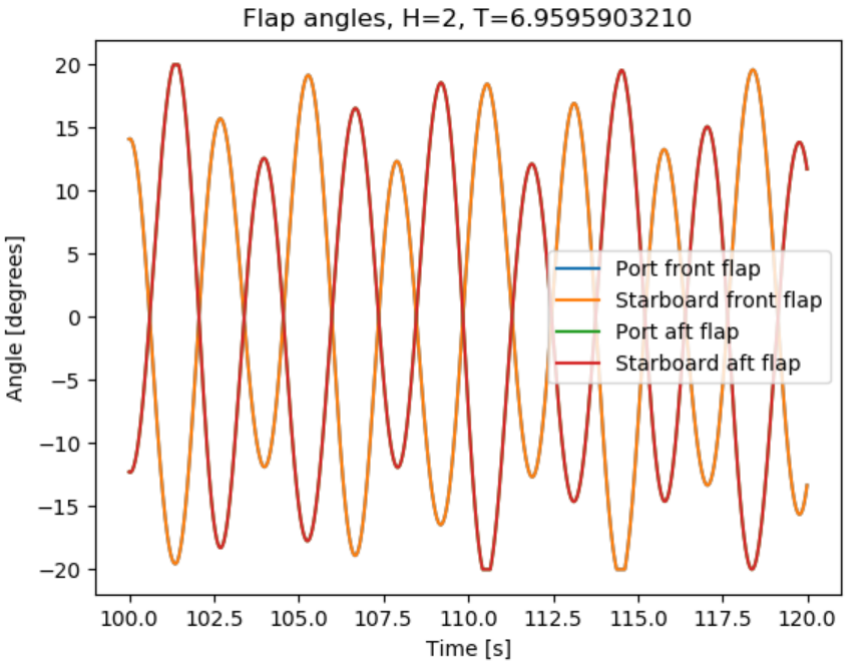

Figure 9.34: Flap angles, H=2 m T=6.959590 s

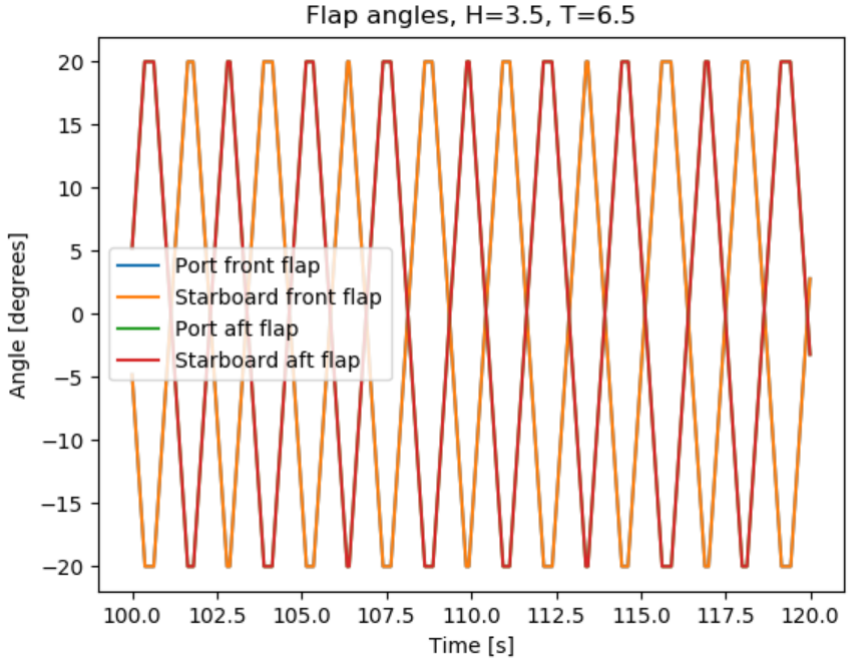

Figure 9.35: Flap angles, H=3.5 m T=6.5 s

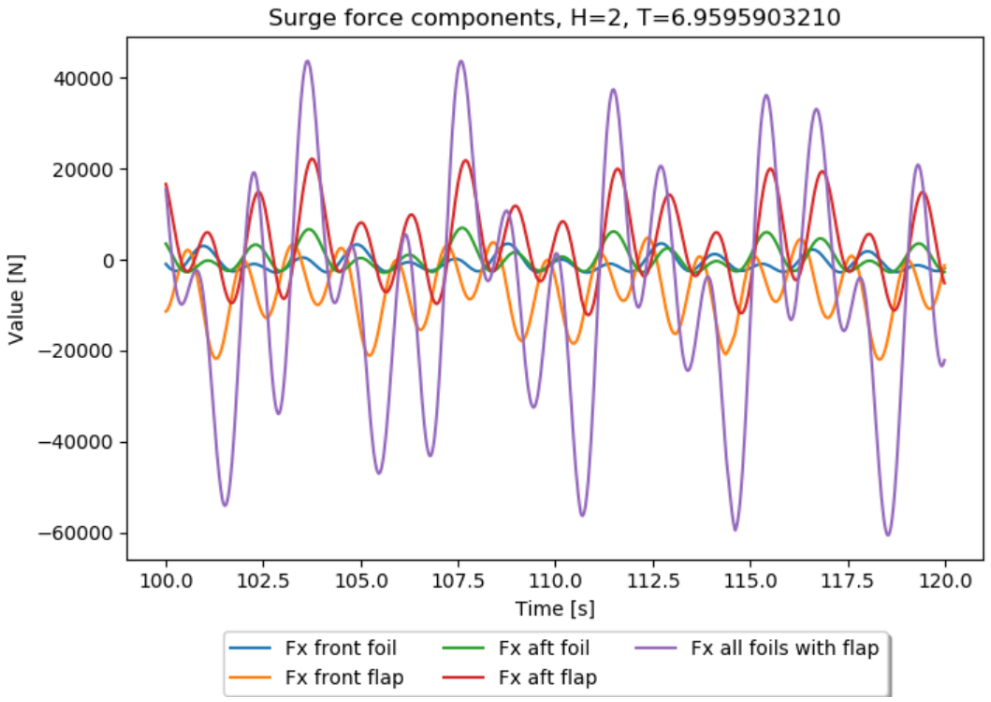

Figure 9.36: Surge force components foil and flap, H=2 m T=6.959590 s

Figure 9.37: Heave force components foil and flap, H=2 m T=6.959590 s

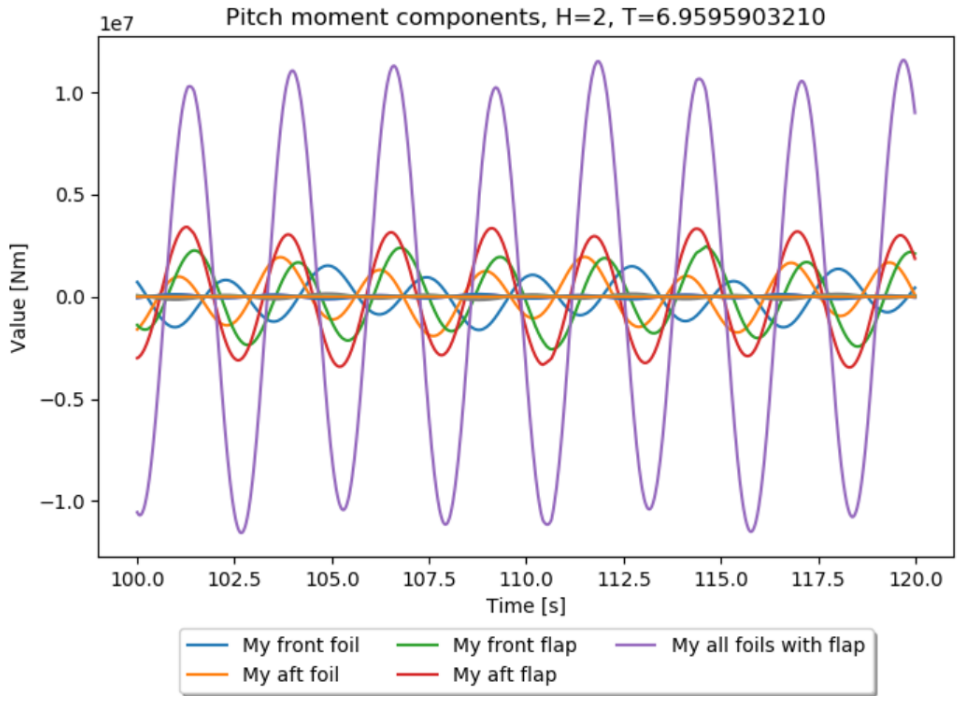

Figure 9.38: Pitch force components foil and flap, H=2 m T=6.959590 s

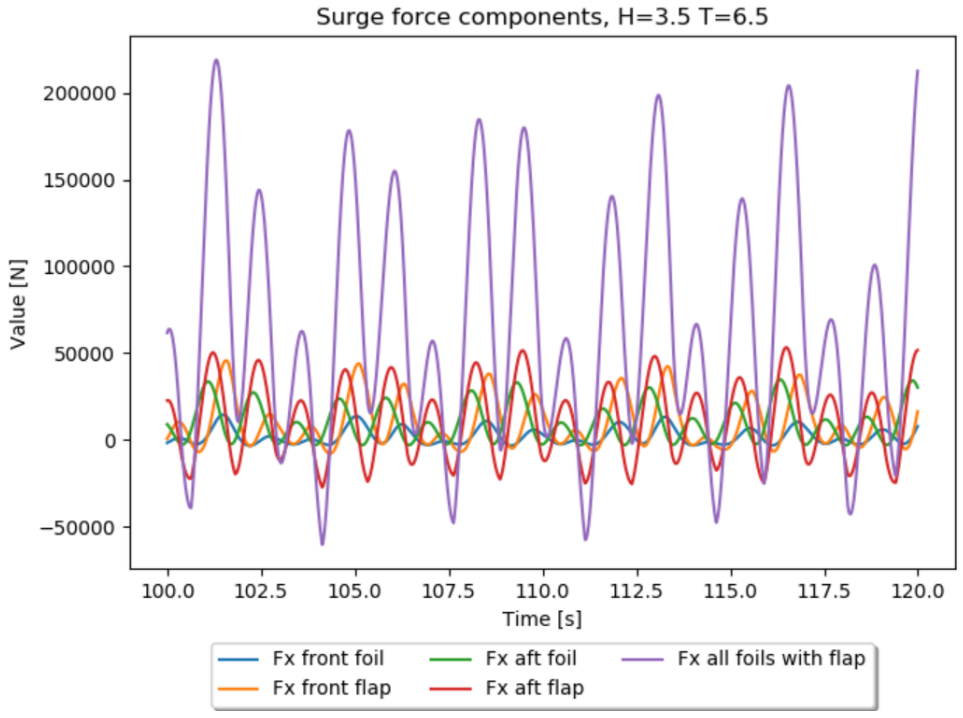

Figure 9.39: Surge force components foil and flap, H=3.5 m T=6.5 s

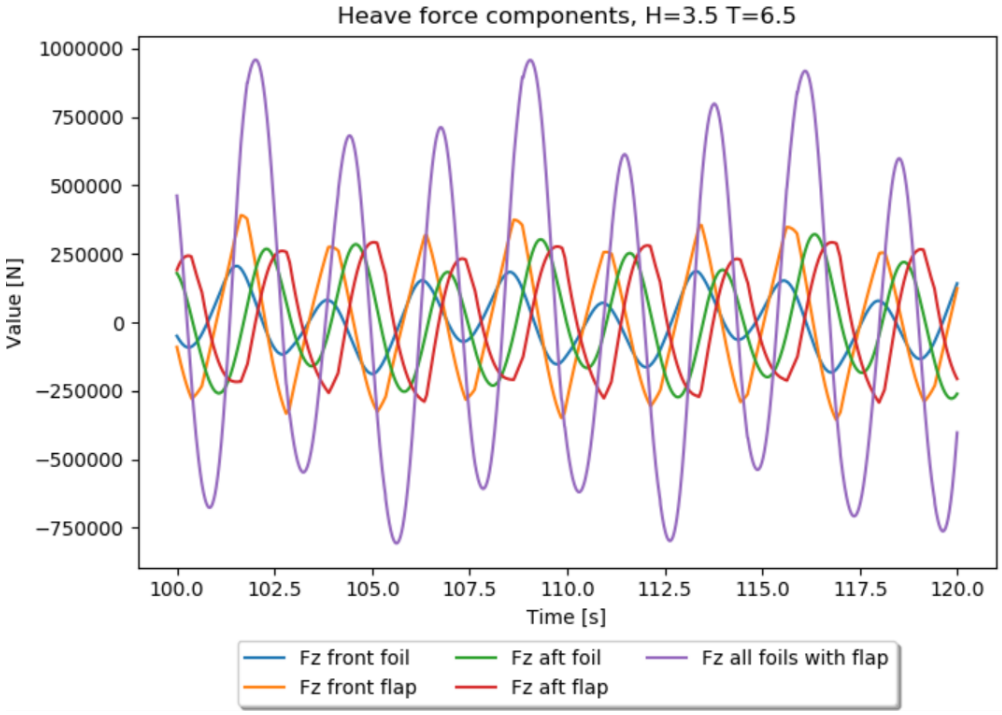

Figure 9.40: Heave force components foil and flap, H=3.5 m T=6.5 s

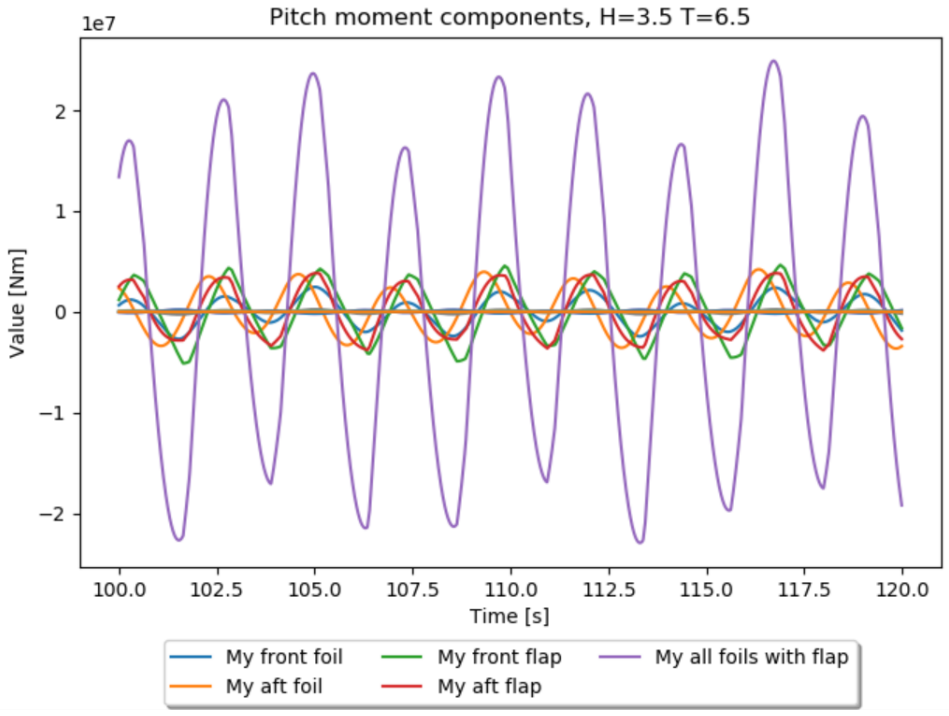

Figure 9.41: Pitch force components foil and flap, H=3.5 m T=6.5 s

The controller was tuned to provide damping in pitch while creating zero lift and surge force. From the motion RAOs in figure 9.26 and the time series in Figure 9.30, this goal can be seen to be very well achieved. In pitch, the motions and accelerations are reduced to practically zero, and the resonance is killed. As heave and pitch are coupled degrees of freedom, the reduction in pitch motion also leads to damping in heave, which is desirable. The reduction of motion in pitch and heave leads to a corresponding reduction of the acceleration in heave and pitch. This leads to a significant decrease in the probability of motion sickness. The surge motion and acceleration is also considerably reduced. The time series for the acceleration can be found in Figure B.3 to Figure B.5. The same frequency components can be observed in the time series as discussed in Section 9.4. Overall, the foil motion control system has a satisfactory influence on the vessel when exposed to Wave 1.

The surge motion for both waves is not changed much with regards to amplitude, shown by Figure 9.28 and 9.31. The phase is, however, slightly shifted. When viewing the horizontal force F_x in Figure 9.36 and Figure 9.39, the results differ for each of the waves. For Wave 1, the surge force is predominantly negative, while for Wave 2 it is generally positive. This points to, as mentioned in Section 9.4 that the initialized thrust effect increases with increasing waves. The negative horizontal force is due to the flaps creating a negative drag force when producing the heave force and pitch moment. Decreasing the angle of the flaps, and therefore, the pitch moment and heave force would also decrease the drag force. When operating in different sea states, the maximum flap angle or controller gain should be altered for optimal operation.

Figure 9.34, which shows the angles of the flaps for Wave 1, illustrates that the two flaps located fore, and the two flaps located aft, move correspondingly in pairs. This is as expected when the control goal is decreasing the pitch motion. The period of the motion of the foil flaps is T=2.5 s, coinciding with the encounter frequency and pitch motion frequency. The phase of the aft and fore flaps is 180°, as the foil actuating arms are equal in value but opposite in sign, maximizing the available pitch moment caused by the flaps. From Figure 9.37 and 9.40 it can be seen that the vertical forces of the aft and fore flaps are approximately 180° out of phase, following the phase of the flap angles, while the pitch moment caused by the flaps, in Figure 9.38 and Figure 9.41, are more or less in phase.

For Wave 1, the controller could have been tuned further to create larger damping, as the foils only operate at the maximum allowed angle (20°) at a fraction of the time. However, doing this would also cause a further increase in the drag forces. Therefore, these decisions should be made considering what the main goal for the operation is, whether it is limiting the motions as much as possible, or in general, increasing the operability and thrust of the vessel. In the simulations, the effective flap angle is a sum of the effective foil angle and the flap angle. In the control allocation algorithm, the effective foil angle was not taken into consideration. This is possibly the cause of the flap moments and forces being

larger for the fore foils than for the foils aft.

For Wave 2, the flaps operate at the saturation point. This can be seen in Figure 9.35. The forces produced by the flaps are therefore abruptly "cut off" when the maximum flap angle is reached, causing nonlinearities. The forces produced by the flap angles can from Figure 9.40 and 9.41 be seen to be pointy and uneven due to this saturation of the angles.

The motion in heave and pitch is only slightly reduced with the inclusion of motion control for Wave 2, shown by Figure 9.32 and Figure 9.33. This is most likely due to the flaps reaching saturation, and the flaps not being allowed to produce the desired control force. To increase the influence of the controlled flaps, a more fitting control algorithm could be found, or the geometry of the flaps could be altered to produce larger damping forces and moments. However, the current influence of the foils with controlled flaps is considered satisfactory for the study, as the responses overall are decreased significantly.

In addition to the results presented, a PD-controller, PI-controller, and PID-controller were tested in the phase of selecting a final controller. However, the results obtained for the other controller types showed to be less satisfactory than for the pure D-controller with regards to pitch motion control. As pitch motion reduction was selected the main goal of the study, the D-controller was kept as the final controller.

9.6 Vertical motion at bow

Pitch motion induces vertical motions that will be largest at the bow. This can be both uncomfortable for passengers, and can lead to phenomena such as slamming and deck-diving. Reducing the vertical motion at the bow is, therefore, an important aspect of pitch motion control. The vertical motion of the point $[L, 0, z_{mrp}]$, where L is the length of the vessel and z_{mrp} is the z-coordinate of the motion reference point, is shown in Figure 9.42. The results are for Wave 1: H=2 m, T=6.9595903210 s.

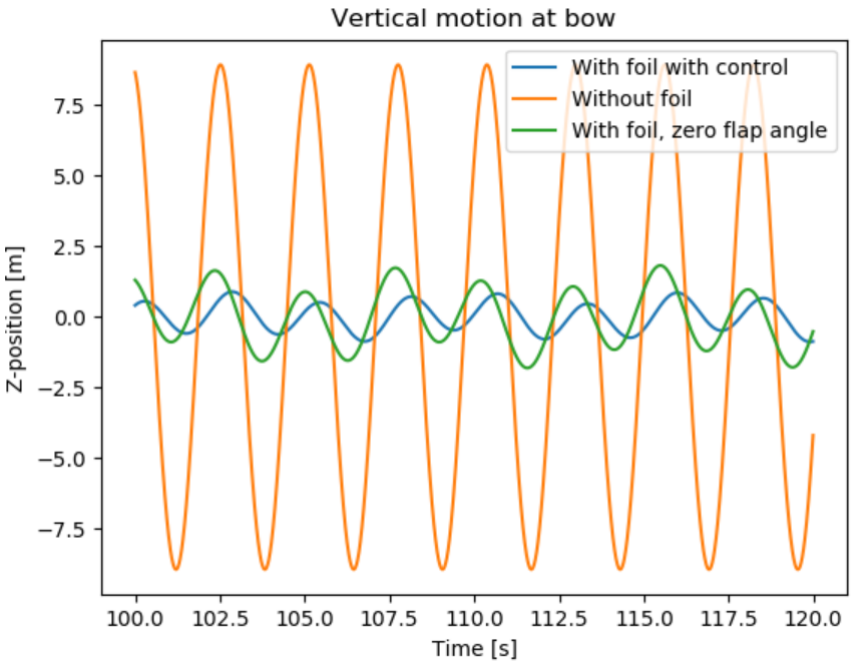

Figure 9.42: Vertical motion at bow

The vertical motion can be seen to be heavily reduced with the use of passive foils, and even further reduced with the use of foil motion control. This indicates that the risk of slamming and deck-diving is significantly reduced for the vessel with the foil motion control system.

9.7 Quantification of results

To quantify the influence of the passive and active foil system, the root-mean-square (RMS) and reduction efficiency ratio (ER) for the time series for heave and pitch motion were calculated. The RMS indicate the ensemble characteristics for the time series, and is defined as Equation 9.1 for a given time series $\{x_1, x_2 \ldots x_n\}$ where μ is the mean value and n the number of elements, Huang et al. (2018). The root-mean-square values and ERs for heave and pitch motion for a selection of regular waves are presented in Table 9.13 and Table 9.14.

$$RMS = \sqrt{\frac{1}{N}\sum_{i=1}^{n}(x_i - \mu)^2} \tag{9.1}$$

λ/Lpp	T [s]	H [m]	No foils [°]	Passive foils [°]	ER%	Active foils [°]	ER%
1.95	6.95	2	13.10	3.43	73.81	0.49	96.25
1.75	6.5	2	5.46	2.92	46.52	0.47	91.39
1.75	6.5	3.5	10.03	4.19	58.23	3.67	63.41

Table 9.13: Reduction efficiency ratios of pitch angle RMS in regular waves

λ/Lpp	T [s]	H [m]	No foils [m]	Passive foils [m]	ER%	Active foils [m]	ER%
1.95	6.95	2	3.78	0.91	75.93	0.56	85.19
1.75	6.5	2	1.22	0.59	51.64	0.35	71.31
1.75	6.5	3.5	2.25	0.71	68.44	0.53	76.44

Table 9.14: Reduction efficiency ratios of heave motion RMS in regular waves

For H=2 m, T=6.95 m, the reduction efficiency ratio is 96% in pitch and 85% in heave. As this is the wave initiating the most significant responses for the vessel, it is here the highest damping should occur for a well functioning foil motion control system. For H=3.5 m, T=6.5 s, the reduction efficiency ratio is 63% in pitch and 76% in heave. The study *Ship pitch-roll stabilization by active fins using a controller based on onboard hydrodynamic prediction* by Huang et al. (2018) can be used for conceptual comparison of the obtained reduction efficiency ratios. In this study, a foil motion control system was simulated numerically in regular waves obtaining the ER for pitch motion for λ/Lpp=1.75 and H=0.6 m. In the mentioned study, the ER was found to be 30.90 for the uncontrolled to the controlled angles. In this thesis, the ER is approximately three times the size. However, several simplifications were done with regards to the computation of the foil loads. It is unknown whether Huang et al. (2018) included similar relevant simplifications. In addition, several parameters differ in the studies regarding for instance the vessel geometry. Therefore, a direct comparison can not be made. However, the paper can be used as an indication that the foil motion control system in this thesis is very efficient concerning the control goal.

9.8 Discussion of method

The geometry selected is considered relevant concerning operational areas and speeds. Design decisions were made with inspiration from similar existing operating vessels. This points to that the market for foil motion control of vessels as the one investigated here is definitely existing. As for the dimensioning of the submerged foil system, *Hydrodynamics of High-speed Marine Vehicles* by Faltinsen (2006) was used thoroughly. Simplifications and assumptions were assessed such that a solid foundation was set for implementation in the seakeeping solver. These simplifications, such as the inclusion of 3D effects, could have been investigated further for increased verification.

The construction of the vessel model was based on geometry from another file format where coordinates for bow and stern were not included. Therefore, the bow and stern were created simply from visual comparison with the line drawings and with inspiration from similar vessels. As seen in Figure 1.2 a considerable amount of the geometry is above the waterline, and is not included in the computations as the software only takes the geometry below the waterline into consideration. However, as also a part of the geometry in bow and stern is located below the waterline, this may lead to inaccuracy in the results.

When selecting the foil geometry, more emphasis could have been put on evaluating the parameters and decisions concerning the relevant environmental conditions. A relevant area was identified for the study, and the statistical environmental conditions in this area were found. Therefore, the foil system could have been assessed with respect to typically sized loads in this environment. As the study was not considered an optimization study, the emphasis was instead put on understanding the mathematical equations. However, re-evaluating the foil parameters on the background of the environmental conditions would most likely have provided better results with regards to foil pitch damping.

A rather simple controller was selected for the study. More research could have been done with regards to selecting a more robust control strategy. The final controller limits pitch very well, which was the selected control goal. However, more time could have been devoted to combining this control goal with other desirable effects, such as for instance decreasing the global loads.

The meshing was executed following the meshing rules and guidelines for structures in *Wasim*. The mesh was compared qualitatively to the meshing of a similar structure used by DNV GL, and a mesh convergence study was executed selecting a suitable grid for the geometry. A position test was run using *Wasim Harmonic* balancing the mass and geometry and checking the numerical stability of the model. Through this test, the quality of the mesh was assessed and found to be sufficient.

The RAOs obtained from *Wasim* were validated by comparison with RAOs for a high-

speed catamaran found in the works by Faltinsen (2006). In retrospect, additional methods could have been considered for verifying the created model and the results obtained. The foil loads were computed according to two different computational methods corresponding to the theory presented by Fossen and by Faltinsen. The results obtained showed to be equal, and the mathematical equations for calculating the angle of attack for computing the foil loads was therefore considered validated.

Waqum was used as the solver for executing the sea-keeping analyses. *Waqum* is mainly built for larger vessels operating at lower Froude numbers. The model used in this study is a rather short vessel operating at a relatively high Froude number. As a result, some effects of importance for high-speed vessels may not be included in the program. This may lead to inaccuracy of the results obtained. Another issue encountered, that may be the cause of inaccurate results, was the numerical instability of the geometry encountered executing the sea keeping analyses in *Waqum*. This instability was solved by adding a spring with damping in surge, and as the RAO's obtained with this damping were found equal to the RAOs from *Wasim*, this was assumed to be a satisfactory solution.

Chapter 10

Conclusion

A high-speed catamaran was selected for the study of the effect of foil motion control. This high-speed catamaran was modeled for numerical investigation, and hydrodynamic simulations were executed to validate the numerical model. The results were validated with results from earlier relevant studies, and the responses were found to be similar in both shape and size. This pointed to that the geometry of the catamaran is modeled satisfactorily for the purpose.

An underwater fore-aft foil system was selected and defined in terms of geometry and positioning. This geometry was assessed with respect to the forward speed, and simplifications and assumptions were discussed. The foil loads were implemented in the seakeeping solver, and the influence of the foil loads on the mean catamaran configuration was investigated. However, as little change in trim with an increase in speed was found due to inaccurate numerical computational methods, only an increase in resistance could be observed in still water.

A seakeeping analysis of the vessel with zero flap angle was executed to investigate the influence of passive foils on the catamaran motions in waves. The static foils were found to provide a significant surge, heave and pitch damping both of the vessel motions and accelerations, reducing the risk of seasickness. The passive foil system was also seen to produce a resulting positive force in the x-direction. Overall, the results provided by the passive foil system are assumed to increase the efficiency of the vessel.

The control strategy consisting of a D-controller and a control allocation algorithm was implemented in the seakeeping solver, and a seakeeping analysis was executed investigating the behavior of the catamaran in relevant wave conditions and the influence of the controller features. Overall, the controlled flaps contribute to significant damping concerning the pitch motions and accelerations with a resulting reduction efficiency ratio for the pitch motion of 96% for H=2, T=6.95 s, and 64% for H=3.5 m, T=6.5 s. The heave

motions and accelerations were also reduced considerably with the control algorithm, while not much change was found for the motion and acceleration in surge. Furthermore, the vertical motion of the bow was investigated and was found to be reduced significantly.

Conclusively, the use of passive foils on the selected high-speed catamaran can be seen to be beneficial both with regards to the reduction of motions and accelerations, reducing the risk of seasickness, in addition to increasing the vessel efficiency. Incorporating the selected foil motion control algorithm reduces the motions and accelerations further. Tuning the controller differently or selecting a different control law could improve the efficiency of the vessel to a greater extent. However, several simplifications and assumptions were made during the course of the work. Therefore, the results can rather be seen as an indication of how the foil motion control system would influence the vessel when implemented in reality than an exact forecast. Nevertheless, a foil motion control system as the one studied in the thesis can be assumed to be of great benefit for high speed vessels similar to the one investigated.

Chapter 11

Further Work

The seakeeping analyses were only executed in regular waves due to issues in the source code when including the irregular wave model. In further studies, the responses of the vessel with foil motion control in irregular waves should be investigated. This would also test the robustness of the control system, as the controller currently implemented is rather simple.

One important aspect that should be considered regarding foil motion control in general, is the structural strength of the foils and the risk of fatigue. The foils and flaps experience large forces and moments, and the structural capacity is often a limiting factor with regards to the ride-control system. The vessel forces and moments are proportional to the wave amplitude, while fatigue is proportional to the wave amplitude cubed. As a result, fatigue is an important issue that should be investigated when realizing a foil motion control concept.

The influence of the struts was not viewed in detail in this study due to time limitation. The struts could cause a significant drop in the lift force as they could cause ventilation and steady free-surface effects. Another possible issue caused by the struts is the added resistance. These effects could together lead to a notable reduction of the lift force, and therefore of the damping efficiency of the foil motion control system.

Several simplifications were done with regards to the computation of the foil loads, including not accounting for foil interaction, cavitation or ventilation. These phenomena could lead to loss of lift, and therefore a decrease in the resulting pitch reduction. As a result, the obtained results in this study can only be used as an indication of how a foil motion control system could influence a high-speed catamaran in reality. Further studies should be executed investigating the influence of leaving out the effects of these phenomena to validate the results obtained in this study. Another method that could be used to validate the results obtained in the study is executing a model test. This would, in addition, test

whether the assumptions done with regards to the foil load computations were satisfactory.

In this study, several non-linear effects are occurring due to, for instance, the unsteady control force occurring when the flap angle reaches maximum deflection, and the increase of angle is abruptly stopped. Effects such as this, and their influence on the foil motion control, could be analyzed more closely.

An interesting focus for future studies of foil motion control of high-speed catamarans is optimizing the foil geometry. A parameter study could be executed with a focus on e.g. selecting the optimal aspect ratio to maximize damping and minimize resistance. The geometrical parameters could be varied with the goal of, for instance, investigating what parameters are dominating concerning the foil loads, and what parameters should be considered less important.

Bibliography

Alavimehr, J., Lavroff, J., Davis, M., Holloway, D., and Thomas, G. (2017). An experimental investigation of ride control algorithms for high-speed catamarans part 1: Reduction of ship motions. *Journal Of Ship Research*.

Avis, J. S. (1989). Reducing added resistance using an anti-pitch foil. *University of British Columbia*.

Baird, N. (1998). The world fast ferry market. *Baird Publications*.

Colicchio, G., Greco, M., and Faltinsen, O. M. (2006). A bem level set domain decomposition strategy for non linear and fragmented interfacial flows. *International Journal for Numerical Methods in Engineering*.

DNV GL (2014a). SESAM User Manual - Wasim. *Wave Loads on Vessels with Forward Speed*.

DNV GL (2014b). Waqum Explorer User Manual.

DNV GL (2018a). Energy Transition Outlook: Maritime Forecast to 2050.

DNV GL (2018b). SESAM Hydro D - Advanced stability and hydrodynamic analysis made easy.

Faltinsen, O. M. (1990). *Sea loads on ships and offshore structures*. Cambridge University Press, Cambridge.

Faltinsen, O. M. (1992). Global loads on high-speed catamarans. *Division of Marine Hydrodynamics, NTH*.

Faltinsen, O. M. (2006). *Hydrodynamics of High-Speed Marine Vehicles*. Cambridge University Press, Cambridge.

Fossen, T. I. (1996). Guidance and control of ocean vehicles. *NTNU*, (8).

Fossen, T. I. (2011). Handbook of marine craft hydrodynamics and motion control. *NTNU*.

Frahm, H. H. (1911). Results of trials of the anti rolling tanks at sea. *Journal of the American Society for Naval Engineers*.

Froude, W. (1865). On the practical limits of the rolling of a ship in a sea-way. *The Institution of Naval Architects*.

Hardwood, C. M. (2006). Hydrodynamic design of a foil system for a high speed catamaran. *Webb Institute, Glen Cove New York*.

Huang, L., Han, Y., Duan, W., Zheng, Y., and Ma, S. (2018). Ship pitch-roll stabilization by active fins using a controller based on onboard hydrodynamic prediction. *Ocean Engineering*.

INCAT (2018). Specifics of INCAT Natchan Rera. *https://www.incat.com.au/wp-content/uploads/2018/02/hull-064-112m-mini-spec.pdf*, [Accessed: 20/2/2019].

Loveday, H. (2006). The design of a hydrofoil system for sailing catamarans. *University of Stellenbosch*.

Migoette, G. and Hoppe, K. G. (1999). Developments in hydrofoil assistance for semi-displacement catamarans. *Icarus Marine*.

NACA (2019). Airfoil tools: NACA 64A410 (naca64a410-il). *http://airfoiltools.com/airfoil/details?airfoil=naca64a410-il* , [Accessed: 19/2/2019].

Ogilvie, T. F. (1964). Recent progress towards the understanding and prediction of ship motions. *Proceedings of the 5th Symposium on Naval Hydrodynamics*.

Perez, T. and Blanke, M. (2012). Ship roll damping control. *Annual Reviews in Control*.

Schlick, E. (1904). The gyroscopic effect of flywheels on board ship. *Trans. Inst. Naval Architects*.

SKYbrary (2019). Angle of attack. *https://www.skybrary.aero/index.php/Angle_of_Attack*, Accessed: [27.2.2019].

Stena Line Scandinavia (2019). *https://www.stenaline.no/vaare-ferger/Stena-Carisma*, Accessed: [10.2.2019].

Stensvold, T. (2016). Halefinnebevegelse kan revolusjonere hurtigbåtmarkedet. *Teknisk Ukeblad*.

Townsend, N., Murphy, A., and Shenoi, R. (2007). A new active gyrostabiliser system for ride control of marine vehicles. *Ocean Engineering*.

World Geodetic System (1984). Its definition and relationship with local geodetic systems. *DMA TR 8350.s 2nd ed. Defense Mapping Agency, Fairfax VA*.

Zhang, S., Li, S., Liang, L., and Sun, M. (2014). Ride control method of wave-piercing catamaran with T-foil and flaps. *2014 IEEE International Conference on Mechatronics and Automation, ICMA*.

Appendices

Appendix A

A.1 Dimensions of catamaran used for verification

Parameter	Symbol	Value
Length	L	25m
Center of gravity lengthwise	LCG	1.7m
Center of gravity above keel	KG	3m
Draft	d	1.75m
Beam at waterline midship	B	2m
Displacement	∇	$40.48m^3$

Table A.1: Dimensions of comparison catamaran for verification

A.2 Dimensions of catamaran model for scaling

Designation	Symbol	Unit	Value
Length between perpendiculars	L	[m]	3.778
Beam at waterline amidships	B	[m]	0.918
Draft - even keel	d	[m]	0.235
Displacement	∇	[m^3]	0.257
Block coefficient	C_B		0.542
Breadth of one hull at waterline amidships	b	[m]	0.267
Distance between centre of hulls	2p	[m]	0.652
Transverse metacentric height	GM	[m]	0.556
Centre of gravity above keel	KG	[m]	0.332
Centre of gravity aft of amidships	LCG	[m]	0.296
Pitch radius of gyration with respect to axis through centre of gravity	r_{55}	[m]	0.981
Roll radius of gyration with respect to axis through centre of gravity	r_{44}	[m]	0.334
Yaw radius of gyration with respect to axis through centre of gravity	r_{66}	[m]	1.022
Distance from centerline to centre of gravity of one half part[1]	y_A	[m]	0.298
Coupled inertia moment in roll-pitch of one half part[1]	$-\int_A xydM$	[kgm^2]	0.366
Coupled inertia moment in roll-yaw of one half part[1]	$-\int_A xzdM$	[kgm^2]	-1.118
Coupled inertia moment in pitch-yaw of one half part[1]	$-\int_A yzdM$	[kgm^2]	0.0170

[1] Half part ($y > 0$) obtained by intersecting along the centre plane of the catamaran

Figure A.1: Dimensions of vessel geometry, model scale

Appendix B

B.1 Motion time series for catamaran with passive foils

B.1.1 H=3.5 m, T=6.959590 s

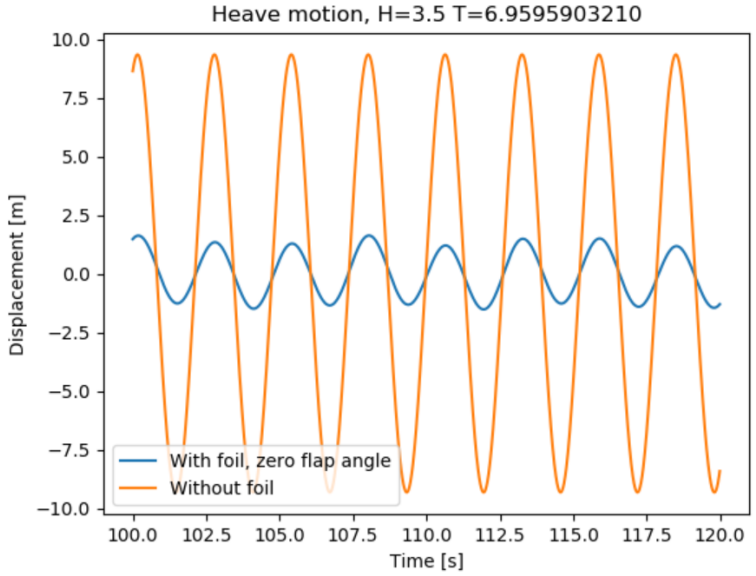

Figure B.1: Heave acceleration time series, H=3.5 m T=6.959590 s

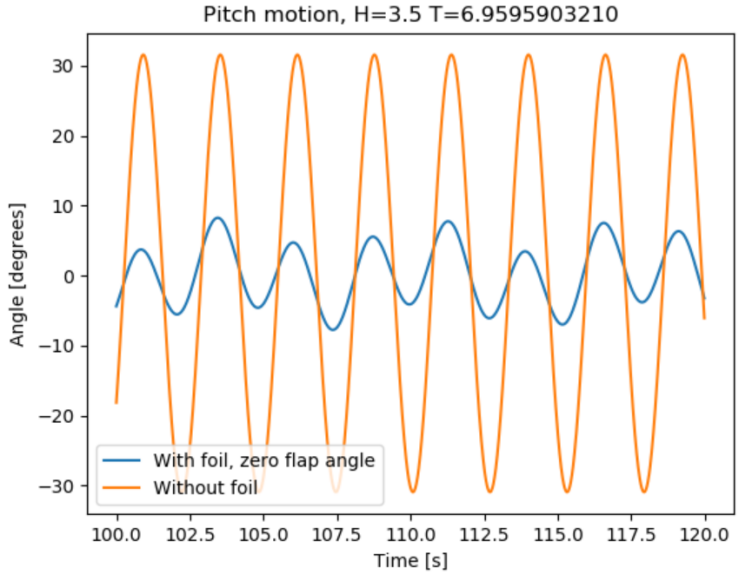

Figure B.2: Pitch acceleration time series, H=3.5 m T=6.959590 s

B.2 Acceleration time series for catamaran with passive and active foils

B.2.1 H=2 m, T=6.959590 s

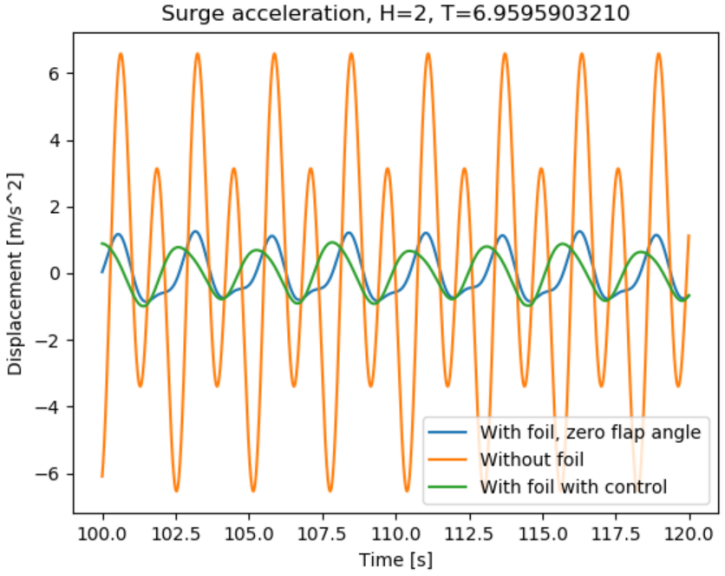

Figure B.3: Surge acceleration time series, H=2 m T=6.959590 s

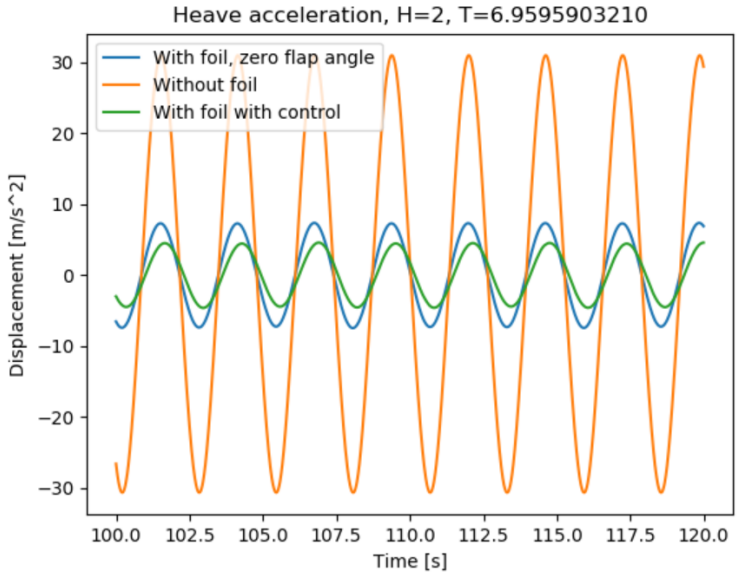

Figure B.4: Heave acceleration time series, H=2 m T=6.959590 s

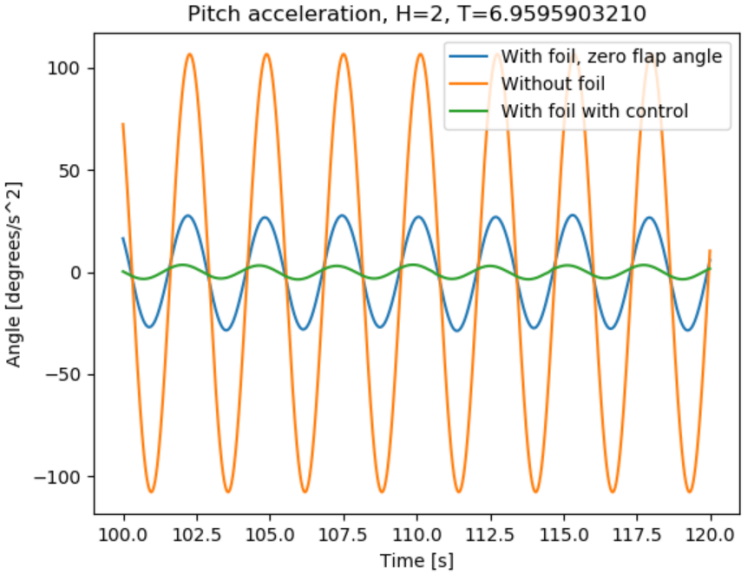

Figure B.5: Pitch acceleration time series, H=2 m T=6.959590 s

B.2.2 H=3.5 m, T=6.5 s

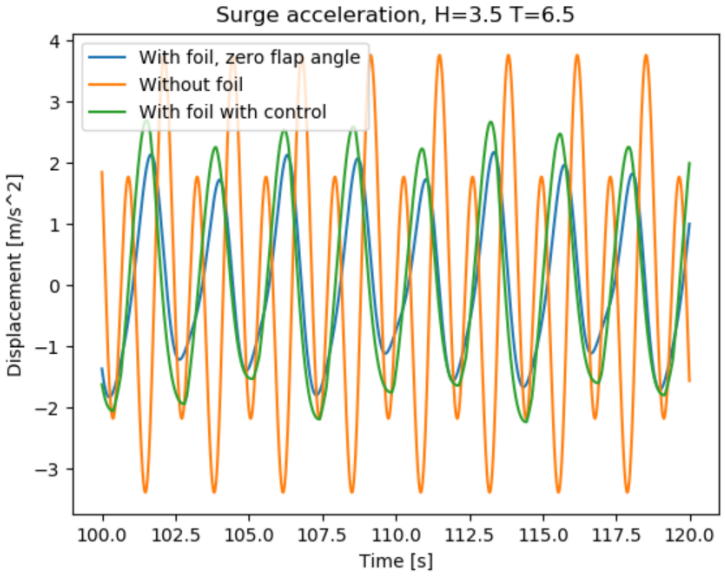

Figure B.6: Surge acceleration time series, H=3.5 m T=6.5 s

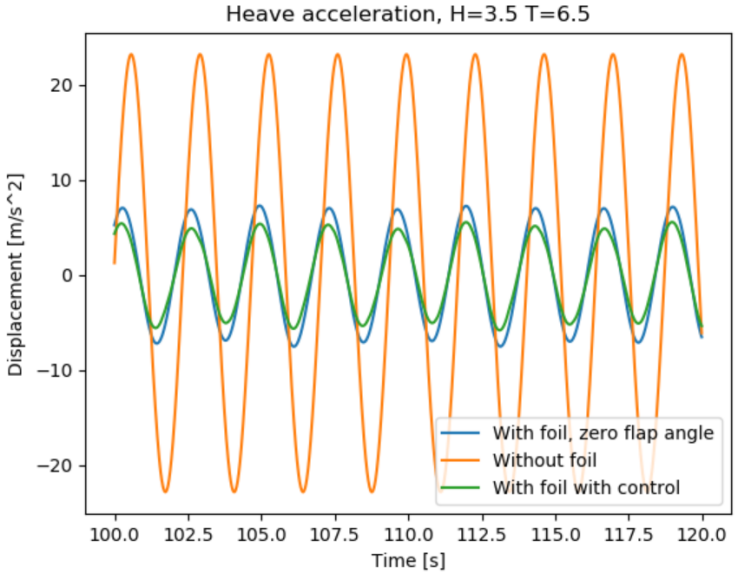

Figure B.7: Heave acceleration time series, H=3.5 m T=6.5 s

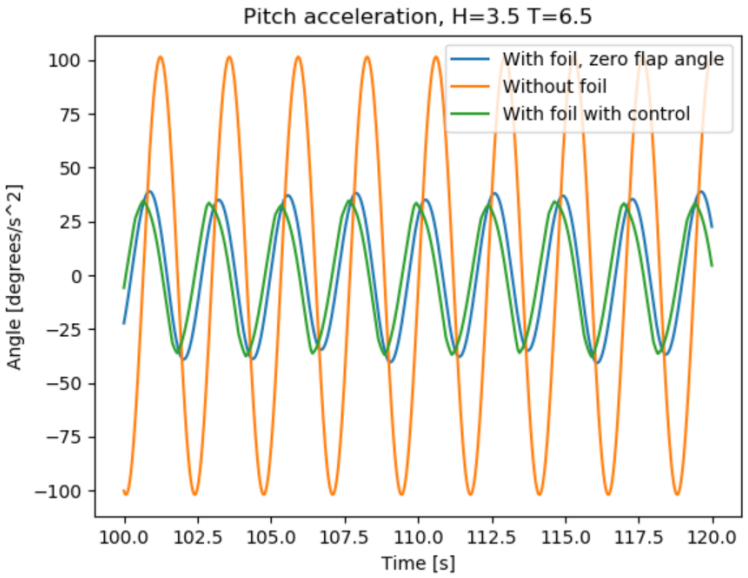

Figure B.8: Pitch acceleration time series, H=3.5 m T=6.5 s

Ida Oline Håberg

Foil Motion Control of High-Speed Catamarans

NTNU
Norwegian University of
Science and Technology